NONLINEAR COHERENT STRUCTURES IN PLASMAS

by

Sayanee Jana

(Enrolment No.-PHYS05201204001)

Saha Institute of Nuclear Physics, Kolkata

A thesis submitted to the

Board of Studies in Physical Sciences

In partial fulfillment of requirements

for the degree of

DOCTOR OF PHILOSOPHY

of

HOMI BHABHA NATIONAL INSTITUTE

October, 2017

Homi Bhabha National Institute

Recommendations of the Viva Voce Committee

As members of the Viva Voce Committee, we certify that we have read the dissertation prepared by Sayanee Jana entitled "Nonlinear Coherent Structures in Plasmas" and recommend that it may be accepted as fulfilling the thesis requirement for the award of Degree of Doctor of Philosophy.

M.S. Janaki — 9.2.2018

Chairman - **Prof. M. S. Janaki** — **Date:**

N. Chakrabarti — 9th Feb, 2018

Guide / Convener - **Prof. Nikhil Chakrabarti** — **Date:**

Co-guide - (if any) — **Date:**

N S Saini — 9/2/18

Examiner - **Prof. N.S. Saini** — **Date:**

M Munshi — 9/2/18

Member 1- **Prof. Munshi Golam Mustafa** — **Date:**

Abhik Basu — 9/2/18

Member 2- **Prof. Abhik Basu** — **Date:**

Final approval and acceptance of this thesis is contingent upon the candidate's submission of the final copies of the thesis to HBNI.

I/We hereby certify that I/we have read this thesis prepared under my/our direction and recommend that it may be accepted as fulfilling the thesis requirement.

Date: 9th Feb, 2018

Place: SINP, Kolkata

N. Chakrabarti

Co-guide (if applicable) **Guide**

STATEMENT BY AUTHOR

This dissertation has been submitted in partial fulfillment of requirements for the doctoral degree at Homi Bhabha National Institute (HBNI) and is deposited in the Library to be made available to borrowers under rules of the HBNI.

Brief quotations from this dissertation are allowable without special permission, provided that accurate acknowledgement of source is made. Requests for permission for extended quotation from or reproduction of this manuscript in whole or in part may be granted by the Competent Authority of HBNI when in his or her judgment the proposed use of the material is in the interests of scholarship. In all other instances, however, permission must be obtained from the author.

Sayanee Jana

DECLARATION

I, hereby declare that the investigation presented in the thesis has been carried out by me. The work is original and has not been submitted earlier as a whole or in part for a degree / diploma at this or any other Institution / University.

Sayanee Jana

List of Publications arising from the thesis

Peer reviewed journals

1. *Stability of an elliptical vortex in a strongly coupled dusty plasma.*
   S. Jana, D. Banerjee and N. Chakrabarti, *Physics of Plasmas*, **2015**, 22, 083704.

2. *Formation and evolution of vortices in a collisional strongly coupled dusty plasma.*
   S. Jana, D. Banerjee and N. Chakrabarti, *Physics Letters A*, **2016**, 380, 2531.

3. *Nonlinear coherent structures of Alfvén wave in a collisional Plasma.*
   S. Jana, S. Ghosh and N. Chakrabarti, *Physics of Plasmas*, **2016**, 23, 072304.

4. *Effect of electron inertia on dispersive properties of Alfvén waves in cold plasmas.*
   S. Jana, S. Ghosh and N. Chakrabarti, *Physics of Plasmas*, **2017**, 24, 102307.

Sayanee Jana

Dedicated to my "Family" and "Teachers"

Acknowledgements

The thesis would not have come to a successful completion, without the help, support and encouragement that I have received from so many people over the years. I would like to express my gratitude and heartfelt thanks to all of them.

First and foremost, I would like to express my deepest and sincere gratitude to my supervisor, Prof. Nikhil Chakrabarti, for considering me as his student when I was in an unfortunate condition of my Ph.D. career. I have been amazingly fortunate to have a supervisor who gave me his precious guidance, caring and moral support, and provided me an excellent atmosphere for doing research. His immense knowledge and deep understanding of the subject helped me a lot. His guidance helped me to successfully overcome all the difficulties I faced in attempting problems, writing papers and finishing this thesis too. Sir, I am very thankful to you for everything you did to make my Ph.D. a success.

I am grateful for having a chance to work with Prof. Samiran Ghosh whose ideas of performing numerical analysis helped me to solve various problems using numerical simulation. I am also thankful to one of my senior colleagues, Dr. Debabrata Banerjee, for his guidance in learning and writing the numerical code. Their patience and support helped me to overcome many crisis situations and finish this thesis.

I would like to thank my doctoral committee members Prof. M. S. Janaki (Chairman), Prof. M. G. Mustafa and Prof. A. Basu for their timely comments on the progress of my thesis. Specially, I am highly obliged to our divisional head, Prof. M. S. Janaki, for helping me a lot in official paper processing during the division change. I also humbly appreciate her motivating ideas and valuable suggestions that helped me a lot in my research work. I would also like to acknowledge Prof. R. N. Pal and Prof. A. N. S. Iyenger for their fruitful comments and discussions during academic reviews.

It is my pleasure to acknowledge my seniors, Subir-da, Debu-da, Chandan-da, Sudip-da, Anwesa-di and Avik-da for their help and support. I am thankful to my lab-mates, Sourav-da, Abhijit-da, Sabuj, Debu, Pankaj, Satyajit, Mithun and Subha for sharing light and joyful moments in lab and canteen. I would like to extend my words of appreciation to Subhasish-da, Monobir-da, Santanu-da, Partha-da, Dipankar-da, Ashok-da and many other colleagues at SINP.

I sincerely thank my Post M.Sc batch-mates at SINP for accompanying me to enjoy a stress free and cheerful life. Special thanks to my best friend, Achyut for his unconditional support and encouragement throughout this endeavor. It was really the happiest coincidence to start together our Ph.D. career. I feel very lucky to have met you, friends. Your friendship makes my life a wonderful experience. Wherever you end up in your future I wish you all the success in life.

I am blessed to have friends who are constant source of laughter, joy and support. I am thankful to my childhood and university friends, specially Piyali, Sudipta, Priyankadi, Anindya, Avik, Sruti and Hrishit for supporting me throughout the years. Particular thanks goes to Oindrila and Deya, you have always been there for me through all these years along with your love, wishes and advice. You redefined the word family to me with your love and affection.

I very respectfully acknowledge all my teachers who, throughout my student life, have given me quality education.

Above and beyond all, I thank the people who mean a lot to me, my parents, Maa and Bapi, for their unconditional love, support, faith, encouragement and confidence in me which encourage me to reach my goal. Also I would like to express my loving thanks to my brother, Babai. My didi and her husband Avik-da, you both deserve heartiest thanks for your love and constant support and a special love goes to our beloved Mr. Golubabu. I would also like to thank you for providing me a homely ambience during thesis writing period. I also take this opportunity to thank all my relatives and well-wishers for their support throughout the journey.

Finally, I would like to thank everyone, whose contributions were important for the successful realization of this thesis, but I could not mention them personally.

SINP, Kolkata
October, 2017 Sayanee Jana

Contents

Synopsis **ix**

List of figures **xvi**

1 Introduction **1**

1.1 Overview 2
1.2 Motivation 7
1.2.1 Nonlinear phenomena 7
1.2.2 Alfvén waves in plasmas 12
1.2.3 Transverse shear wave in strongly coupled dusty plasma . . . 15
1.3 Lagrangian fluid description: An useful way to treat the convective nonlinearity 23
1.4 Pseudo-spectral method: An efficient numerical method to handle plasma nonlinearity 27
1.5 Outline of the thesis 30

2 Effect of electron inertia on linearly polarized Alfvén wave propagation in a collisional electron-ion plasma **33**

2.1 Introduction 34
2.2 Basic equations to describe dispersive Alfvén waves 36
2.3 Linear analysis 42
2.4 Nonlinear analysis by Lagrangian mass variable 43
2.4.1 Weak amplitude nonlinear wave 43
2.4.2 Moving-frame nonlinear analysis 45
2.5 Wave modulation for small wave number: nonlinear Schrödinger equation 49
2.5.1 Effect of electron-ion collision on modulational instability . . 51
2.5.2 Approximate analytical solution: Weakly dissipative envelope (bright) soliton 54
2.6 Numerical simulation 55
2.6.1 Numerical solutions of modified Korteweg-de Vries-Burgers equation 56
2.6.2 Numerical solutions of damped nonlinear Schrödinger equation 59

2.7 Summary 62

3 Effect of electron inertia on circularly polarized Alfvén wave propagation in an electron-ion plasma 66

3.1 Introduction 67
3.2 Basic equations 68
3.3 Linear analysis 73
3.4 Weak amplitude nonlinear dynamics 74
3.5 Modulational instability 77
3.6 Analytical solution 78
3.7 Summary 81

4 Vortex dynamics in a strongly coupled dusty plasma in presence of dust-neutral collisional drag 82

4.1 Introduction 83
4.2 Governing equations 85
4.3 Numerical investigation 87
4.4 Dynamical evolution of vortices 89
4.5 Summary 98

5 Stability analysis of an elliptical vortex in a strongly coupled dusty plasma in presence of dust-neutral collisional drag 104

5.1 Introduction 105
5.2 Governing equations 106
5.3 Equilibrium 107
5.4 Stability analysis of two dimensional elliptical vortex 108
5.5 Summary 115

6 Conclusion 117

6.1 Summary 118
6.2 Future scope of the work 122

Bibliography 125

Synopsis

Formation of coherent structures, their stability and their interactions have been an important area of research in fluid dynamics as well as in plasmas as they play a very important role in energy and particle transport in such medium. This thesis is focused on the studies related to formation of coherent structures and their stability that help in understating transport phenomena in space and astrophysical plasmas as well as in laboratory plasma experiments. As is well known, a plasma comprising of electrons, ions and neutral particles is basically a highly nonlinear system. In presence of different free energy sources (velocity shear, density gradient, temperature gradient, current etc.), any small wavy disturbance inside the plasma can grow up due to different types of instabilities like drift, Kelvin Helmholtz , Rayleigh-Taylor etc. Consequently several nonlinear phenomena such as the harmonic generation involving fluid advection, the nonlinear Lorentz force, trapping of particles in the wave potential, wave-wave interactions, pondermotive force etc. become effective and together with the wave dispersion contribute to the localization of waves, leading to different types of nonlinear coherent structures like solitons, [1] shock waves, [2] vortices, [3, 4] rogue waves [5] etc. These structures not only occur in space plasmas such as in the Earth's bow shock, bow shock's at the boundary of the heliosphere, shock waves in interstellar plasma, vortices in the auroral plasma, outer part of the sun and the stars etc., but also can be obtained in the laboratory experiments. [6, 7, 8] So, the detailed studies of such nonlinear phenomena have utmost importance to the physicists from experimental as well as theoretical point of view.

In a plasma, a great variety of waves arises spontaneously due to the coherent motions of the charged plasma particles depending on the internal and external physical conditions. Besides different kinds of electrostatic waves, several electromagnetic waves such as magnetosonic wave, Alfvén wave etc. can also be generated in a magnetized plasma. [6, 9, 10] The magnetic field with the twisted field lines generates low frequency transverse shear Alfvén wave of phase velocity $V_A = B_0/\sqrt{4\pi n_0 m_i}$ (where B_0 is the magnitude of the externally applied magnetic field, n_0 is the number density and m_i is the ion inertia) in which the restoring force and inertia are provided by the magnetic field pressure and ion mass, respectively. The dispersion relation for the Alfvén waves is obtained from the magnetohydrodynamic (MHD) equations which is non-dispersive in nature. [9, 10] Several studies have been reported on Alfvénic solitons which owe their existence to the interplay between the nonlinearities and the wave dispersion where the latter arises from various plasma effects described by the generalized Ohms law. By using the basic model equations describing weakly nonlinear dispersive MHD waves, Kennel *et al.* have shown that parallel propagating Alfvén waves obey the Derivative Nonlinear Schrödinger (DNLSE) equation, which describes Alfvénic soliton, Alfvén wave turbulence etc. [11, 12] In this above mentioned model, they did not consider electron inertia effect on the wave dynamics. And the wave dispersion arises due to the coupling between the elliptically polarized magnetic field components. However, recently it is found that electron inertia plays an important role in dispersive effects of Alfvén waves which can create nonlinear structures responsible for discrete auroral arcs. [13, 14] This fact motivates us to investigate how the electron inertia affects the Alfvén wave propagation in an electron-ion plasma.

In this context, we have investigated the dynamics of the linearly polarized Alfvén wave in the framework of Lagrangian two-fluid theory [15, 16, 17] in a cold electron-ion plasma in presence of finite electron inertia effect. However, the effect of collisions in plasma is always inevitable and leads to many phenomena of fundamental importance. Therefore, electron-ion collision induced dissipation effects are taken into consideration in our study. In the framework of two fluid dynamics, finite electron inertia together with ion inertia is found to act as a source of wave dispersion which can balance the nonlinear steepening of waves leading to the formation of a soliton. In the quasi-linear limit, the dynamics of the nonlinear Alfvén waves is shown to be governed by a modified Korteweg-de Vries equation (mKdV), which can be extended to a modified Korteweg-de Vries Burgers equation (mKdVB) in presence of finite dissipation. In this mKdvB equation, the electron-ion collisional dissipation is eventually responsible for the Burgers term and as mentioned before, the electron inertia is responsible for the dispersive term. These nonlinear equations have been analyzed by means of analytic calculation and numerical simulation to elucidate the phase space dynamics of the nonlinear wave. The numerical investigations reveal that the nonlinear wave exhibits both oscillatory and monotonic shock structures depending on the strength of the dissipation. Furthermore, another important nonlinear phenomenon i.e. the effects of self interaction of the Alfvén waves that introduces self focussing effect (modulational instability) in the system has also been investigated in the long wavelength limit. Our investigation shows that there is a possibility of the trapping of Alfvén wave in a hole created by the wave itself in the medium, and the dynamics of this modulated wave is governed by a damped Nonlinear Schrödinger equation (NLSE) in which the damping is provided by the electron-ion collision. This nonlinear equation has been analyzed both analytically and numerically. The analytical and numerical simulations reveal that this modulated wave exhibits weakly dissipative bright envelope solitons. Numerical simulation also predicts the formation of rogue waves, giant breathers and rogue wave holes.

Next, we have investigated circularly polarized Alfvén wave propagation in a collisionless electron-ion plasma keeping all the parameters unchanged. The complete linear analysis indicates the saturation of right-hand polarized wave in presence of the dispersive effect of electron inertia. In the finite amplitude limit, the weakly nonlinear Alfvén wave dynamics is found to be governed by a new type of Derivative Nonlinear Schrödinger equation (DNLSE) modified by third order dispersion arising due to finite electron inertia effect. This nonlinear equation is found to be completely integrable like the DNLSE [18] and soliton like solutions are obtained.

In plasmas, apart from electrons and ions, dust particles are omnipresent ingredients which can be found in space and astrophysical environment such as planetary ring systems, cometary tails, white dwarf matter, interplanetary and interstellar clouds, Stars, Solar systems etc. [19] and also in human made systems like plasma processing and plasma etching equipments in industry, magnetic fusion plasmas, space stations, rocket exhausts, plasma torches etc. [20, 21] The dust particles which are massive, as large as of micron sized and highly charged (either positively or negatively depending on the surrounding environments), together with normal electron-ion plasma form dusty plasma system. A very interesting aspect of dusty plasma is that it can be found in a strongly coupled state as the interaction potential energy between the dust particles exceeds the kinetic energy. The strength of the coupling between the dust particles can be characterized by the coulomb coupling parameter [22] $\Gamma = q_d^2/(k_B T_d a)$, the ratio of the average potential energy to the average kinetic energy per particle, where q_d, $a(\simeq n_d^{-1/3})$, n_d, T_d and k_B are the charge on the dust particle, the average inter-particle distance, the dust number density, the temperature of the dust component and the Boltzman constant respectively. In the regime where Γ varies from 1 to Γ_c (~ 170, a critical value beyond which the system becomes crystalline), both viscosity and elasticity are equally important and the system behaves as a viscoelastic medium. The dynamics of such a visco-elastic medium has been in the past provided by the Generalized

Hydrodynamic (GH) model that incorporates the Maxwell's relaxation parameter τ_m to mimic this behavior. [23, 24] It has been shown in past studies that the strong coupling enables the system to support a novel low frequency transverse shear mode along with the longitudinal modes. [24, 25] Hence, the presence of the dust particles make the system more complex and provide a possibility to generate entirely new collective modes of oscillation, linear and nonlinear instabilities as well as nonlinear coherent structures.

It has been shown analytically as well as by molecular dynamics simulations that convective nonlinearity of the GH model plays an important role to generate vortex like structures in strongly coupled system. [26, 27] In such system the effect of strong coupling on vortices makes them quite different from normal viscous fluid. Recently, evolution and interaction of vortex like structures have been studied numerically by varying the strong coupling parameter ranging from hydrodynamic to strongly coupled limit in dusty plasma without considering collisions. [28] But, collisions always takes place between plasma and dust particles in laboratory as well as astrophysical and space plasma environment. The dust-neutral collisional drag force is, therefore, incorporated in our study to investigate it's effect on the vortex phenomena in strongly coupled plasma. We have studied vortex formation, its evolution and interactions for different initial structures having gaussian profile in the framework of the GH model modified by dust-neutral collisional drag. Our main objective is to study how the interplay between the nonlinear elastic stress (coming from the convective nonlinearity of the GH model along with the elasticity) and dust-neutral collisional drag determines the dynamics of vortices in such system. All the studies have been done by numerically integrating GH model after transforming into fourier space using doubly periodic pseudo-spectral simulation code with Runge-Kutta-Gill time integrator. [29] It is shown that the interplay between the nonlinear elastic stress and the dust-neutral collisional drag results in the generation of non-propagating monopole vortex before it starts to propagate like transverse shear wave. It is also found that the interaction between two unshielded monopole Gaussian vortices having both same rotation (co-rotating) and opposite rotation (counter rotating) produce two propagating dipole vortices of equal and unequal strength respectively when there is a sensitive balance between the nonlinear elastic stress and the dust-neutral collisional drag.

Next, we have carried out a stability analysis of a long scale two dimensional equilibrium vortex (with finite ellipticity at the core) to short scale perturbation in presence of dust-neutral collisional drag in strongly coupled dusty plasma. The analysis has been done using a mathematical technique employed by Bayly [30] in the context of a fluid dynamics problem. A numerical study has also been done to obtain the stability domain of the vortex for arbitrary values of ellipticity and estimates of growth rate is obtained by using multiple time scale method. It is seen that for circular vortices there is no instability because these vortices rotate rigidly and hence have no sources of free energy. But for vortices with finite ellipticity, it is seen that the free energy associated with the velocity shear of the vortex can perimetrically drive secondary instabilities consisting of transverse shear waves when the collision modified secondary wave frequency matches with the mean rotation frequency of the vortex or one of its multiples. Thus the secondary instability can act as a seed for the onset of turbulence by transferring the energy from the long scale vortex to the short scale secondary wave and may in turn act as a nonlinear saturation mechanism of the vortex structures in plasmas.

In summary, the results and conclusion on the analysis of the weakly nonlinear, dispersive Alfvén wave propagation, could be useful for understanding the the observed physical phenomena like particle energization and plasma heating and also in interpreting the nonlinear phenomena behind the observed magnetic structures in space plasmas. Moreover, our studies on vortex phenomena may lead a better way to understand the transport phenomena in strongly coupled plasmas.

Bibliography

[1] S. I. Popel, S. V. Vladimirov and P. K. Shukla, Phys. Plasmas **2**, 716 (1995).

[2] D. A. Tidman and N. A. Krall, *Shock waves in collisionless plasma*, John Wiley and Sons, New York, (1971).

[3] A. B. Mikhalovskii, V. P. Lakhin, L. A. Mikhailovskaya and O. G. Onishchenko, Sov. Phys. JETP **86**, 2061 (1984).

[4] A. Hasegawa, C. G. Maclennan and Y. Kodama, Phys. Fluids **22**, 2122 (1979).

[5] E. I. El-Awady and W. M. Moslem, Phys. Plasmas **18**, 082306 (2011).

[6] V. M. Chmyrev, S. V. Bilichenko, O. A. Pokhotelov, V. A. Marchenko, V. I. Lazarev, A. V. Streltsov and L. Stenflo, Physica Scripta. **38**, 841 (1988).

[7] A. Retinò, D. Sundkvist, A. Vaivadsand, F. Mozer, M. André and C. J. Owen, Nat. Phys. **3**, 235 (2007).

[8] S. D. Bale, P. J. Kellogg, D. E. Larson, R. P. Lin, K. Goe and R. P. Lepping, Geophys. Res. Lett. **25**, 2929 (1998).

[9] H. Alfvén, Nature (London) **150**, 405, (1942).

[10] N. F. Cramer, *The Physics of Alfvén Waves*, WILEY-VCH, Germany, (2001).

[11] C. F. Kennel, B. Buti, T. Hada, and R. Pellat, Phys. Fluids **31**, 1949, (1988).

[12] E. Mjølhus, J. Plasma Phys. **19**, 437, (1978).

[13] K. Stasiewicz, J. Geophys. Res.: Space Physics **110**, A3, (2005).

[14] K. Stasiewicz, P. Bellan, C. Chaston, C. Kletzing, R. Lysak, J. Maggs, O. Pokhotelov, C. Seyler, P. Shukla, L. Stenflo, A. Streltsov and J.-E. Wahlund, Space Sci. Rev. **92(3-4)**, 423, (2000).

[15] J. M. Dawson, Phys. Rev. **113**, 383, (1959).

[16] R. C. Davidson, *Methods in Nonlinear Plasma Theory*, Academic, New York, (1972).

[17] H. Schamel, Phys. Reports. **392**, 279, (2004).

[18] J. M. Ablowitz and A. P. Clarkson, *Solitons, nonlinear evolution equations and inverse scattering*, Cambridge university press, (1991).

[19] F. Verheest, *Waves in dusty space plasma*, Kluwer Academic, Dordrecht (2000).

[20] G. Federicia, C. H. Skinner, J. N. Brooksc, J. P. Coadd, C. Grisoliae, A. A. Haaszf, A. Hassaneing, V. Philippsh, C. S. Pitcheri, J. Rothj, W. R. Wamplerk and D. G. Whytel, Rep. Prog. Phys. **41**, 1967, (2001).

[21] E. C. Whipple, Rep. Prog. Phys. **44**, 1197, (1981).

[22] H. Ikeji, Phys. Fluids **29**, 1764, (1986).

[23] Y.I. Frenkel, *Kinetic Theory of Liquids*, Clarendon, Oxford (1946).

[24] P.K. Kaw and A. Sen, Phys. Plasmas **5**, 3552, (1998).

[25] J. Pramanik, G. Prasad, A. Sen and P.K. Kaw, Phys. Rev. Lett. **88**, 17500 (2002).

[26] J. Ashwin and R. Ganesh, Phys. Rev. Lett. **106**, 135001 (2011).

[27] M. S. Janaki and N. Chakrabarti, Phys. Plasmas **17**, 053704 (2010).

[28] V. S. Dharodi, S. K. Tiwari, A. Das, Phys. Plasmas **21** (2014) 073705.

[29] E. A. Coutsias, F. R. Hansen, T. Huld, G. Knorr and J. P. Lynov, Phys. Scripta **40** (1989) 270.

[30] B. J. Bayly, Phys. Rev. Lett. **57**, 2160, (1986).

List of Figures

2.1 (color online) Phase-space trajectories in the $\phi - \psi$ plane of the dynamical system. The left figure (blue solid curve) is drawn for $M = 0.5$ and the right figure (black solid curve) is drawn for $M = 4$. 48

2.2 (color online) Numerical solution of the dynamical system (2.43) in absence of dissipation ($\nu = 0$) with $D = 0.1$. Formation of single soliton for ϕ (dimensionless magnetic field fluctuations) in the traveling wave frame χ. The left figure (red solid curve) is drawn for $M = 0.5$ and the right figure (magenta solid curve) is drawn for $M = 3$. 56

2.3 (color online) Numerical solution of the dynamical system (2.43) in presence of dissipation ($\nu \neq 0$) with $M = 4$. Formation of shock-like structure for ϕ in the traveling wave frame χ. The left figure (red solid curve) shows oscillatory shock structure for weak dissipation ($\nu = 0.1$). The right figure (magenta solid curve) shows monotonic shock structure for strong dissipation ($\nu = 1$). 57

2.4 (color online) Breather solution of the dimensionless dynamical system (2.43) with $M = 4$ and $(\phi^*, 0)$ as the initial condition. The left figure (red solid curve) shows breather structure without dissipation, whereas, the right figure (magenta solid curve) shows the same with dissipation ($\nu = 0.1$). 58

2.5 (color online) Time-dependent numerical solution of the equation (2.72) with $\bar{\gamma} = 0.1$ and initial amplitude $a = 1$. 59

2.6 (color online) Time-dependent numerical simulation of the equation (2.72) with Eq. (2.76) as the initial condition. The numerical values of the parameters are $\phi_{00} = 1$, $\sigma = 0.05$ and $\epsilon = 0.05$. The left figure is drawn for no dissipation, whereas, the right figure is drawn in presence of dissipation with $\bar{\gamma} = 0.05$. In the left figure, the solid (black) curve is the initial perturbation pulse and the dotted curve (red) represents the typical profile of a bright Peregrine Soliton at $\bar{\tau} = 5$. The right figure represent the same in presence of dissipation. 61

2.7 (color online) The typical profiles of Breathers. The left figure (red dashed) represents the Breather profile in absence of dissipation at time $\bar{\tau} = 8$. The right figure (blue solid) represents the same profile in presence of dissipation with $\bar{\gamma} = 0.05$ at time $\bar{\tau} = 11$. The initial condition is same as in Fig. 2.6. 62

2.8 (color online) Time-dependent numerical simulation of the equation (2.72) with Eq. (2.76) as the initial condition. The numerical values of the parameters are $\phi_{00} = 1$, $\sigma = 0.05$ and $\epsilon = -0.05$. The left figure is drawn for no dissipation, whereas, the right figure is drawn in presence of dissipation with $\bar{\gamma} = 0.05$. In the left figure, the solid (black) curve is the initial perturbation pulse and the dotted curve (red) represents the typical profile of a dark or hole Peregrine Soliton at $\bar{\tau} = 5$. The right figure represent the same in presence of dissipation. 63

3.1 (color online) Comparison of the dispersion curve for right-hand polarized wave in absence and presence of electron inertia with $\lambda = 42.8$. The left figure (blue solid curve) is drawn in absence of electron inertia ($\delta = 0$) and the right figure (red solid curve) is drawn in presence of inertia ($\delta = 1$). 74

3.2 (color online) Formation of single soliton in moving frame ξ with $u = 1$ 81

4.1 (Color online) Evolution of large amplitude (amplitude 5.8 in normalized unit) Gaussian formed monopole vortex in time with length scale $L = 1mm$ and velocity scale $U = 1mm/s$ so that the simulation box would be $20mm \times 20mm$. Velocity scale is chosen keeping in mind the typical shear wave velocity in mm/s. Mode numbers are taken as 512×512 and collision frequency $\nu = 0.0225, Re = 0.1$ and $\tau_m = 20$. Here, vorticity is plotted as 3D surface on $x - y$ plane. 92

4.2 (Color online) Evolution of small amplitude (1.0 in normalized unit) Gaussian formed monopole vortex in time. Others parameters remain same like previous Fig. 4.1. Nonlinearity could not exceed the strength of linear term and thus initial structure propagates with shear wave velocity. 93

4.3 (Color online) Normalized enstrophy per unit area is plotted for comparison of linear and nonlinear case. Graph on left side represents nonlinear case and the right one is for linear case. 94

4.4 (Color online) Normalized energy per unit area is plotted for comparison of linear and nonlinear case. Graph on left side represents nonlinear case and the right one is for linear case. 95

4.5 (Color online) Formation and evolution of dipole vortices from two counter rotating monopole Gaussian vortices in time. Mode numbers are taken as 512×512 and initial amplitude 50 in normalized unit. Collision frequency $\nu = 45.5, Re = 0.1$ and $\tau_m = 20$. The simulation box size is $20mm \times 20mm$ but here we have taken $10mm \times 10mm$ for better resolution. Here, vorticity is plotted as contour on $x - y$ plane. 97

4.6 (Color online) Formation and evolution of dipole vortices from two counter rotating monopole Gaussian vortices in time. Mode numbers are taken as 512×512 and initial amplitude 50 in normalized unit. Collision frequency $\nu = 45.5, Re = 0.1$ and $\tau_m = 0.1$. The simulation box size is $20mm \times 20mm$ but here we have taken $10mm \times 10mm$ for better resolution. Here, vorticity is plotted as contour on $x - y$ plane. 98

4.7 (Color online) Formation and evolution of dipole vortices from two counter rotating monopole Gaussian vortices in time. Mode numbers are taken as 512×512 and initial amplitude 16 in normalized unit. Collision frequency $\nu = 7.36, Re = 0.1$ and $\tau_m = 20$. The simulation box size is $20mm \times 20mm$ but here we have taken $10mm \times 10mm$ for better resolution. Here, contour plot of vorticity on $x - y$ plane is shown. 99

4.8 (Color online) Formation and evolution of dipole vortices from two co-rotating monopole Gaussian vortices in time. Mode numbers are taken as 512×512 and initial amplitude 50 in normalized unit. Collision frequency $\nu = 47.5$, $Re = 0.1$ and $\tau_m = 20$. The simulation box size is $20mm \times 20mm$ but here we have taken $10mm \times 10mm$ for better resolution. Here, vorticity is plotted as contour on $x - y$ plane. 100

4.9 (Color online) Formation and evolution of dipole vortices from two co-rotating monopole Gaussian vortices in time. Mode numbers are taken as 512×512 and initial amplitude 16 in normalized unit. Collision frequency $\nu = 7.36$, $Re = 0.1$ and $\tau_m = 20$. The simulation box size is $20mm \times 20mm$ but here we have taken $10mm \times 10mm$ for better resolution. Here, contour plot of vorticity on $x - y$ plane is shown. 101

5.1 (color online) Plot of $[k_0^2 c_{sh}^2 - \frac{1}{4}\left(\nu + {\tau_m}^{-1}\right)^2]/\Omega^2$ vs. ϵ (ellipticity of the vortex). The pink colored regions show the unstable domains. . 114

Chapter 1

Introduction

An objective of this thesis is to contribute to the knowledge of some novel phenomena associated with nonlinear coherent structures in the context of the nonlinear plasma theory. A detailed study on nonlinear coherent structures related to both Alfvén wave in an electron-ion plasma as well as transverse shear wave in a strongly coupled plasma has been presented here. In case of Alfvén wave study, the Lagrangian two fluid model has been adopted and both analytical and numerical analysis have been done in a very extensive way. The generalized hydrodynamic (GH) model, coupled with the Poisson's equation, has been adopted for the purpose of describing strongly coupled plasma e.g. dusty plasma in strongly coupled regime. For the numerical simulation of GH equations, a de-aliased doubly periodic pseudo-spectral code has been employed. The results of our investigations could be useful in understating transport phenomena in space and astrophysical plasmas as well as in laboratory plasma experiments. This chapter describes an overview of our investigations followed by the motivation in studying nonlinear coherent structures associated with both the Alfvén wave in an electron-ion plasma and also transverse shear wave in a strongly coupled plasma.

1.1 Overview

A plasma, often referred as the fourth state of matter, is basically a gas of charged particles which behaves as an electrically conducting medium. As we increase the heat added to a solid, it will transform to the gaseous state followed by the liquid state, and then finally the bonds binding the electrons and the ions together are broken and the gas becomes an electrically conducting plasma. The term "plasma", which came from the Greek word plasma (meaning "moldable substance or jelly"), was first introduced to describe ionized gas by Tonks and Langmuir in 1929. [1] Since plasma is made up of electrically charged particles, it behaves differently from those of neutral gases due to the strong electromagnetic influences generated from localized charge and current concentrations in medium. These electromagnetic influences affect the motion of the other charge particles residing far away in the plasma which results in the generation of collective behavior in plasma. Plasma can be treated as a neutral medium on a large scale because of the presence of the equal number of positively and negatively charged particles, whereas, there is localized charge concentrations in plasma, hence the plasma is often treated as a "quasi-neutral medium". So the standard definition of plasma is as follows: "*A plasma is basically a quasi-neutral gas of charged and neutral particles which exhibits collective behavior*". [2]

The outer layers of the Sun and stars in general are made up of ionized gases and from these regions winds blow through interstellar space contributing, along with stellar radiation, to the ionized state of the interstellar gas. Thus more than ninety nine percent of the known universe is in the plasma state and the rest consisting of non plasma states of matter (the other three states of matter: solid, liquid and gas). The Earth and its lower atmosphere form a plasma-free oasis in a plasma universe whereas the upper atmosphere, stretching into the ionosphere and beyond the magnetosphere, is rich in plasma effects. Hence the physics of plasma is very important to study the dynamics happening inside the space environment, stellar medium and the upper atmospheric region of earth. [2–5]

Since 99% of the observable universe is in the plasma state, so it is quite obvious to have the dust particles embedded inside the plasmas in space and astrophysical environments such as comet tails, planetary nebula, interstellar space, planetary rings, atmospheric aerosols, planetary upper atmosphere, Solar nebulae etc. [6] Generally, dust means many things to different people, but in view of plasma physics we need to be more specific. Dust particles are massive (billions times heavier than the protons) and their sizes are of macroscopic dimensions compared to atoms and ionized nuclei, and are typically of the order of a micron. Hence, a plasma impregnated with heavier macroscopic sized dust particles is termed as a dusty plasma when the charged (due to electron/ion impingement on the dust surface) dust species behaves in a collective manner. In a normal plasma the potential energy of a typical charged particle due to its nearest neighbor is much smaller than its kinetic energy, so the plasmas like electron-ion plasma are treated as a weakly coupled plasmas. In contrast the typical low thermal velocity and high charge density on the macroscopic dust species often render a dusty plasma medium in a strongly coupled state. [6] Such dusty plasmas can be prepared artificially and/or get formed inherently in certain laboratory situations, for example, in Tokamaks due to plasma wall interactions, rocket exhausts, plasma torches etc. The presence of dust particles introduces new features to the plasma dynamics which are otherwise absent in the usual electron-ion plasma. This thesis is concerned in studying plasma dynamics both in electron-ion plasma as well as strongly coupled dusty plasma (commonly known as complex plasma).

Although plasmas do not usually occur naturally on earth, there are well known phenomena related to natural plasmas including visible glows in the polar auroras, upper-atmospheric lightning (e.g. Blue jets, Blue starters, Gigantic jets), polar wind etc. In laboratory, artificially produced plasmas are used in technological applications such as plasma displays, fluorescent lamps (low energy lighting) and neon signs. Plasmas are also used for welding, sterilizing medical instruments, lighting home and industries, cleaning up pollution, purifying contaminated water, treating harmful wastes etc. The presence of dust particles also makes the plasma system an important field of interest to the industrial purposes, such as, dry powder coatings, micro electronics, semiconductor and nanoparticle physics, solar cell and so on. [7–10]

Apart from these usefulness of plasma applications in daily life; large projects on controlled nuclear fusion and confinement technologies in plasmas have drawn a great attention to the plasma community because of their strong potential in providing a cheap, long time sustainable and hazard-free source of energy, which could eradicate energy crisis in the near future. [11] A main purpose of using a plasma in the controlled nuclear fusion is to create a favorable situation for the thermal-ion-fusion process to happen at the center of a fusion device like the stellar-core, so that the process can release energy. By employing various nonlinear processes, plasma heating can be possible to attain temperatures comparable to a stellar-core in plasma based fusion devices. [12–18] The three inevitable processes, i.e. creation, heating and confinement of the plasma drive the system away from the thermodynamic equilibrium state and thus, macroscopic changes occur inside it. In this complicated plasma dynamics inside the plasma based devices, excitations of plasma waves are very common phenomena. The characteristics of the plasma waves, generated due to auto capturing by the fields of the collective effects are different, depending on their sources. In presence of various free energy sources (velocity shear, density gradient, temperature gradient, current etc.) in the plasma, the waves no longer be in a linear regime but grow without any bound which results instabilities. There are numerous processes via which unstable modes can saturate and attain large amplitudes. When the amplitudes of the waves are sufficiently large, nonlinearities play a significant role. Basically, the nonlinearities come from the harmonic generation involving fluid advection, the nonlinear Lorentz force, trapping of particles in the wave potential, ponderomotive force etc. The nonlinearity together with the dispersion contributes to the localization of waves, leading to different types of interesting coherent structures formation; namely solitons, [19] shock waves, [20] vortices, [21, 22] rogue waves [23] etc. which are mainly responsible for the enhancement of transport of heat and particles in the system. These structures not only occur in space plasmas such as in the Earth's bow shock, bow shock's at the boundary of the heliosphere, shock waves in interstellar plasma, vortices in the auroral plasma, outer part of the sun and the stars etc., but also can be obtained in the laboratory experiments. [24–26] Studies on such nonlinear phenomena have attracted more profound interest to the plasma physicists from both experimental as well as theoretical point of view due to two reasons: the first one is to create a confined plasma environment so that a controlled thermonuclear fusion for energy requirements can be achieved and the second one is to explore several phenomena related to various types of structures observed in space and astrophysical plasma environment. Therefore, the rigorous study, regarding the various phenomena associated with nonlinear coherent structures in plasmas in different physical scenario has been pursued in this thesis.

Interestingly plasmas support various types of waves that cannot be present in any other medium. One of the most notable and extensively studied wave is the low frequency magnetohydrodynamic Alfvén wave which is commonly observed in the natural environment of plasmas in space, such as the auroral ionosphere and the interplanetary plasma, and in the solar wind. [27, 28] In this thesis, we have explored the linear and nonlinear behavior of this wave taking into account the electron inertial effect which is found to act as a source of dispersion. Specifically, we have concentrated on the formation of different nonlinear coherent structures like solitons, shocks, envelope solitons, rouge waves of Alfvén wave considering different aspects of plasma such as presence of collisions, wave-wave nonlinear interactions etc. We have tried to picturise such nonlinear structures by employing the Lagrangian transformation technique.

As stated earlier dust particles are also ubiquitous in space and laboratory plasmas, so the effect of dust particles on the plasma dynamics has also grabbed the attention of plasma physicists from decades. One of the main attributes of dusty plasma is that it can be found in the strongly coupled regime where it can mimic the physical characteristics of a broad range of fluids (both viscous and elastic properties appear) and crystalline solids as well. [6, 29] This strong coupling effect enables the system to support transverse shear wave of low frequency (few HZ) which has been obtained in the framework of generalized hydrodynamic model (GH) [30] and experimentally verified later on. [31, 32] Such strongly coupled system can support vortex like structures which are formed due to the nonlinear saturation of transverse shear wave [6, 33–35]. In such structures the dust particles rotate in a 2-D plane. We have explored formation, interactions and stability of such structures analytically as well as numerically in the frame-work of the GH model in presence of dust-neutral collisional drag. The vortex dynamics has been investigated by numerically integrating GH equation after transforming into Fourier space using the de-aliased doubly periodic pseudo-spectral code with Runge-Kutta-Gill time integrator. [36]

This thesis mainly presents the analytical and numerical studies on the various nonlinear phenomena of coherent structures related to the Alfvén waves in an electron-ion plasma and also transverse shear wave in a strongly coupled dusty plasma which could lead to proper understanding of the transport phenomena in space and astrophysical plasmas and also in laboratory plasmas. In recent days, advancement of both analytical and computational techniques enables us to do intense research in this areas.

1.2 Motivation

1.2.1 Nonlinear phenomena

Nowadays, nonlinear phenomena have become a topic of immense research interest to the physics community. Plasma is inherently a highly nonlinear system. A great varieties of nonlinear effects arise in the plasma medium which influence the dynamics of plasma and lead to large amplitude phenomena in it. Like the fluid medium, convective nonlinearity in fluid momentum equation in plasma plays an important role to generate different structures like soliton and vortex motion, and turbulence associated there with. Plasma contains mobile charged particles that continuously interact with the wave via Lorentz force, which introduces nonlinearity to the system. A large wave can also trap particles in its potential troughs, thus changing the properties of the medium in which it propagates. This type of particle trapping is also an example of nonlinear phenomena and can lead to nonlinear damping. Parametric instabilities and self modulation appear in plasma due to the nonlinear wave-wave interactions. Hence, these different types of nonlinearities present in the plasma give rise to many interesting phenomena, making the plasmas very interesting and a challenging research topic.

The nonlinear phenomena in plasma can be grouped into two main categories: the first one is the coherent phenomena which refer to circumstances where the system developed nonlinearly keeping consistency with the phase information carried by the waves and the second one is the incoherent or turbulent phenomena which refer to circumstances where a large number of random collective oscillations are excited by a linear instability resulting waves with random phases. [37] Plasma supports a great varieties of nonlinear coherent structures such as solitons, shocks, vortices, rouge waves etc. which involve dispersion and nonlinearities together with or without collisional effect. However, most of the phenomena in nature are found to be incoherent or turbulent.

In this thesis we have studied the formation of several types of nonlinear coherent structures, their stabilities and evolution for different physical scenarios.

Here, we will discuss briefly on different types of nonlinear coherent structures, their probable causes and governing equations.

1.2.1.1 Nonlinear coherent structures

Human beings are fascinated by various kinds of linear waves (for example: 1. when a stone is thrown into a still pond, the waves spread in a circular pattern with crests and troughs, but overall in the form of a wave packet, 2. when a girl plays a veena, then notes are generated as a result of vibrations pulsating through the air, 3. when a radio station broadcasts its signals, the electromagnetic energy from its transmitter radiates outward in an identical fashion, and several such phenomena) in their day to day live. In presence of dispersion, the amplitude of these waves diminish over distance leading to the water waves in the pond to settle, the melody to fade and the broadcasting signal to weaken. However, there are various examples of waves having permanent form which can travel over a long distance without any change in size and shape. All these waves can be described by the nonlinear wave equations. In 1834, John Scott Russell first discovered such type of wave, known as the "Russell's solitary" wave, having hump or dip shaped of permanent profile while conducting experiment on fluid dynamics. [38] He investigated such phenomena experimentally as well as theoretically and concluded that, the nonlinearity present in the system balances the wave dispersion (when the effect of dissipation is negligible in comparison with those of the nonlinearity and dispersion) which results in the formation of non-diminishing stable wave structure i.e known as solitary wave. However, when the dissipation effect becomes comparable or more dominant to the dispersion present in the system then shock waves are generated. Korteweg and de Vries described the finite and small amplitude localized solitary wave propagation by the Korteweg-de Vries (KdV) equation, [39] while shock waves are described by a KdV-Burgers equation. A remarkable property of these solitary waves is that they preserve their shapes and speeds even after collisions with other solitary waves. Observing such particle like properties, Zabusky and Kruskal coined the name 'soliton' to the solitary waves. [40] Besides single solitons, envelope solitons can propagate in dynamical system at a balanced condition between the broadening effects of anomalous dispersion and the narrowing effects of focusing nonlinearity. Nonlinear variation of the Schrödinger equation known as the Nonlinear Schrödinger equation (NLSE) has become the simplest model to define such type of envelope soliton propagation. Actually, solitons are fundamental phenomena in nonlinear dynamics and have attracted the attention of researchers from the physical and mathematical sciences over the last few decades. Solitons were observed in many physical systems: localized vibrational modes in biological systems, [41] high-energy physics, sound waves, [42] matter waves in Bose-Einstein Condensates [43, 44] and nonlinear waves in optics [45] etc. In the late 50s the soliton concept entered into plasma physics. Various studies on ion acoustic solitons, dust ion acoustic solitons, Alfvénic solitons have been reported depending on different physical aspects of plasma. [24, 46–48] Soliton carries energy within a nonlinear medium without energy loss, so they are very useful in transportation of energy in that medium. Unlike solitons, the energy of a shock wave dissipates relatively quickly with distance while propagating through plasma medium. After the saturation of the shock waves, the energy stored in the wave is transferred back to the plasma particles, leading to the strong plasma heating and the generation of high energy particles. These high-energy particles are responsible for the particle acceleration mechanism.

There are another kind of large, unexpected and suddenly appearing surface waves in nature, known as rouge waves, which was first observed in the ocean with amplitudes much higher than the average wave crests around them. [49, 50] The NLSE also describes such waves produced due to the self focussing effect like the envelope solitons. Nonlinear wave studies related to the rogue wave phenomena can also be found in fiber optics, [51, 52] superfluid He4, [53] optical cavities [54], Bose-Einstein condensates [55] and also in relativistic laser-plasma interactions, as well as plasma waves in atmosphere and astrophysical situations. [56, 57]

Besides such nonlinear structures, there are another well known coherent structures, known as vortex structures. Such structures can be generated in fluid medium and also plasma due to their powerful self organizing capacity. Before going to detailed discussion about vortex in plasmas, we here explain what the term 'vortex' signifies. The fluid motion can be divided into three main categories 1) laminar or potential flow, 2) pure rotation or vortex motion and 3) fully turbulent or disorderly motion. In a real physical situation all of three types combine together in fluid motion. The velocity of such fluid can be well described by a vector function of space and time and its curl gives the vorticity of the flow. It actually represents a region in a fluid in which the flow rotates around an axis line, which may be straight or curved. Physically, vorticity can be regarded as angular momentum density. Thus the vortices are regarded as coherent structures with non zero curl of the velocity field which survive for few turn over time. Vortices are commonly occurring in nature. They form during atmospheric disturbances in the vicinity of high and low pressure areas and are also vividly seen in the shapes of dust devils and in tornadoes. Vortices are also very often observed in fluid and plasma environment like planetary fluid environment, [58] astrophysical plasma [59, 60] and fusion plasmas. [61]

So, various types of coherent structures are generated in the fluid and also in plasma environment; and hence a thorough understanding of the probable causes of formation of such structures, their stabilities and evolution have been a topic of intense interest to the physics community.

1.2.2 Alfvén waves in plasmas

Waves in plasmas have been the subject of theoretical and experimental research work for many years because of its wide relevance in understanding space plasma phenomena. Plasmas are basically a complex medium for the propagation of different types of waves having wide range of frequencies and characteristics. Among the several waves, some low frequency magnetohydrodynamic waves (MHD) (much smaller than the ion cyclotron frequency ω_{ci}) arise inside the plasma medium when it is immersed in a uniform, constant magnetic field (B_0). Alfvén wave, discovered by a Swedish space physicist H. Alfvén, [62] is the most dominant low frequency (kHz) MHD wave which propagates along the constant magnetic field at the Alfvén speed $V_A = B_0/\sqrt{4\pi n_0 m_i}$ (where B_0 is the magnitude of the externally applied magnetic field, n_0 is the ion number density and m_i is the ion inertia). The existence of such wave is not surprising if one considers that the wave motion of ordinary neutral gas sound wave is $\omega = kV$ with $V = \sqrt{\gamma P/\rho}$, where P is the gas pressure and ρ is the gas density and the magnetic stress tensor scales as $\sim B_0^2/4\pi n_0 m_i$ so that Alfvén type velocities will result if P is replaced by $B_0^2/8\pi$ i.e. the restoring force and inertia are provided by the magnetic field pressure and ion mass, respectively. Thermal motions of the plasma components are not important for such kind of waves, thereby in low β_p plasma (where $\beta_p = 8\pi nT/B_0^2 (\ll 1)$, n is the plasma density, T is the plasma temperature and B_0 is the strength of the magnetic field i.e. the case where the magnetic pressure is considered to be large enough compared to the kinetic pressures of plasma species) region like solar system, auroral region such types of waves appear. [27, 28, 63] In Alfvén wave propagation the fluid and field lines oscillate together as if the particles are stuck to the field lines. It involves twisting, shearing and plucking motions of the magnetic field lines perpendicular to the applied magnetic field. [63]

In laboratory, finite amplitude Alfvén waves are excited by many sources such as external antennae, energetic charged particle beams, nonuniform plasma parameters, electrostatic and electromagnetic waves, and in space plasma such waves may be observed by direct measurement of electric and magnetic fields in the waves by artificial satellites, or via optical evidence, in the case of waves in the Sun's atmosphere. [63, 64] These waves in a plasma were firstly excited and detected by Allen Baker, Pyle and Wilcox at Berkely, California and by Jephcott in England in 1959 during an experiment done in a hydrogen plasma created in a "slow pinch" discharge between two electrodes aligned along a magnetic field. In the experiment of Wilcox *et al.*, such waves were observed with a Alfvénic speed of $2.8 \times 10^5 m/sec$ for applied magnetic field $1T$ and plasma density $6 \times 10^{21} m^{-3}$.

Alfvén wave is basically a long wavelength mode. It can be thought as a possible candidate for solar corona heating as it can transport energy fluxes over a large distance. It may also play an important role in driving field aligned currents, in particle energization in magnetized plasma, [65, 66] in self-modulation in strongly magnetized plasma, [67] in tokamak plasma heating [68, 69], in space plasma related issues like coronal heating, [70, 71] in auroral electron acceleration, [72, 73] in interplanetary shocks [74], turbulence [75] etc. Because of its several such applications, the propagation of Alfvén waves including their linear and nonlinear aspects has been a subject of great interest in succeeding decades. [63, 64, 76–78]

The dispersion relation for the Alfvén wave is obtained from the MHD equations, [62, 63] which is non-dispersive. The dispersion arises from various plasma effects described by the nonideal Ohm's law and this leads to the nonlinear pondermotive acceleration, wave-particle interactions and the formation of nonlinear localized structures. In a recent text book, [5] the descriptions of Alfvén waves have been highlighted using two fluid theory besides the usual single fluid description (MHD). Various interesting physics have come out especially related to spatial scale associated with ion and electron inertia (represented by inertial length $\lambda_i = c/\omega_{pi}$ and $\lambda_e = c/\omega_{pe}$ where ω_{pi} and ω_{pe} are the ion and electron plasma frequency respectively) in laboratory and space plasmas. Recently, it has been found that electron inertia plays an important role in dispersive effects of the Alfvén waves which can create nonlinear structures responsible for discrete auroral arcs. [72, 79]

Inspired by these formulations, we have shown in this thesis that how the electron inertia (normally undermined compared to ion) could be an important issue in Alfvén wave propagation both in linear and nonlinear regimes. An important nonlinear effect known as the wave-wave interaction which is mainly responsible for the wave modulation has been investigated. The second and third chapter of this thesis are devoted to the study of Alfvén wave propagation and its nonlinear phenomena.

1.2.3 Transverse shear wave in strongly coupled dusty plasma

As discussed previously in the overview part, a dusty plasma is basically a system of normal electron-ion plasma with highly charged, micron-sized dust particles embedded in it. These additional dust particles are bigger in size and more massive compared to the electrons and ions. The constant interaction of electrons and ions on the surface of these particles causes them to acquire large amount of charges, enabling them to respond strongly to electromagnetic forces and also to contribute towards the collective dynamics of the system. Due to their large mass, the natural time scales of their dynamics (time scale $\sim$ 1-100 Hz, size $\sim$ few micrometer and mean inter particle separation $\sim 100\ \mu m$) are much longer compared to that of the normal electron-ion plasma and therefore the collective dynamics associated with them are easily observable in laboratory experiments. In 1989, first laboratory observation of dust cloud levitation was done in a laser induced plasma processing device. [80] Since then, theoretical and experimental research on laboratory dusty plasma have been progressed rapidly in exploration of dusty plasma dynamics.

The charged dust particles interact through the long range Coulomb interaction which enables them to make strong coupling with each other. This strong coupling arises at low temperature when the potential energy between the dust particles exceeds the average thermal energy. The measure of the strength of the coupling between the dust particles is provided by the Coulomb coupling parameter, [29] $\Gamma = q_d^2/(k_B T_d a)$, the ratio of the average potential energy to the average kinetic energy per particle; where q_d , $a(\simeq n_d^{-1/3})$, n_d, T_d and k_B are the charge on the dust particle, the average inter particle distance, the dust number density, the temperature of the dust component and the Boltzmann constant respectively. However, the potential on each particle is shielded out due to the screening effect, resulting the coupling strength to get modified with the factor of $\exp(-r/\lambda_D)$; where λ_D is the Debye length. The presence of strong coupling in dusty plasma was first predicted by Ikeji theoretically [29] and thereafter it has been experimentally verified by several observations. [81–85] In the regime where Γ varies from 1 to Γ_c (~ 170, a critical value beyond which the system becomes crystalline), both viscosity and elasticity become equally important and the system can be classified as a visco-elastic medium. [29, 86] This strong coupling enables the system to support transverse shear wave like the wave generated in elastic rod due to the elastic deformation of particles perpendicular to the wave motion. This transverse shear wave is a very low frequency wave (few Hz) compared to other compressional waves present in the dusty plasma like dust acoustic wave ($\sim$ kHz), dust ion acoustic wave (a few tens of kHz) etc. Existence of transverse shear wave was first predicted by Kaw and Sen theoretically in 1998 [30] and later it has also been experimentally verified. [31, 32] After its discovery the investigation to explore different properties in different parametric regime has grabbed a great deal of interest.

1.2.3.1 Generalized hydrodynamic model (GH) equations

One of the fundamental characteristics which differentiates solid from liquid is that, the former one has long range ordered elastic property, whereas the latter one has short range ordered viscous property. But at low temperature both elastic property and viscous property coexist in case of visco-elastic fluid like dusty plasma. In 1867, Maxwell made a connection between these two properties by proposing an experimental model, as a series connection of a purely viscous damper and a purely elastic spring, known as the Maxwell's 'relaxation theory of elasticity'. For a particular external stress, strain rates are added combining the properties of an idealized elastic solid and an idealized viscous liquid and it is shown that the strain would die out after certain relaxation time. In case of viscoelastic medium, stress relaxes exponentially as $\sim \exp(-t/\tau_m)$, where τ_m is called Maxwell's relaxation time. For time scales longer than τ_m, the medium behaves like a fluid whereas at time scales shorter than τ_m, the medium retains its memory and exhibits elastic properties. This relaxation time explicitly depends on the coupling parameter Γ and various other parameters of the system. [87, 88] Frenkel generalized the well known Navier Stoke's equation of the hydrodynamics using the Maxwell's model of relaxation time and obtained the generalized hydrodynamic equation which has been used in studying medium having visco-elastic phenomena. [89] In this model, the Galilean invariant form of the dust fluid momentum equation can be written as: [30]

$$\left[1 + \tau_m \left(\frac{\partial}{\partial t} + \mathbf{v}\cdot\nabla\right)\right] \left[\rho_d \left(\frac{\partial}{\partial t} + \mathbf{v}\cdot\nabla\right)\mathbf{v} + \nabla p_d + q_d n_d \mathbf{E}\right] = \frac{\partial \sigma_{ij}}{\partial x_j}, \tag{1.1}$$

where $\rho_d = n_d m_d$ is the dust density; n_d and m_d are the number density and mass of the dust respectively, q_d is the charge on the individual dust particle, $\mathbf{v}$ is the dust fluid velocity, p_d is the dust pressure and $\mathbf{E}$ is electric field and σ_{ij} is the viscous tress tensor defined by [74]

$$\sigma_{ij} = \eta\left(\frac{\partial v_i}{\partial x_j} + \frac{\partial v_j}{\partial x_i}\right) + \left(\zeta - \frac{2}{3}\eta\right)\delta_{ij}(\nabla\cdot\mathbf{v}), \tag{1.2}$$

where η and ζ are the shear and bulk dynamic viscosity coefficients respectively. Since we are concerned to study the wave with very low frequency of the order $\omega \ll kv_{th\ e(i)}$; where $v_{th\ e}$ and $v_{th\ i}$ denote thermal velocities of electron and ion respectively, therefore the electrons and ions being light fluids compared to dust can be modeled by the standard Boltzmann distributions as:

$$n_e = n_{e0} \exp\left(\frac{e\phi}{T_e}\right),$$
$$n_i = n_{i0} \exp\left(-\frac{e\phi}{T_i}\right), \tag{1.3}$$

where $n_{e(i)}$ is the electron (ion) number density, $|e|$ is the magnitude of charge on the electron (ion), $T_{e(i)}$ denotes the electron (ion) temperature which is assumed to be constant throughout and ϕ is the electrostatic potential. The mass conservation of the fluid is described by the continuity equation

$$\frac{\partial \rho_d}{\partial t} + \nabla \cdot (\rho_d \mathbf{v}) = 0. \tag{1.4}$$

The above momentum equation and continuity equation are closed through the Poisson's equation

$$\nabla \cdot \mathbf{E} = 4\pi(en_i - en_e - q_d n_d), \tag{1.5}$$

where the dust charge is assumed to be negative. The above four Eqs. (1.1-1.5) constitute the complete set of equations for the analysis of the strongly coupled dusty plasma.

1.2.3.2 Existence of transverse shear wave

As we are interested in studying low frequency phenomena ($k\lambda_D \ll 1, \lambda_D$ is the dust Debye length); therefore the following charge neutrality condition holds both in the equilibrium and in presence of perturbations; $0 = en_i - en_e + q_d n_d \Rightarrow$

$(n_i - n_e)\, e = q_d n_d$. With this charge neutrality condition, replacing the electric field term by the pressure term as $q_d n_d \mathbf{E} = -\nabla(p_e + p_i)$, [90] the Eq. (1.1) is modified as:

$$\left[1 + \tau_m \left(\frac{\partial}{\partial t} + \mathbf{v} \cdot \nabla\right)\right] \left[\rho_d \left(\frac{\partial}{\partial t} + \mathbf{v} \cdot \nabla\right) \mathbf{v} + \nabla p\right] = \eta \nabla^2 \mathbf{v} + \left(\zeta + \frac{\eta}{3}\right) \nabla(\nabla \cdot \mathbf{v}), \tag{1.6}$$

where $p = p_d + p_e + p_i$ is the total pressure of the system. The dust pressure is assumed to obey the adiabatic equation of state which is given by $p_d = \gamma_d \mu_d n_d T_d$, where γ_d is the adiabatic index, $\mu_d = (\partial p_d / \partial n_d)_{T_d} / T_d$ is the compressibility parameter [91] and T_d is the temperature of the dust fluid. A model dependence of the compressibility coefficient on the excess internal energy, i.e., $u(\Gamma)$ can also be written as, [30, 91] $\mu_d = 1 + u(\Gamma)/3 + (\Gamma/9)\partial u(\Gamma)/\partial \Gamma$, where $u(\Gamma) = -0.81 - 0.89\Gamma + 0.95\Gamma^{1/4} + 0.19\Gamma^{-1/4}$. [92, 93] As both the electron and ion temperatures are taken to be constant throughout, therefore the system pressure can be written as: $p = n_e T_e + n_i T_i + \gamma_d \mu_d n_d T_d$.

Here the dust fluid is considered as homogeneous and incompressible i.e. the case where $\nabla \cdot \mathbf{v} = 0$, so that the density fluctuation can be ignored for simplicity. With this condition the continuity Eq. (1.4) of dust fluid leads to the constant dust density $\rho_d = \rho_{d0}$. Under this condition, the modified dust momentum equation for the incompressible dust fluid can be written as:

$$\left[1 + \tau_m \left(\frac{\partial}{\partial t} + \mathbf{v} \cdot \nabla\right)\right] \left[\rho_{d0} \left(\frac{\partial}{\partial t} + \mathbf{v} \cdot \nabla\right) \mathbf{v} + \nabla p\right] = \eta \nabla^2 \mathbf{v}. \tag{1.7}$$

Under small amplitude limit, neglecting the convective nonlinearity in Eq. (1.7) we have the following linearized form of the dust momentum equation

$$\left(1 + \tau_m \frac{\partial}{\partial t}\right) \left[\rho_{d0} \frac{\partial \mathbf{v}}{\partial t} + \nabla p\right] = \eta \nabla^2 \mathbf{v}. \tag{1.8}$$

Here no dust flow is taken in equilibrium. The variable $\mathbf{v}$ and p are the perturbed dust fluid velocity and pressure respectively. Let us take curl of the Eq. (1.8) to obtain

$$\left(1+\tau_m\frac{\partial}{\partial t}\right)\frac{\partial}{\partial t}(\nabla\times\mathbf{v})=\frac{\eta}{\rho_{d0}}\nabla^2(\nabla\times\mathbf{v}). \tag{1.9}$$

As a consequence of ($\nabla\cdot\mathbf{v}=0$), $\mathbf{v}$ can be expressed as $\mathbf{v}=\hat{e}_z\times\nabla\psi$, where $\psi(x,y)$ is the velocity stream function with $\nabla\times\mathbf{v}=\hat{e}_z\Omega$ and vorticity $\Omega=\nabla^2\psi$. Let us investigate the above Eq. (1.9) in both hydrodynamic and kinetic limit.

In hydrodynamic limit (defined as $\tau_m\partial/\partial t\ll 1$), z-component of the equation (1.9) is written as:

$$\frac{\partial\Omega}{\partial t}=\frac{\eta}{\rho_{d0}}\nabla^2\Omega \tag{1.10}$$

which represent the diffusion equation. Considering the plane wave form $\Omega\sim\exp(i\mathbf{k}\cdot r-i\omega t)$, the dispersion relation is obtained as $\omega=-i\eta k^2/\rho_{d0}$, which arises only due to the presence of the viscosity.

In kinetic limit (defined as $\tau_m\partial/\partial t\gg 1$), the linearized vorticity equation (1.9) reduces to

$$\frac{\partial^2\Omega}{\partial t^2}=c_{sh}^2\nabla^2\Omega \tag{1.11}$$

which represents wave equation where phase velocity of shear wave is $c_{sh}^2=\eta/(\tau_m\rho_{d0})$; where τ_m can be expressed as:

$$\tau_m=\frac{4\eta m_d}{3\rho_{d0}T_{d0}}\frac{1}{(1-\gamma_d\mu_d+4u(\Gamma)/15)},$$

and using this relation, expression of the velocity of shear wave is given by, [30]

$$c_{sh}^2=\frac{3T_{d0}}{4m_d}\left(1-\gamma_d\mu_d+\frac{4}{15}u(\Gamma)\right). \tag{1.12}$$

Therefore, the elastic effect arising due to the strong coupling between the dust particles enables the system to support transverse shear wave which has no counterpart in weakly coupled state of the system. The shear wave has been identified in the molecular dynamics simulation study [94] and observed to be spontaneously excited with phase velocity $c_{sh} = 4.2\ mm/s$ for dust particle density $5 \times 10^{11}\ m^{-3}$ and dust particle temperature 0.03 eV in an experimental setup of a glow discharge dusty plasma. [31] This experimentally obtained wave velocity agrees quiet well with theoretically calculated value from the relation (1.12). The linear and nonlinear behavior of this wave in strongly coupled plasma have been studied extensively under different physical conditions both theoretically and experimentally.

1.2.3.3 Earlier investigations on dust vortex flows

As described in the Sec. 1.2.1 of this chapter, different types of coherent structures like solitons, shocks, vortices, rouge waves have been observed in fluid as well as plasma medium. In case of dusty plasma, as the governing dynamics is different than that of Newtonian fluids, the existence of various coherent structures as well as their stabilities and evolution must have significant differences. Study on dust vortices is an interesting fundamental issue which has been reported by many experimental and theoretical investigations.

Formation of different types of dust vortices have been studied in presence as well as in absence of magnetic field. In plasma crystal experiment under microgravity condition, different types of dust vortices have been observed around the dust voids in the cloud of fine dust particles. [95] Later, in simulation, it has been concluded that the dust vortices around the void get generated due to the nonconservative forces such as, ion drag force, electric force and coulomb force, but thermophoretic force has no driving role for their generation. [96] Experiment carried out in the laboratory rf (radio-frequency) plasma has reported the formation of dust vortices at the wake flow regime of dust particles behind voids. [97] The phenomena of thermal creep gives rise to the formation of Vortex like structures of convective dust clouds in a complex plasma experiment [98]. Bockwoldt *et al.* have explained in experimental and numerical studies that stable dust vortices are generated due to the balance between the driving torques from charge gradients and ion drag and the loss of torque by friction with the neutral gas. [99] They have also explained that charge gradient alongwith ion drag force is essential for the generation of quadrupole vortices. Konopka *et al.* and Sato *et al.* have shown the rotation of dust particles experimentally in the magnetized dusty plasma. [100, 101] Recently, Schwabe *et al.*, have studied the properties of dust vortices in light of turbulence and reported that velocity structure functions scale very close to the predictions by Kolmogorov theory [102]. Agarwal *et al.* have observed spontaneous rotation of a strongly coupled dusty plasma cloud in the absence of any external magnetic field induced by charge gradients perpendicular to the gravity [103].

In strongly coupled dusty plasma, there are also some theoretical observations of transverse shear wave generating vortex like flows in unmagnetized situation. P. K. Shukla [34] has reported different types of dust vortex flows such as monopolar dust vortex, a row of identical dust vortices, and a row of counter-rotating dust vortices which are generated from the nonlinear saturation of the transverse shear wave. Such vortex flows are capable of describing the salient features of nonlinear coherent waves and structures observed in laboratory dusty plasma discharges. [95]

Later on, M. S. Janaki *et al.* have shown dipolar vortex like solutions exploiting the convective nonlinearity of the generalized momentum equation of the dust fluid. [33] Molecular dynamic simulation has also shown the formation of tripole and dipole vortices from the perturbed shielded Gaussian vortex in strongly coupled dusty plasma. [104]

Therefore, the vortices forming in strongly coupled dusty plasma provide the opportunity to proper understanding of the flow of strongly coupled medium such as elastic polymer solutions, condensed matter system and astrophysical systems, and hence, have become topic of our research interest. The fourth chapter of this thesis is devoted to study vortex phenomena associated with transverse shear wave in strongly coupled dusty plasma. The physical relevance of any vortex depends on wheatear it is stable or not, hence its stability analysis is very important. In the fifth chapter, stability analysis of a vortex has been presented.

1.3 Lagrangian fluid description: An useful way to treat the convective nonlinearity

There are two different approaches to study plasma dynamics. The first one is the kinematic description based on microscopic view point, which includes effects of motion of all individual charged particles and takes appropriate averages to obtain a fundamental plasma kinetic equation. The other one is the fluid model which describes the plasma based on macroscopic quantities (velocity moments of the distribution such as density, mean velocity, mean energy, pressure etc. and their evolution in space and time). Together with the Maxwell's equations the fluid approach can almost provide a complete dynamic evolution of a plasma. In our problem, we have adopted fluid description in studying nonlinear plasma dynamics.

Within fluid description, there are also two different methods that are widely used to observe and analyze fluid flows, commonly known as the Eulerian and Lagrangian description of fluid flows. The Eulerian fluid description corresponds to a coordinate system fixed in space and measures fluid properties, like velocity, density, temperature, etc. as a function of time as the flow passes fixed location in the flow field. Whereas, the Lagrangian fluid description involves observing the trajectories of specific fluid parcels as they move in space-time and also monitoring any changes in their properties.

While studying plasma dynamics, the inherent nonlinear property of plasma is reflected through the 'convective derivative' term, $\partial/\partial t + \mathbf{v}\cdot\nabla$ in the fluid equations. In the Eulerian fluid description, this convective term appears in the governing equations as operating on an Eulerian field $f(x, y, z, t)$ where the first term inside the bracket gives the change of the function $f(x, y, z, t)$ with t and the second term gives the change due to the spatial variation. [2, 3] Within this framework, the nonlinear equations governing the wave dynamics of plasma are very tough to solve analytically. Under weak amplitude limit, linear analysis can be done by neglecting the higher order terms, but for large amplitude the nonlinearity can be handled mainly by visualizing a stationary picture from moving frame, where the dynamical variables are considered as functions of the variable, $\zeta = x - Mt$, M being the constant velocity of the moving frame. This method is valid only if the solutions are isolated and stable for a long time i.e. to find out solitary structures. However, it has disadvantages regarding to know about the dynamics, which is the time evolution of the system and also to have any information about the initial state from which the stationary state evolved. Thus any method which allows one to study the time evolution explicitly would be extremely useful. One such method is based on the utilization of a Lagrangian fluid description. [37]

In the Lagrangian fluid description, a transformation is carried out from the conventional Eulerian coordinate to Lagrangian coordinate, through which the nonlinear convective derivative merely reduces into a local time derivative, thereby making the governing equation very easier to handle. The transformation from the Eulerian variables (x,t) to Lagrangian variables (ξ, τ) can be written as:

$$\xi = x - \int_0^{\tau} v(\xi, \tau')d\tau' \quad , \quad \tau = t. \tag{1.13}$$

This is basically generalization of the Galilean transformation where the fluid velocity v is a function of space and time. This transformation shows that ξ is a function of x and t, while, initially, when $\tau = t = 0$, fluid element is located at $\xi(x, 0) = x$. From Eq. (1.13) time derivative transforms according to,

$$\frac{\partial}{\partial \tau} \equiv \left(\frac{\partial}{\partial t} + v\frac{\partial}{\partial x} \right). \tag{1.14}$$

The relationship between the Eulerian and Lagrangian derivatives becomes

$$\frac{\partial}{\partial x} \equiv \left[1 + \int_0^{\tau} \frac{\partial v}{\partial \xi} d\tau' \right]^{-1} \frac{\partial}{\partial \xi}. \tag{1.15}$$

The continuity equation in fluid can be rewritten in the newly defined Lagrangian coordinate as:

$$\left(\frac{\partial}{\partial t} + v\frac{\partial}{\partial x} \right) n + n\frac{\partial v}{\partial x} = 0 \Rightarrow \frac{\partial}{\partial \tau} \left[n(\xi, \tau) \left(1 + \int_0^{\tau} \frac{\partial v}{\partial \xi} d\tau' \right) \right] = 0. \tag{1.16}$$

The relation between the old and new space derivative at a certain time is determined by the Eqs. (1.15) and (1.16) as:

$$\frac{\partial}{\partial x} = \frac{n(\xi, \tau)}{n(\xi, 0)} \frac{\partial}{\partial \xi}. \tag{1.17}$$

The above expression clearly indicates that relation between old and new space derivative is determined by the initial and instantaneous density profile. Thus the calculations become very simple in this newly defined coordinate system and analytical solution of the relevant physical quantities can be obtained. Further we can revert back the solution in the laboratory frame i.e., the Eulerian coordinates system and the effect of the fluid nonlinearity reappears resulting more explicit visualization of the underlying physical processes related to the study.

A great deal of attention has been paid to investigate nonlinear effects in plasmas involving Alfvén waves. Theoretical analysis of such kind of nonlinear effects in most cases has been performed using reductive perturbation theory, where the nonlinearity is considered to be very weak. [105–110] But the finite-amplitude Alfvén waves are subjected to a great variety of nonlinear effects, which can be explored in detail exploiting the Lagrangian fluid method. In 1988, Kennel et al., [77] in their pioneering work, have derived governing equation for the dispersive nonlinear Alfvén wave using Lagrangian coordinates and a two time scale method, since then this method has become very much popular in case of Alfvén wave study. However, there are some limitations of such techniques which are very important to be mentioned here. This method is applicable in plasma situation where the physical quantities have only one dimensional variation over space. On the other hand, if any kind of multi-stream flow is developed in certain plasma situation then this method loses its functionality in describing such system, as the transformation from the Eulerian to Lagrangian coordinate does not remain unique for all x and t. Hence, all our study related to Alfvén waves have been restricted to one dimensional spatial variation and all types of complications have been avoided.

1.4 Pseudo-spectral method: An efficient numerical method to handle plasma nonlinearity

Spectral methods are a class of numerical methods that are often applied in solving nonlinear partial differential equations (PDE) with certain approximations. Among several spectral methods such as pseudo-spectral method or spectral collocation method, spectral Galerkin method, Chebyshev spectral method etc., [111–113] the pseudo-spectral method has been an efficient one in solving convective nonlinear term ($\mathbf{v} \cdot \nabla \mathbf{v}$) in fluid dynamics using the Fast Fourier Transform (FFT). This method is only applicable in solving problems with periodic boundary conditions. So this method have been very popular in direct simulation of vortices in fluid dynamics, in weather modeling and also in certain areas of plasma physics with periodic domain. [114, 115]

The basic idea in applying numerical method to solve PDE is that: first try to write the solution of the PDE as a linear combination of basis functions, and then select the coefficients in such a way that the resulting linear combination approximates the solution decently. Many different functions can be employed as basis in the expansion, e.g. Bessel, Chebyshev, Legendre Series and Fourier etc. The coefficients of this expansion are used to represent the solution. Differentiation in configuration space then becomes an algebraic operation in transformation space. The Fourier expansions which are used as basis function for the pseudo-spectral method are best suited for computational purpose due to the availability of the FFT algorithm.

To describe the method, let us consider a continuous, periodic function $\phi(x)$

on the interval $0 \ll x \ll 2\pi$. The Fourier expansion of $\phi(x)$ is

$$\phi(x) = \sum_{k=0}^{\infty} \phi_k e^{ikx}, \tag{1.18}$$

where

$$\phi_k = \frac{1}{2\pi} \int_0^{2\pi} \phi(x) e^{-ikx} dx. \tag{1.19}$$

The expansion in Eq. (1.18) requires infinitely many coefficients, so it can not be used in numerical scheme. A finite approximation, $\phi_N(x)$, where

$$\phi(x) \sim \phi_N(x) = \sum_{k=0}^{N-1} \tilde{\phi}_k e^{ikx}, \tag{1.20}$$

can be obtained in many ways. The pseudo-spectral method determines the values of $\tilde{\phi}_k$ by solving the N linear equations

$$\phi_N(x_i) = \phi(x_i), \quad i = 0, 1, ..., N-1; \tag{1.21}$$

where x_i are the collocation points. In the case of Fourier expansion, the choice of

$$x_i = \frac{2\pi}{N} i, \quad i = 0, 1, ..., N-1; \tag{1.22}$$

allows one to use FFT algorithm. The differentiation is performed by

$$\frac{\partial \phi}{\partial x} \sim \frac{\partial \phi_N}{\partial x} = \sum_{k=-N/2}^{N/2-1} ik\tilde{\phi}_k e^{ikx}, \tag{1.23}$$

where the limits of the summation are determined by the shortest detectable length being $2\Delta x$.

As mentioned earlier pseudo-spectral is used in numerical plasma simulation extensively due to its efficient ability in solving the convective nonlinear term ($\mathbf{v} \cdot \nabla \mathbf{v}$) using FFT. If we expand the nonlinear term in fourier series in transformation space then it yields

$$v(x)\frac{\partial v(x)}{\partial x} = ik \sum_{k=p+q} v(p)v(q) = \sum_{k=p+q} v(p)v'(q) = w(k). \tag{1.24}$$

This Eq. (1.24) contains convolution, which is very difficult to handle by normal finite difference method. The computational operation required in this method is of the order of N^2, which is unacceptable for high resolution job with higher values of N. Fortunately, the number of operations involved in a FFT is only of the order of $N \log N$, which is very much handy in this respect.

In this FFT method, one should first transform $v(p)$ and $v'(q)$ back into the configuration space to obtain $V(x_i)$ and $V'(x_i)$, where x_i are the gridpoints, then form the product

$$\tilde{W}(x_i) = V(x_i)V'(x_i), \tag{1.25}$$

and finally, transform into k-space to obtain

$$\tilde{w}(k) = \frac{1}{N}\sum_{x_i} \tilde{W}(x_i)e^{-ikx_i}. \tag{1.26}$$

Under this FFT method, it is easily shown that

$$\tilde{w}(k) = \frac{1}{N}\left[\sum_{k=p+q} v(p)v'(q) + \sum_{p+q=k+N} v(p)v'(q) + \sum_{p+q=k-N} v(p)v'(q)\right], \tag{1.27}$$

which is not equal to the expression for $w(k)$ [Eq. (1.24)]. In addition to the term [Eq. (1.24)] we are interested in, two extra terms are present here, known as "aliasing" errors.

The aliasing errors can be eliminated by imposing restriction on the k-variation from the original $-N/2 \leq k \leq N/2 - 1$ to $(-N/2)\cdot 2/3 \leq k \leq (N/2)\cdot 2/3 - 1$ and putting the remaining values of $v(k)$ and $v'(k)$ out side these limits equal to zero before doing the inverse FFT to come back to the configuration space. The same should also be applied in case of $\tilde{w}(k)$ after doing the final FFT. In this way, effect of any additional terms produced by the nonlinear multiplication operation could be avoided. This fruitful method is known as the "2/3 de-aliasing" method. [116, 117]

Hence, the pseudo-spectral method has been used very popularly due to its high accuracy and low computational effort compared to ordinary finite difference methods. However there are some limitations. They are only applicable to solve problems with periodic boundary conditions and require the input data to be sampled at evenly spaced gridpoints.

In case of strongly coupled dusty plasma, the dust momentum equation (1.1) has higher order convective nonlinearity as described earlier. In our study on vortex dynamics, we have employed a de-aliased doubly periodic pseudo-spectral code to tackle the nonlinearity using a fourth order Runge-Kutta-Gill time integrator for time stepping.

1.5 Outline of the thesis

The outline of the thesis is briefly described below:

In chapter-II governing equation describing linearly polarized weakly nonlinear dispersive Alfvén wave propagation has been derived in the framework of Lagrangian two-fluid approach in a cold collisional magnetized plasma in presence of finite electron inertial effect. The small amplitude nonlinear dynamics of the Alfvén wave described by a modified Korteweg-de Vries-Burgers (mKdVB) equation has been investigated. It has been shown that the electron inertia provides the dispersive effect and the electron-ion collision is responsible for the Burgers term. In the long-wavelength limit, the wave modulational characteristic of the nonlinear wave governed by a damped nonlinear Schrödinger equation (NLSE) has also been investigated. All the obtained nonlinear equations have been analyzed by means of analytical calculation and numerical simulation to elucidate the various aspects of the phase-space dynamics of the nonlinear wave. The numerical calculations and results have been discussed in detail.

In continuation of the previous study **chapter-III** describes the circularly polarized Alfvén wave propagation and associated nonlinear phenomena. In this study collisional effect has not been taken into consideration. A complete linear analysis has been presented which indicates the saturation of right-hand circularly polarized wave in presence of the dispersive effect of electron inertia. A new type of modified nonlinear equation same as the Derivative Nonlinear Schrödinger equation (DNLSE) has been obtained where third order dispersion arises due to finite electron inertia. An analytical solution has also been presented with vanishing boundary conditions.

chapter-IV is devoted to investigate formation, evolution and interaction of vortices in a strongly coupled dusty plasma in the framework of the GH model modified by dust-neutral collisional drag. Nonlinear dynamical response of this strongly coupled system in presence of dust-neutral drag has been mainly presented. All the studies have been carried out using a de-aliased doubly periodic pseudo-spectral code with Runge-Kutta-Gill time integrator.

chapter-V extends the investigation in studying stability analysis of the long scale equilibrium elliptical vortex structure (with finite ellipticity (ϵ) at the core) to short scale secondary transverse shear wave perturbations. An extensive study has been carried out to obtain the stability domain of the vortex for arbitrary values of ellipticity. The estimates of the growth rate of the instability have also been obtained by using a multiple time scale method.

In chapter-VIII, a summary of the results and discussions made in this doctoral research work has been presented. The problems, remain unsolved, have also been discussed point wise which could be interesting to pursue further.

Chapter 2

Effect of electron inertia on linearly polarized Alfvén wave propagation in a collisional electron-ion plasma

In this chapter, the linearly polarized Alfvén wave propagation has been investigated using the Lagrangian fluid approach in a collisional cold electron-ion plasma. In the framework of two fluid dynamics, electron inertia is found to act as a source of dispersion acting against the convective nonlinearity. Weak amplitude Alfvén wave is found to be governed by a modified Korteweg-de Vries equation (mKdV), which extends for finite dissipation to a mKdV-Burgers equation. In the long wavelength limit, this weakly nonlinear Alfvén wave is shown to be governed by a damped nonlinear Schrödinger equation (NLSE). Furthermore, these nonlinear equations have been analyzed by means of analytical calculation and numerical simulation. It has been found that, the nonlinear Alfvén wave exhibits the dissipation mediated shocks, envelope solitons and breather like structures. Numerical simulations also predict the formation of dissipative Alfvénic rogue waves, giant breathers and rogue wave holes.

2.1 Introduction

As described in the first chapter, the Alfvén wave is the fundamental low frequency magnetohydrodynamic wave (MHD) and is important both in the laboratory [118] and space plasma [63] because of nonlinear structures formation leading to several applications in various physical processes related to particle energization in magnetized plasma, [65] self-modulation in strongly magnetized plasma, [67] tokamak plasma heating, [68] interplanetary shocks [74] etc. Nonlinear structures are formed due to the combining effects of nonlinearity and dispersion, mentioned earlier in Sec. 1.2.1 of the first chapter. Several extensive studies have been done on Alfvénic localized structures where it has been reported that the nonideal Ohm's law is responsible for the wave dispersion. In 1988, Kennel *et al.* in their pioneering work, [77] have shown that, dispersive fast and slow wave, propagating at large angles to the magnetic field, are governed by the Korteweg-de Vries (KdV) equation, whereas, a modified KdV (mKdV) equation governs the dynamics of the nonlinear intermediate frequency wave. However, in presence of Hall effects, in the limit of wavelengths much larger than the ion inertial length, the dynamics of the nonlinear Alfvén wave propagating along a direction either parallel or making a small angle with the magnetic field, is governed by a derivative nonlinear Schrödinger equation (DNLSE) which describes Alfvénic soliton, Alfvén wave turbulence etc. [77, 119] In this above mentioned model, wave dispersion arises due to coupling of the elliptically polarized magnetic field components. [77] Several theoretical works have also been reported on the propagation of nonlinear Alfvén wave [107–109] where the electron inertia response has been overlooked. In our present model we have not considered two component magnetic field, rather it has been shown that one component magnetic field is sufficient to describe the essential features of nonlinear and dispersive Alfvén wave in electron-ion plasma where the electron inertia provides dispersive effect.

Moreover, the MHD waves are highly dissipative [120] and the dissipation leads to the coronal heating in solar plasma. The Alfvén wave is thought to be a possible candidate for solar corona heating as it can transport energy fluxes over a large distance. The resonant absorption and plasma heating enhance the chance of dissipation (via viscosity and/or resistivity) that leads to the Alfvén wave heating. [121, 122] In recent past, various nonlinear phenomena of Alfvén waves from the kinetic to inertial regime have been established by means of numerous laboratory observations as well as theoretical analysis. [123–129] Nonlinear phenomena of Alfvén waves in low beta plasmas now become a very important research area to the plasma physicists. [130]

In the present work, we have investigated the dynamics of the weakly nonlinear linearly polarized Alfvén wave in the framework of Lagrangian two-fluid theory in a cold plasma [37, 131–133] in presence of finite electron inertial effect. The electron-ion collision induced dissipative effect is also taken into account. Interestingly, the effect of finite electron inertia acts as a source of wave dispersion. In the quasi-linear limit, the dynamics of the nonlinear Alfvén mode is shown to be governed by a mKdV-Burgers (mKdVB) equation, where the electron-ion collision is responsible for the Burgers term and as mentioned before the electron inertia is responsible for the dispersive term. In the long wavelength limit, we have also investigated another important physical phenomena known as the modulational instability. It is a destabilization mechanism for plane waves that results from the interplay between nonlinearity and dispersive effect. [134–136] The nonlinearity mainly originates from the ponderomotive force. A slow parallel modulation of a finite amplitude monochromatic plane wave can grow and in some limit leads to the formation of a bright (envelope) soliton. In our study, the dynamics of the modulated wave is shown to be described by a nonlinear Schrödinger equation (NLSE) with a linear damping term arising due to electron-ion collision. These two nonlinear equations (mKdVB and damped NLSE) have been analyzed by means of analytic calculation and numerical simulation.

2.2 Basic equations to describe dispersive Alfvén waves

We have considered the two-fluid model of a cold plasma, in which each distinct species of particle is specified by the index α, with mass m_α and charge q_α, Each collection of particles of a specific type is supposed to act as a fluid, with its own velocity U_α, number density n_α. Each fluid is collision dominated and acted on by the electric and magnetic fields, and may act on the other fluids via collisions. We have also assumed low-β_p plasma, (where $\beta_p = 8\pi nT/B_0^2 (\ll 1)$, n is the plasma density, T is the plasma temperature and B_0 is the strength of the magnetic field) so that the cold plasma approximation is justified. [137] The uniform external magnetic field is in the $\hat{e_x}$ direction ($B_0\hat{e}_x$). To investigate the propagation of the nonlinear Alfvén wave in the direction of the external magnetic field, we have considered the equation of motion for the fluid corresponding to the species α:

$$m_\alpha n_\alpha \left(\frac{\partial}{\partial t} + \mathbf{U}_\alpha \cdot \nabla\right) \mathbf{U}_\alpha = n_\alpha q_\alpha \left(\mathbf{E} + \frac{1}{c}\mathbf{U}_\alpha \times \mathbf{B}\right) + m_\alpha n_\alpha \nu_{\alpha\beta}(\mathbf{U}_\beta - \mathbf{U}_\alpha), \quad (2.1)$$

where $\nu_{\alpha\beta}$ is the collision frequency of particle of species α with particles of species β. In this work we have considered only electron-ion plasma with singly ionized ions ($\alpha \equiv e, i$) in which $q_e \equiv -e$ and $q_i = e$, where e is the fundamental unit of electronic charge.

The continuity equation for each fluid is

$$\frac{\partial n_\alpha}{\partial t} + \nabla \cdot (n_\alpha \mathbf{U}_\alpha) = 0, \tag{2.2}$$

and the following Maxwell's equations are

$$\nabla \times \mathbf{E} = -\frac{1}{c}\frac{\partial \mathbf{B}}{\partial t}, \tag{2.3}$$

$$\nabla \times \mathbf{B} = \frac{4\pi \mathbf{J}}{c} + \frac{1}{c}\frac{\partial E}{\partial t}, \tag{2.4}$$

where summation convention is used. All symbols have their usual meaning. In this work, we are interested in the low-frequency mode where ω is smaller than the electron plasma frequency $\omega \ll \omega_{pe}$, so that we have neglected the displacement current compared to particle current in Eq. (2.4) and obtained

$$\nabla \times \mathbf{B} = \frac{4\pi \mathbf{J}}{c} = \frac{4\pi}{c} q_\alpha n_\alpha U_\alpha. \tag{2.5}$$

Now, if we restrict that all the dynamical variables has only one space dimension, say in x direction, then the x component of the Eq. (2.5) yields $J_x \approx 0$. This implies that the electron current can balance the ion current in the x direction, i.e. $n_e U_{ex} = n_i U_{ix}$. In this condition, from the continuity equations (2.2) for both species, we can write,

$$\frac{\partial}{\partial t}(n_i - n_e) + \frac{\partial}{\partial x}(n_i U_{ix} - n_e U_{ex}) = 0. \tag{2.6}$$

Now, using $n_e U_{ex} = n_i U_{ix}$, in Eq. (2.6) we have obtained $\partial(n_i - n_e)/\partial t = 0$, which simply shows that 'quasi-neutrality approximation' $n_i \sim n_e \sim n$ is a reasonable approximation for this problem. Hereafter all the analysis will be done in one spatial variable x. Consequently, we have assumed that all the variables are functions of x and t. Furthermore, we have assumed that the applied magnetic field, propagation of the wave and the inhomogeneity are all in the x direction. Using all the above stated approximation, from Eq. (2.6) we obtain

$$\frac{\partial}{\partial x}\left[n(U_{ix}-U_{ex})\right]=0 \Rightarrow U_{ix}=U_{ex}=u \text{ (say)}, \tag{2.7}$$

where we have assumed that $U_{ix}(0,t) = U_{ex}(0,t) = 0$. Using this fact we can introduce a Lagrangian transformation in double species wave dynamics problem.

In Alfvén wave dynamics the perturbed magnetic field B arises from the spatial variation of polarization current and directed along the z-direction. In component form, Eq. (2.5) can be written as:

$$\frac{\partial B}{\partial x} = -\frac{4\pi en}{c}(U_{iy}-U_{ey}), \tag{2.8}$$

$$0 = \frac{4\pi en}{c}(U_{iz}-U_{ez}). \tag{2.9}$$

Equation (2.8) implies that the conduction current flows along y, the direction perpendicular to the plasma motion. From Eq. (2.9) we find $U_{iz} = U_{ez} = v$ (say). Since the quasineutrality condition and equal velocity of both the species in z direction rule out the x and z components of electric field, so the total wave electric field becomes $\mathbf{E}(x,t) = E_y(x,t)\hat{e}_y$. The velocity filed is $U_j = U_{jx}(x,t)\hat{e}_x + U_{jy}(x,t)\hat{e}_y + U_{jz}(x,t)\hat{e}_z$, with $U_{jx} = u(x,t)$ and $U_{jz} = v(x,t)$ for both the species, where $j \equiv e,i$. Since, the compressional Alfvén wave propagates parallel to the ambient magnetic field directed along x, i.e., $B_0\hat{e}_x$, the magnetic field arising from the fluctuation of electric field will be directed along the z direction. Therefore, the total magnetic field can be written as $\mathbf{B} = B_0\hat{e}_x + B(x,t)\hat{e}_z$. In view of these above mentioned conditions, from the continuity equations (2.2) for both species, we have

$$\left(\frac{\partial}{\partial t} + u\frac{\partial}{\partial x}\right) n = -n\frac{\partial u}{\partial x}, \tag{2.10}$$

whereas momentum equations (2.1) can be written separately for electrons and ions as:

$$m_e\left(\frac{\partial}{\partial t} + u\frac{\partial}{\partial x}\right)\mathbf{U}_e = -e\left(\mathbf{E} + \frac{1}{c}\mathbf{U}_e \times \mathbf{B}\right) + m_e\nu_{ei}(\mathbf{U}_i - \mathbf{U}_e), \tag{2.11}$$

$$m_i\left(\frac{\partial}{\partial t} + u\frac{\partial}{\partial x}\right)\mathbf{U}_i = e\left(\mathbf{E} + \frac{1}{c}\mathbf{U}_i \times \mathbf{B}\right) + m_i\nu_{ie}(\mathbf{U}_e - \mathbf{U}_i). \tag{2.12}$$

Equations (2.10)-(2.12) has a symmetry in the convective operator. This nonlinear operator can be simplified by introducing the Lagrangian variables (ξ, τ) through the following transformation:

$$\xi = x - \int_0^\tau u(\xi, \tau')d\tau' \quad , \quad \tau = t. \tag{2.13}$$

With this transformation the derivative operators are transformed accordingly similar to discussed in the Sec. 1.3 of the first chapter. Using these transformations, the continuity equation (2.10) is simplified and expressed as $n(\xi, \tau)/n(\xi, 0) = \partial\xi/\partial x$. Expressing momentum equations (2.11) and (2.12) in terms of these newly defined variables and combining the equations we have

$$\frac{\partial}{\partial \tau}(m_e\mathbf{U}_e + m_i\mathbf{U}_i) = \frac{e}{c}(\mathbf{U}_i - \mathbf{U}_e) \times \mathbf{B}, \tag{2.14}$$

where we have used $m_e\nu_{ei} = m_i\nu_{ie}$. Expressing $\mathbf{B} = \hat{e}_x B_0 + \hat{e}_z B(x, t)$, the x, y and z components of Eq. (2.14) are

$$\frac{\partial u}{\partial \tau} = \frac{eB(x, t)}{(m_e + m_i)c}(U_{iy} - U_{ey}), \tag{2.15}$$

$$\frac{\partial}{\partial \tau}(m_e U_{ey} + m_i U_{iy}) = 0, \tag{2.16}$$

and

$$\frac{\partial v}{\partial \tau} = -\frac{eB_0}{(m_e+m_i)c}(U_{iy}-U_{ey}), \tag{2.17}$$

respectively. From Eq. (2.16), it is evident that total momentum is conserved along the y direction. Taking $U_{ey}(\xi,0) = U_{iy}(\xi,0) = 0$, we find

$$U_{iy} = -\frac{m_e}{m_i}U_{ey}. \tag{2.18}$$

Since the magnetic field associated with the wave under study is along the z direction i.e. $B(x,t)\hat{e}_z$, the current flows in y direction. This can be further verified from Eq. (2.8) which is given by

$$ne(U_{iy}-U_{ey}) = -\frac{c}{4\pi}\frac{\partial B}{\partial x}. \tag{2.19}$$

Substituting $(U_{iy}-U_{ey})$ in Eqs. (2.15) and (2.16) we obtain

$$\frac{\partial u}{\partial \tau} = -\left[\frac{B}{4\pi(m_e+m_i)n(\xi,0)}\right]\frac{\partial B}{\partial \xi}, \tag{2.20}$$

$$\frac{\partial v}{\partial \tau} = \left[\frac{B_0}{4\pi(m_e+m_i)n(\xi,0)}\right]\frac{\partial B}{\partial \xi}. \tag{2.21}$$

The evolution equation for magnetic field can further be expressed by taking curl in the electron momentum equation (2.11) as:

$$m_e\nabla\times\left(\frac{\partial}{\partial t}+u\frac{\partial}{\partial x}\right)\mathbf{U}_e = -e\nabla\times\left(\mathbf{E}+\frac{1}{c}\mathbf{U}_e\times\mathbf{B}\right)+m_e\nu_{ei}\nabla\times(\mathbf{U}_i-\mathbf{U}_e). \tag{2.22}$$

Considering only z component of the above Eq. (2.22), we get

$$\left(\frac{\partial}{\partial t}+u\frac{\partial}{\partial x}\right)B + B\frac{\partial u}{\partial x} - B_0\frac{\partial v}{\partial x} = -\frac{cm_e}{e}\frac{\partial}{\partial x}\frac{\partial U_{ey}}{\partial \tau} + \frac{m_e c^2\nu_{ei}}{4\pi e^2}\frac{\partial}{\partial x}\left(\frac{1}{n}\frac{\partial B}{\partial x}\right). \tag{2.23}$$

In Eq. (2.19), substituting U_{iy} from Eq. (2.18) we have

$$\left(1+\frac{m_e}{m_i}\right)U_{ey} = \frac{c}{4\pi en}\frac{\partial B}{\partial x}. \tag{2.24}$$

Substituting u_{ey} in Eq. (2.23) (in terms of Lagrangian variable) we have

$$\frac{\partial B}{\partial \tau}+\frac{Bn}{n(\xi,0)}\frac{\partial u}{\partial \xi}-\frac{B_0 n}{n(\xi,0)}\frac{\partial v}{\partial \xi}=\frac{c^2}{4\pi e^2}\left(\frac{m_e m_i}{m_e+m_i}\right)\frac{n}{n(\xi,0)}\frac{\partial}{\partial \xi}\left[\frac{\partial}{\partial \tau}\left(\frac{1}{n(\xi,0)}\frac{\partial B}{\partial \xi}\right)\right] +\frac{m_e c^2 \nu_{ei}}{4\pi e^2}\frac{n}{n(\xi,0)}\frac{\partial}{\partial \xi}\left(\frac{1}{n(\xi,0)}\frac{\partial B}{\partial \xi}\right). \tag{2.25}$$

Now we normalize Eqs. (2.10), (2.20), (2.21), and (2.25) by $n \to n/n_0$, $v \to v/v_A$, $B \to B/B_0$, $\xi \to \xi/L$ and $\tau \to \tau v_A/L$, with n_0, v_A, and L denoting a constant equilibrium density, the Alfvén velocity, and an arbitrary length scale respectively. Then Eqs. (2.10), (2.20), (2.21) and (2.25) respectively become

$$\frac{\partial}{\partial \tau}\left(\frac{1}{n}\right)=\frac{1}{n(\xi,0)}\frac{\partial u}{\partial \xi}, \tag{2.26}$$

$$\frac{\partial u}{\partial \tau}=-\frac{1}{2n(\xi,0)}\frac{\partial B^2}{\partial \xi}, \tag{2.27}$$

$$\frac{\partial v}{\partial \tau}=\frac{1}{n(\xi,0)}\frac{\partial B}{\partial \xi}, \tag{2.28}$$

and

$$\frac{\partial B}{\partial \tau}=-\frac{Bn}{n(\xi,0)}\frac{\partial u}{\partial \xi}+\frac{n}{n(\xi,0)}\frac{\partial v}{\partial \xi}+D\frac{n}{n(\xi,0)} \frac{\partial}{\partial \xi}\frac{\partial}{\partial \tau}\left(\frac{1}{n(\xi,0)}\frac{\partial B}{\partial \xi}\right)+\nu\frac{n}{n(\xi,0)}\frac{\partial}{\partial \xi}\left(\frac{1}{n(\xi,0)}\frac{\partial B}{\partial \xi}\right), \tag{2.29}$$

where $D=(\delta/L)^2$ is the dispersion parameter arising from electron's finite mass, and $\nu=(m_e c^2/4\pi n_0 e^2)(\nu_{ei}/L v_A)$ is the dissipation parameter which arises due to collision, δ is the skin depth defined by $\delta=(c^2 m_e m_i/[4\pi(m_e+m_i)n_0 e^2])^{1/2}$. Equations (2.26), (2.28) and (2.29) can now be combined together to give the following equation in a more compact form as:

$$\frac{\partial^2}{\partial \tau^2}\left(\frac{B}{n}\right)-\frac{1}{n(\xi,0)}\frac{\partial}{\partial \xi}\left[\frac{1}{n(\xi,0)}\frac{\partial B}{\partial \xi}\right]=\frac{1}{n(\xi,0)}\frac{\partial^2}{\partial \tau \partial \xi}\left[\frac{1}{n(\xi,0)}\frac{\partial}{\partial \xi}\left(D\frac{\partial B}{\partial \tau}+\nu B\right)\right]. \tag{2.30}$$

Furthermore, Eqs. (2.26) and (2.27) can be combined to give

$$\frac{\partial^2}{\partial \tau^2}\left(\frac{1}{n}\right) = -\frac{1}{2n(\xi,0)}\frac{\partial}{\partial \xi}\left(\frac{1}{n(\xi,0)}\frac{\partial B^2}{\partial \xi}\right). \tag{2.31}$$

These two coupled nonlinear partial differential equations (2.30) and (2.31) are the governing equations that describes the dynamics of the nonlinear, dispersive Alfvén wave in an electron-ion plasma. It is to be noted that the above model is appropriate for low-dense plasma as the analysis is valid for $(v_A/c) \leq D \ll (m_e/m_i)$ i.e. for small dispersion parameter D and Alfvén velocity v_A.

2.3 Linear analysis

Before going to the details of the nonlinear analysis, let us linearize equations (2.30) and (2.31) by assuming $n = 1 + \tilde{n}$ and $B = \tilde{b}$ and obtain the following linear equation:

$$\left(\frac{\partial^2}{\partial t^2} - \frac{\partial^2}{\partial x^2}\right)\tilde{b} = D\frac{\partial^4 \tilde{b}}{\partial^2 t \partial^2 x} + \nu\frac{\partial^3 \tilde{b}}{\partial t \partial^2 x}. \tag{2.32}$$

Then assuming the solution in the form of Fourier mode $\tilde{b} \sim \exp[-i(\omega t - kx)]$ (where ω and k are the oscillation frequency and wave number), we obtain the following dispersion relation for the linear Alfvén wave

$$\left(1 + Dk^2\right)\omega^2 + i\nu k^2 \omega - k^2 = 0, \tag{2.33}$$

where the collisional parameter ν represents the usual wave damping. In absence of collision the above dispersion relation (in dimensional unit) becomes

$$\omega = \frac{k v_A}{\sqrt{1 + k^2 \delta^2}}. \tag{2.34}$$

This dispersion relation clearly shows that the Alfvén wave is dispersive because of the term δ which arises due to the finite electron inertia. Thus finite electron mass effect acts as a source of dispersion of the Alfvén wave in electron-ion plasma.

2.4 Nonlinear analysis by Lagrangian mass variable

In this section we have tried to analyze the nonlinear system derived above by means of a more simplified description that utilizes the Lagrangian mass variable. The system of coupled differential Eqs. (2.30) and (2.31) can be substantially simplified without the loss of generality by switching to the Lagrangian mass variable. [132, 138] For this, let us define the following new Lagrangian mass variable ζ instead of ξ

$$\zeta = \int^{\xi} n(\xi', 0) d\xi',$$

which yields the mathematical operator

$$\frac{\partial}{\partial \zeta} = \frac{1}{n(\xi, 0)} \frac{\partial}{\partial \xi}.$$

Then introducing this new mass variable ζ, from Eqs. (2.30) and (2.31), we obtain the following simplified couple equations

$$\frac{\partial^2}{\partial \tau^2}\left(\frac{B}{n}\right) - \frac{\partial^2 B}{\partial \zeta^2} = \frac{\partial^2}{\partial \zeta^2}\left[D\frac{\partial^2 B}{\partial \tau^2} + \nu \frac{\partial B}{\partial \tau}\right], \tag{2.35}$$

$$\frac{\partial^2}{\partial \tau^2}\left(\frac{1}{n}\right) = -\frac{1}{2}\frac{\partial^2 B^2}{\partial \zeta^2}. \tag{2.36}$$

These equations (2.35) and (2.36) are complicated nonlinear equations and it is difficult to find an exact analytical solution with its full nonlinearity. Therefore, in the next subsection, we will investigate the finite amplitude nonlinear solutions keeping up to third order nonlinear term.

2.4.1 Weak amplitude nonlinear wave

To study the dynamics of the finite amplitude nonlinear Alfvén wave, we write

$$n = 1 + \tilde{n} \text{ and } B = \tilde{b} \text{ with } \mid \tilde{n} \mid, \mid \tilde{b} \mid < 1.$$

Now substituting and keeping up to second order term, from Eq. (2.35), we obtain

$$\frac{\partial^2 \tilde{b}}{\partial \tau^2} - \frac{\partial^2 \tilde{b}}{\partial \zeta^2} = D\frac{\partial^2}{\partial \tau^2}\left(\frac{\partial^2 \tilde{b}}{\partial \zeta^2}\right) + \nu\frac{\partial}{\partial \tau}\left(\frac{\partial^2 \tilde{b}}{\partial \zeta^2}\right) - \frac{\partial^2}{\partial \tau^2}\left(\frac{\tilde{b}}{\tilde{n}}\right). \tag{2.37}$$

The LHS of the above equation represents linear Alfvén wave whereas the RHS implicates that the wave is modified by dispersion dissipation and nonlinearity. Therefore this equation shows the wave steepening by nonlinearity, wave spreading by dispersion and amplitude modulation by dissipation. These three physical phenomena can lead to the well know evolution equation for finite amplitude Alfvén Wave.

Moreover, the small amplitude nonlinear wave equations are derived by assuming that the equilibrium density is homogeneous i.e. $n(\xi, 0) = 1$, therefore $\zeta = \xi$ $[\equiv x - \int v(\xi, \tau')d\tau']$. Also in this weak amplitude limit $\xi(\zeta) \equiv x$ and $\tau \equiv t$ (actually in this case, $\xi(\zeta)$ and τ are no longer remain Lagrangian variables but become equivalent to x and t). Therefore, we rewrite the above equation (2.37) in the following form:

$$\left(\frac{\partial}{\partial t} - \frac{\partial}{\partial x}\right)\left(\frac{\partial}{\partial t} + \frac{\partial}{\partial x}\right)\tilde{b} = D\frac{\partial^2}{\partial t^2}\left(\frac{\partial^2 \tilde{b}}{\partial x^2}\right) + \nu\frac{\partial}{\partial t}\left(\frac{\partial^2 \tilde{b}}{\partial x^2}\right) - \frac{\partial^2}{\partial t^2}(\tilde{V}\tilde{b}). \tag{2.38}$$

Also in absence of dissipation and for negligible dispersion ($D \ll 1$), the linear equation (2.31) can be expressed as:

$$\left(\frac{\partial}{\partial t} - \frac{\partial}{\partial x}\right)\left(\frac{\partial}{\partial t} + \frac{\partial}{\partial x}\right)\tilde{b} = 0. \tag{2.39}$$

For the Alfvén wave propagating in the positive x direction only, from the above relation, we get

$$\frac{\partial}{\partial t} = -\frac{\partial}{\partial x},$$

and this approximation yields (from Eq. (2.36))

$$\tilde{V} \approx -\frac{\tilde{b}^2}{2}.$$

Then substituting all these in Eq. (2.38) and integrating the transformed equation once with the boundary condition at $x \to \infty$, $\tilde{b} \to 0$, we obtain

$$\frac{\partial \tilde{b}}{\partial t} + \left[1 + \frac{3}{4} b^2\right] \frac{\partial \tilde{b}}{\partial x} + \frac{D}{2} \frac{\partial^3 \tilde{b}}{\partial x^3} = \frac{\nu}{2} \frac{\partial^2 \tilde{b}}{\partial x^2}. \tag{2.40}$$

Finally, a further transformation of coordinates

$$\hat{x} = x - t \quad \text{and} \quad \hat{t} = t,$$

renders the following usual form of modified Korteweg-de Vries Burgers (mKdVB) equation with $\tilde{b} \equiv \phi$

$$\frac{\partial \phi}{\partial \hat{t}} + \frac{3}{4} \phi^2 \frac{\partial \phi}{\partial \hat{x}} + \frac{D}{2} \frac{\partial^3 \phi}{\partial \hat{x}^3} = \frac{\nu}{2} \frac{\partial^2 \phi}{\partial \hat{x}^2}. \tag{2.41}$$

For a collisionless plasma $\nu = 0$ the above equation can be reduced to modified Korteweg-de Vries (mKdV) equation.

It is to be noted that the nonlinear equation (2.41) under investigation can also be obtained by the well known reductive perturbation technique. Interestingly, here keeping only up to second order terms of the dynamical variable, we obtain the same equation from arbitrary nonlinear equation formulated in Lagrangian variables.

2.4.2 Moving-frame nonlinear analysis

In this section, we have presented an exact solution of the Eq. (2.41) in a frame moving with the phase velocity of the wave. We have hoped that this will improve our understanding on the behavior of the nonlinear system [Eq. (2.41)]. To investigate the nonlinear solution, we have transformed Eq. (2.41) to the moving frame $\chi = M\hat{t} - \hat{x}$, where M is the Mach number (normalized phase velocity). Then integrating the transformed equation once subject to the boundary conditions $\phi \to 0$, all derivatives $\to 0$ as $\chi \to \infty$, and we have finally obtained the following nonlinear ordinary differential equation:

$$D\frac{d^2\phi}{d\chi^2} + \frac{\phi^3}{2} - 2M\phi + \nu\frac{d\phi}{d\chi} = 0. \tag{2.42}$$

Then we have recast this nonlinear equation (2.42) in the following two simultaneous equations:

$$\frac{d\phi}{d\chi} = \psi, \quad \frac{d\psi}{d\chi} = -\frac{\nu}{D}\psi + \frac{\phi}{D}\left[2M - \frac{\phi^2}{2}\right]. \tag{2.43}$$

In the $\phi - \psi$ plane, this dynamical system has the following two physically possible equilibrium (stationary) points

$$(0,0) \text{ and } \left(\phi^* \equiv 2\sqrt{M},\ 0\right).$$

To investigate the nature of these two stationary points, we have considered the two cases of interest: collisionless and collisional.

In collisionless case, we have neglected the electron-ion collision ($\nu = 0$) in the Eq. (2.42) [i.e. in Eq. (2.43)] and calculate the variational matrix of the system (2.43) at these two stationary points. These matrices are as follows:

$$J_{(0,0)} = \begin{bmatrix} 0 & 1 \\ \frac{2M}{D} & 0 \end{bmatrix}, \; J_{(\phi^*,0)} = \begin{bmatrix} 0 & 1 \\ -\frac{4M}{D} & 0 \end{bmatrix}. \tag{2.44}$$

The corresponding pair of eigen values are determined from the following characteristic (quadratic) equations

$$\lambda^2 - \frac{2M}{D} = 0 \text{ and } \Lambda^2 + \frac{4M}{D} = 0. \tag{2.45}$$

These two characteristic equations determine the pair of eigen values as $\pm\sqrt{2M/D}$ (real and distinct) and $\pm\, i\, 2\, \sqrt{M/D}$ (purely imaginary), respectively. This implies that the stationary point $(0,0)$ is a saddle point and the stationary point $(\phi^*, 0)$ is a center. In case of saddle point (Left panel of Fig 2.1 shows that a small perturbation in the neighborhood of this point forms a homoclinic orbit i.e. separetrix in the $\phi - \psi$ phase-space which is the signature of the soliton solution), the equation (2.41) (with $\nu = 0$) is analytically solvable and the analytical solution gives the following single soliton solution

$$\phi(x,t) \quad = \quad 2\sqrt{2M}\,\mathrm{sech}\left[\sqrt{\frac{2M}{D}}\,\chi\right]. \tag{2.46}$$

This shows that the width of the soliton ($\propto \sqrt{D}$) depends on the electron inertia induced dispersion. Moreover, the numerical solution of the equation (2.41) with $\nu = 0$ are also provided in Sec. V.

Next, we have considered the collisional case and calculate the variational matrix of the system (2.43) at these two stationary points. These matrices are as follows:

$$J_{(0,0)} = \begin{bmatrix} 0 & 1 \\ \frac{2M}{D} & -\frac{\nu}{D} \end{bmatrix}, \; J_{(\phi^*,0)} = \begin{bmatrix} 0 & 1 \\ -\frac{4M}{D} & -\frac{\nu}{D} \end{bmatrix}. \tag{2.47}$$

The corresponding pair of eigen values are determined from the following characteristic (quadratic) equations

$$\begin{aligned} \lambda^2 + \left(\frac{\nu}{D}\right)\lambda - \frac{2M}{D} = 0, \\ \Lambda^2 + \left(\frac{\nu}{D}\right)\Lambda + \frac{4M}{D} = 0. \end{aligned} \tag{2.48}$$

These two characteristic equations determine the following eigen values for the stationary points $(0,0)$ and $(\phi^*,0)$, respectively,

$$\lambda_{(0,0)} \quad = \quad \frac{1}{2D}\left[-\nu \pm \sqrt{\nu^2 + 8DM}\right], \tag{2.49}$$

and

$$\Lambda_{(\phi^*,0)} \quad = \quad \frac{1}{2D}\left[-\nu \pm \sqrt{\nu^2 - 16DM}\right]. \tag{2.50}$$

The eigen values (2.49) corresponding to the stationary point $(0,0)$ are real and distinct which indicate that the stationary point $(0,0)$ is a saddle point. The eigen values (2.50) corresponding to the stationary point $(\phi^*,0)$ are either pair of complex conjugate with negative real part or real (and distinct) with negative sign according as

$$\nu \lesseqgtr 4\sqrt{DM}. \tag{2.51}$$

Thus the stationary point $(\phi^*,0)$ is either stable focus or stable node. In this collisional case, right panel of Fig 2.1 shows that a small perturbation in the vicinity of the point $(0,0)$ forms a heteroclinic orbit between this point and the point $(\phi^*,0)$ which is the signature of the shocklike structures. However, in this collisional case the equation (2.41) is not exactly analytically solvable as its Hamiltonian is not conserved. Therefore to get the insight of the solutions, we have numerically simulated this equation (2.41) and the results are shown graphically in Sec. V.

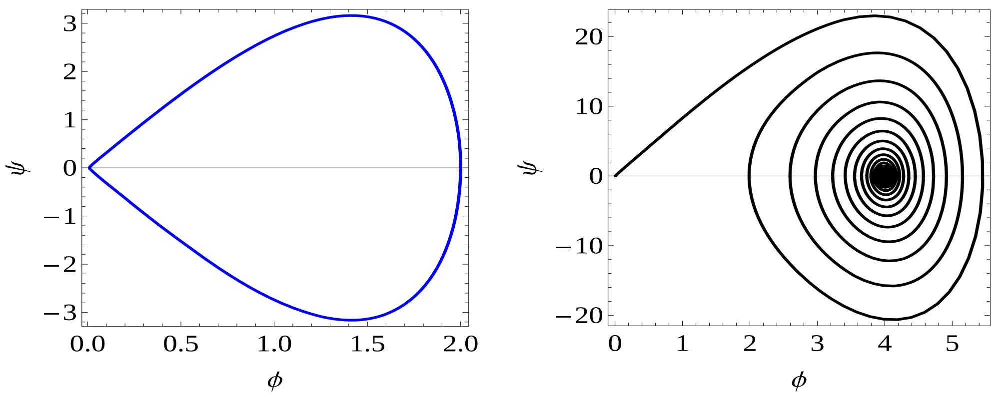

Figure 2.1: (color online) Phase-space trajectories in the $\phi-\psi$ plane of the dynamical system. The left figure (blue solid curve) is drawn for $M = 0.5$ and the right figure (black solid curve) is drawn for $M = 4$.

2.5 Wave modulation for small wave number: nonlinear Schrödinger equation

In the previous section, we have not considered the effects of self-interaction of the Alfvén wave (an intrinsic character of nonlinear wave propagation) that introduces self-focusing effect (modulational instability) in the system. [134–136, 139] In this section, we consider this effect for the nonlinear Alfvén wave in presence of electron-ion collision induced dissipation in the long-wavelength limit. The nonlinear Schrödinger equation (NLSE) with cubic nonlinearity clearly explain such self-interaction effects. [139] Moreover, it is well-known from different physical systems [140–142] that the classical KdV as well as the extended KdV equations can easily be transformed to the NLSE in the long-wavelength limit. Therefore, to study the modulational instability (self-interaction effect) of nonlinear Alfvén waves in presence of dissipation, we derive the NLSE from the above nonlinear mKdVB equation (2.41) in the long-wave length limit. To achieve this, we have introduced the following stretched variable ξ and τ:

$$\hat{\xi} = \epsilon\left(\hat{x} - U_g\hat{t}\right) \text{ and } \hat{\tau} = \epsilon^2\,\hat{t}, \tag{2.52}$$

where U_g is the group velocity of the wave and ϵ is a small parameter that characterizes the strength of nonlinearity. This transformation separates the system into a slowly varying part associated with the amplitude of the wave and a rapidly varying part, which is the phase of the wave. The operators $\partial/\partial\hat{x}$ and $\partial/\partial\hat{t}$ then take the forms

$$\frac{\partial}{\partial\hat{x}} \to \frac{\partial}{\partial\hat{x}} + \epsilon\frac{\partial}{\partial\hat{\xi}},$$

and

$$\frac{\partial}{\partial \hat{t}} \rightarrow \frac{\partial}{\partial \hat{t}} - \epsilon U_g \frac{\partial}{\partial \hat{\xi}} + \epsilon^2 \frac{\partial}{\partial \hat{\tau}},$$

to account for the slow variations of wave amplitude. The wave amplitude ϕ is expanded in powers of ϵ in the following way:

$$\phi(\hat{x}, \hat{t}) = \sum_{j=1}^{\infty} \epsilon^j \sum_{l=-\infty}^{\infty} \phi_l^{(j)}(\hat{\xi}, \hat{\tau}) \exp\left[i(k\hat{x} - \omega\hat{t})l\right] \tag{2.53}$$

with the reality condition $\phi_{-l}^{(j)} = (\phi_l^{(j)})^*$. Also to incorporate the weak collisional effects and for consistent perturbation, we have considered the following scaling:

$$\nu \sim O\left(\epsilon^2\right). \tag{2.54}$$

Now employing (2.52)-(2.54) in the equation (2.41), in the lowest order with $l = \pm 1$, we have obtained the dispersion relation,

$$\omega = -\frac{D}{2}\, k^3. \tag{2.55}$$

The second order terms with $l = \pm 1$ gives the following compatibility condition:

$$U_g = -\frac{3}{2} D k^2 \equiv \frac{d\omega}{dk}. \tag{2.56}$$

Finally, we substitute the above derived equations into third order ($n = 3$) equations and obtain the following damped nonlinear Schrödinger equation (NLSE) for $\phi_1^{(1)}[\equiv \phi]$:

$$i\frac{\partial \phi}{\partial \hat{\tau}} + P\frac{\partial^2 \phi}{\partial \hat{\xi}^2} + Q|\phi|^2\phi + i\gamma\phi = 0. \tag{2.57}$$

In this equation, the group dispersion coefficient

$$P = -\frac{3}{2} D k \equiv \frac{1}{2}\frac{d^2\omega(k)}{dk^2} \tag{2.58}$$

is related to the curvature of the dispersion relation $\omega(k)$ [Eq.(2.55)] which is always negative for all wave number k. The coefficient of nonlinear term

$$Q = -\frac{3}{4}\,k \tag{2.59}$$

is related to the nonlinear frequency shift. The dissipative term

$$\gamma = \frac{\nu k^2}{2} \tag{2.60}$$

is related to the electron-ion collision.

2.5.1 Effect of electron-ion collision on modulational instability

Next, we have analyzed the stability of the above NLSE (2.57) for very low-frequency Alfvén waves in presence of dissipation. In this NLSE [Eq.(2.59)], the term $-Q \mid \phi \mid^2$ plays the role of a potential energy. The local maxima of this potential energy acts as an effective potential well in the plasma. The high frequency waves reflect from the regions of high density, and the amplitude-dependent ponderomotive force forms a low-density region (cavity). As a consequence the low-frequency waves become trapped within these density depleted regions and the wave energy will concentrate at the bottom of the well. The energy concentration makes the well deeper by making this energy even larger. Thus the formation of the cavity is an unstable physical process that occurs due to the energy localization in the medium. This process is known as modulational instability. [139, 143–145] Here, we have investigated this instability for nonlinear Alfvén waves in presence of electron-ion collision.

For this purpose, we have assumed that in presence of collision, the amplitude evolution equation (2.59) possesses the following plane wave solution:

$$\phi = \phi_0(\hat{\tau}) \exp\left(-i \int_0^{\hat{\tau}} \Delta(\tau')d\tau'\right), \tag{2.61}$$

where, $\phi_0(\hat{\tau})$ and $\Delta(\hat{\tau})$ are the amplitude of the pump carrier wave and the non-linear frequency shift in presence of dissipation. Substituting this solution (2.61) in the equation (2.57), we have obtained the following two equations:

$$\begin{aligned} \frac{d\phi_0}{d\hat{\tau}} + \gamma\phi_0 = 0 \Rightarrow \phi_0(\hat{\tau}) = \phi_{00}\exp(-\gamma\hat{\tau}) \ \text{ and} \\ \Delta(\hat{\tau}) = -Q|\phi_0(\hat{\tau})|^2 = -Q|\phi_{00}|^2\exp(-2\gamma\hat{\tau}), \end{aligned} \tag{2.62}$$

where ϕ_{00} is a real constant. Also note that $\phi_0(\hat{\tau}) \to 0$ as $\hat{\tau} \to \infty$ which implies that ϕ_0 is bounded and stable. Therefore for stability analysis, we have considered the perturbation about this stable solution in the following standard procedure:

$$\phi = \left[\phi_0(\hat{\tau}) + \tilde{\phi}(\hat{\xi}, \hat{\tau})\right] \exp\left(-i \int_0^{\hat{\tau}} \Delta(\tau')d\tau'\right), \tag{2.63}$$

where $\tilde{\phi}\left(|\ \tilde{\phi}\ | \ll \phi_0\right)$ is the perturbed amplitude of the modulated wave. Then substituting this equation (2.63) in the equation (2.57), we have obtained the following linearized two coupled equations:

$$\begin{aligned} \frac{\partial\tilde{\phi}_I}{\partial\hat{\tau}} &= P\frac{\partial^2\tilde{\phi}_R}{\partial\hat{\xi}^2} + 2Q|\phi_0|^2\tilde{\phi}_R - \gamma\tilde{\phi}_I \\ \text{and} \quad \frac{\partial\tilde{\phi}_R}{\partial\hat{\tau}} &= -P\frac{\partial^2\tilde{\phi}_I}{\partial\hat{\xi}^2} - \gamma\tilde{\phi}_R. \end{aligned} \tag{2.64}$$

Here $\tilde{\phi} = \tilde{\phi}_R + i\tilde{\phi}_I$, $\phi_{R(I)}$ is the real (imaginary) part of ϕ.

Finally, the space-time dependence of the perturbation of the form $\tilde{\phi} \sim \exp(i\vartheta)$, where $\vartheta\left(= \tilde{k}\hat{\xi} - \int_0^{\hat{\tau}} \tilde{\omega}(\acute{\tau})d\acute{\tau}\right)$ is the modulated phase with $\tilde{k}(\ll k)$ and $\tilde{\omega}(\ll \omega)$ are the wave number and modulation frequency, respectively, yields the following dispersion relation:

$$(\tilde{\omega} + i\gamma)^2 = P^2\tilde{k}^4 - 2PQ\ |\ \phi_0\ |^2\ \tilde{k}^2. \tag{2.65}$$

This shows that the electron-ion collision provides the usual damping. Also, the system is stable for $PQ < 0$. However, there is a possibility of the instability if $PQ > 0$ (both P and Q are of same sign: here both P and Q are negative for all $\tilde{k}$ [Eqs. (2.58) and (2.59)]). Thus the instability occurs if

$$\tilde{k}^2 < \tilde{k}_{cr}^2 = \left(\frac{2Q}{P}\right) \mid \phi_0 \mid^2 = \left(\frac{1}{D}\right) \mid \phi_{00} \mid^2 \exp(-2\gamma\hat{\tau}), \tag{2.66}$$

provided with this values of $\tilde{k}$ the following inequality must holds:

$$\gamma < \sqrt{P^2\tilde{k}^4\left(\frac{\tilde{k}_{cr}^2}{\tilde{k}^2} - 1\right)}. \tag{2.67}$$

This determines the maximum time τ_{max} to observe instability

$$\tau_{max} = \frac{1}{2\gamma}\ln\left(\frac{2PQ\tilde{k}^2 \mid \phi_{00} \mid^2}{\gamma^2 + P^2\tilde{k}^4}\right) = \left(\frac{1}{\nu k^2}\right)\ln\left(\frac{18D\tilde{k}^2 \mid \phi_{00} \mid^2}{k^2\nu^2 + 18D^2\tilde{k}^4}\right). \tag{2.68}$$

Thus, the instability growth will cease for $\hat{\tau} \geq \tau_{max}$. Now by setting $\tilde{\omega} = i\Gamma$, the dispersion relation for instability growth rate becomes

$$(\Gamma + \gamma)^2 = 2PQ \mid \phi_0 \mid^2 \tilde{k}^2 - P^2\tilde{k}^4. \tag{2.69}$$

The maximum growth rate is found by taking the derivative of the Eq. (2.69) with respect to $\tilde{k}^2$, and setting this to zero, we have

$$\tilde{k}_{max}^2 = \left(\frac{Q}{P}\right) \mid \phi_0 \mid^2 = \left(\frac{1}{2D}\right) \mid \phi_{00} \mid^2 \exp\left(-2\gamma\hat{\tau}\right), \tag{2.70}$$

which is just half of the $\tilde{k}_{cr}$ value. With this value of $\tilde{k}_{max}^2$, we can find the maximum growth rate

$$\Gamma_{max} = \mid Q \mid \mid \phi_0 \mid^2 - \gamma. \tag{2.71}$$

Therefore in presence of electron-ion collision, the nonlinear Alfvén waves are modulationally unstable when

$$\mid \phi_0 \mid^2 >= \frac{2\ \nu k}{3}.$$

2.5.2 Approximate analytical solution: Weakly dissipative envelope (bright) soliton

In the above damped NLSE [Eq. (2.57)], the group dispersion coefficient P [Eq. (2.58)] and the nonlinear coefficient Q [Eq. (2.59)] are all negative for all values of the wave number k. Thus, to find the envelope (bright) soliton of the damped NLSE [Eq. (2.57)], we have recast the equation in the following normal form:

$$i\frac{\partial\phi}{\partial\bar{\tau}} - \frac{1}{2}\frac{\partial^2\phi}{\partial\bar{\xi}^2} - \mid\phi\mid^2\phi + i\bar{\gamma}\phi = 0, \tag{2.72}$$

where $\bar{\tau} = \mid Q\mid\hat{\tau}, \bar{\xi} = \hat{\xi}\sqrt{\mid Q\mid/2\mid P\mid}$ and $\bar{\gamma} = \gamma/\mid Q\mid$. This equation exhibits bright or envelope soliton. This equation (2.72) is solved numerically and the solutions are shown graphically in Fig. (2.5). However, here we have solved this equation analytically.

In absence of dissipation ($\nu = 0 \implies \bar{\gamma} = 0$), we have the usual NLSE which is an exactly integrable Hamiltonian system, possesses infinite number of conservation. In this case let us assume a solution of the form $\phi(\bar{\xi},\bar{\tau}) = \rho(\bar{\xi},\bar{\tau})\exp\left[i\varphi(\bar{\xi},\bar{\tau})\right]$ and then solve the ordinary differential equations for φ and ρ subject to the boundary condition $\rho \to 0$ as $\bar{\xi} \to \pm\infty$. We have finally obtained the following single envelope (bright) soliton which in terms of actual parameters reads as:

$$\begin{aligned}\phi(\hat{\xi},\hat{\tau}) = a\ \mathrm{sech}&\left[\frac{a}{2\sqrt{D}}\left(\hat{\xi} + \frac{3}{2}k\sqrt{D}\kappa\hat{\tau}\right)\right] \\ \exp&\left[\frac{i}{2\sqrt{D}}\left(\kappa\hat{\xi} - \frac{3k}{4}\sqrt{D}\left(a^2-\kappa^2\right)\hat{\tau}\right)\right],\end{aligned} \tag{2.73}$$

where a and κ are two soliton parameters in which a is the amplitude of the soliton. This shows that the disturbances resemble with the soliton shape with a exponential factor making oscillation between a maxima and a minima. The resultant structure is the envelope excitation of nonlinear Alfvén wave.

In case of weak dissipation (here it is indeed weak as $\nu \sim O(\epsilon^2)$), we can solve the above damped NLSE [Eq. (2.57)] perturbatively by taking $\varepsilon(\phi)$ as a small perturbed quantity. To apply this perturbation, we have considered the general solution of the perturbed soliton is of the following form: [146]

$$\phi(\bar{\xi},\bar{\tau}) = a(\bar{\tau})\text{sech}\,\left[a(\bar{\tau})\left(\bar{\xi}+b(\bar{\tau})\right)\right]\exp\left[i\bar{\xi}\kappa(\bar{\tau}) - i\sigma(\bar{\tau})\right], \tag{2.74}$$

where a, b, σ and κ are the soliton parameters. Finally, applying the conservation laws for the NLSE (conserved integral relations, [146]) we have obtained the following bright soliton (envelope soliton) in presence of dissipation (electron-ion collision), which in terms of actual variable reads as:

$$\begin{aligned}\phi(\hat{\xi},\hat{\tau}) = a_0\exp\left(-2\gamma\hat{\tau}\right)\text{sech}&\left[a_0\exp\left(-2\gamma\hat{\tau}\right)\frac{1}{2\sqrt{D}}\left(\hat{\xi}+\frac{3k}{2}\sqrt{D}\kappa_0\hat{\tau}\right)\right]\\ &\exp\left\{\frac{i}{2\sqrt{D}}\left[\kappa_0\hat{\xi}+\frac{3k}{4}\sqrt{D}\left(\kappa_0^2\hat{\tau}+a_0^2\left(\frac{\exp\left(-4\gamma\hat{\tau}\right)-1}{4\gamma}\right)\right)\right]\right\},\end{aligned} \tag{2.75}$$

where a_0 and κ_0 are the initial values of a and κ respectively. In the limit $\gamma \to 0$, we recover the previous result (2.73) (with $a_0 = a$ and $\kappa_0 = \kappa$). It is clear that as time elapses the amplitude of the bright (envelope) soliton decreases exponentially with decay rate $\sim 2\gamma$. The numerical solution in Fig. (2.5) also shows similar nature. Thus the electron-ion collisions have damping effect on the bright soliton structure of nonlinear Alfvén waves in electron-ion plasma.

2.6 Numerical simulation

In this section, we have numerically simulated both the nonlinear equations (2.41) and (2.57) with the help of the MATHEMATICA.

2.6.1 Numerical solutions of modified Korteweg-de Vries-Burgers equation

To simulate the equation (2.41) numerically, first we have solved the dynamical system (2.43) in absence of collision $\nu = 0$ by the Runge-Kutta-Fehlberg (RKF) method by taking the stationary point $(0, 0)$ as the initial condition with $D = 0.1$. The solutions are shown graphically in Fig. 2.2. This figure shows that a small perturbation around the equilibrium point $(0, 0)$ (saddle point) develops into a soliton as expected from the analytical solution (2.46). The comparative study between the figures (left and right) demonstrate that single soliton structure observed for low Mach number ($M = 0.5$). In case of high Mach number ($M = 3$) single soliton disintegrate into multi-soliton structures with higher amplitude.

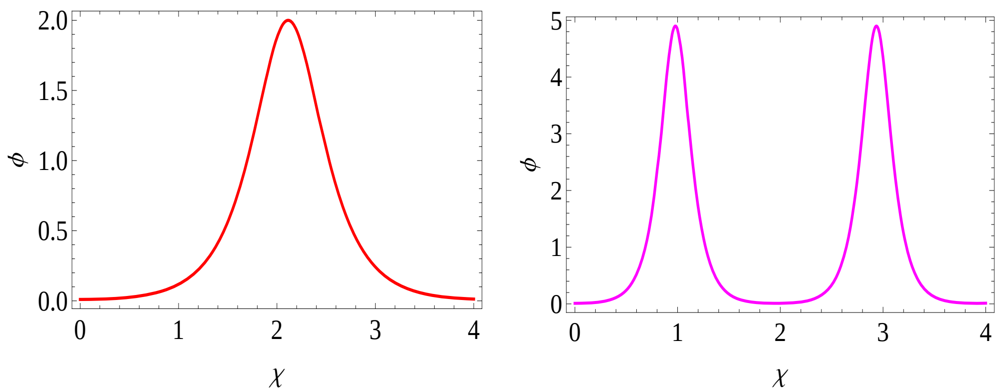

Figure 2.2: (color online) Numerical solution of the dynamical system (2.43) in absence of dissipation ($\nu = 0$) with $D = 0.1$. Formation of single soliton for ϕ (dimensionless magnetic field fluctuations) in the traveling wave frame χ. The left figure (red solid curve) is drawn for $M = 0.5$ and the right figure (magenta solid curve) is drawn for $M = 3$.

Next we have solved the dynamical system (2.43) by RKF method by taking the stationary point $(0, 0)$ as the initial condition with $D = 0.1$ and $M = 4$. Then starting from a small perturbation around the initial condition $(0, 0)$ and upon numerical integration of the dynamical system, it is seen that the perturbation develops into a shock-like structure as illustrated in Fig. 2.3 with oscillating / monotonic transition corresponding to the second stationary point $(\phi^*, 0)$. Actually, if one assumes that for $\chi = -\infty(\hat{x} = \infty)$ the particle was located at $\phi = 0$, then at $\chi = \infty(\hat{x} = -\infty)$, it appears at the point $\phi = \phi^*$ and the solution describes a shocklike structure. The equilibrium point $(0, 0)$ corresponds to the equilibrium downstream state and the point $(\phi^*, 0)$ corresponds to the upstream state. In case of weak dissipation ($\nu = 0.1$), the dispersion dominates over dissipation and therefore the transition occur with an oscillating behavior that forms dispersive (oscillatory) shock structure as illustrated in the left figure of Fig. 2.3. On the other hand for strong dissipation ($\nu = 1$), the dissipation dominates over dispersion and therefore the transition occur with a monotonic behavior that forms monotonic shock structure as illustrated in the right figure of Fig. 2.3. Thus

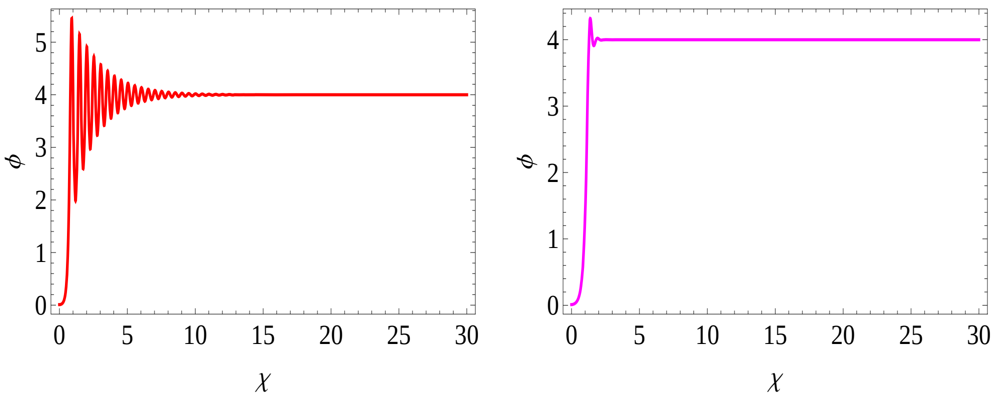

Figure 2.3: (color online) Numerical solution of the dynamical system (2.43) in presence of dissipation ($\nu \neq 0$) with $M = 4$. Formation of shock-like structure for ϕ in the traveling wave frame χ. The left figure (red solid curve) shows oscillatory shock structure for weak dissipation ($\nu = 0.1$). The right figure (magenta solid curve) shows monotonic shock structure for strong dissipation ($\nu = 1$).

according to the condition (2.51), the stable focus always corresponds to the oscillatory nature, whereas the stable node corresponds to the monotonic nature of the solution. In the both cases the observed shock is compressive in nature. The shock strength (related to the extreme upstream and downstream values) is given by $[\phi(+\infty) - \phi(-\infty) =]\phi^* = 2\sqrt{M}$.

Finally we have solved the dynamical system (2.43) by the RKF method with the stationary point $(\phi^*, 0)$ as the initial condition with $M = 4$. The simulation results are shown graphically in Fig. 2.4. This figure illustrated that a small perturbation around this stationary point develops into breather structures.

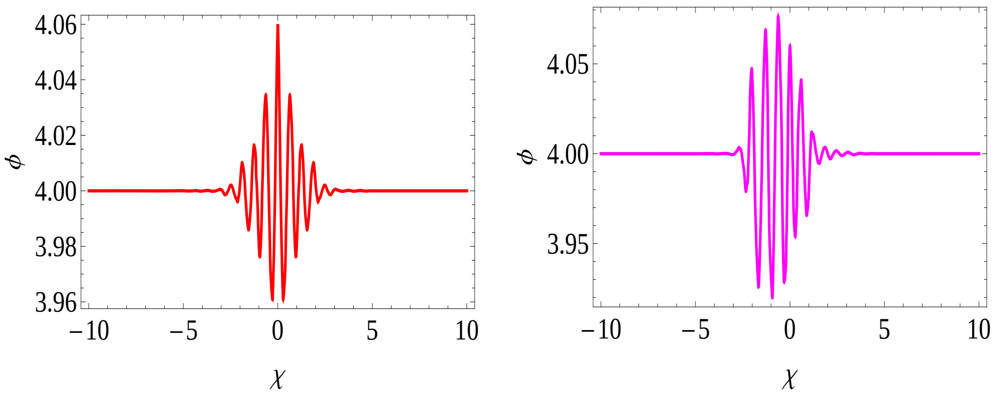

Figure 2.4: (color online) Breather solution of the dimensionless dynamical system (2.43) with $M = 4$ and $(\phi^*, 0)$ as the initial condition. The left figure (red solid curve) shows breather structure without dissipation, whereas, the right figure (magenta solid curve) shows the same with dissipation ($\nu = 0.1$).

A breather is a nonlinear wave in which energy concentrates in a localized and oscillatory manner. It is a localized periodic solutions of a nonlinear system. A breather is described as a oscillatory solution (wave-packet) about a stationary point whose envelope and oscillatory part move with different velocities. [147] We can see from the simulation that indeed the solutions represented in Fig. 2.4 resemble the situation of a breather.

2.6.2 Numerical solutions of damped nonlinear Schrödinger equation

Here we have numerically simulated the nonlinear equation (2.72) using MATHEMATICA based finite difference scheme. For the time-dependent numerical solution, we have used the envelope (bright) soliton solution as the initial waveform:

$$\phi(\bar{\xi}, 0) = a\,\mathrm{sech}\,(a\bar{\xi})\exp(i\bar{\xi}),\ \bar{\xi} \in [-L, L],$$

where a is the amplitude of the initial waveform and L is approximately the system size. The boundary condition is $\phi(-L, \bar{\tau}) = \phi(L, \bar{\tau})$. To obtain adequate results through computation, we take $L = 40$ and $a = 1$. The time-dependent numerical solutions are shown in Fig.2.5. These solutions reveal that the amplitude of the envelope decreases (spatial width increases) with time $\bar{\tau}$ in presence of dissipation (electron-ion collision). This confirms the weakly dissipative nature of the envelope as obtained by the approximate analytical solution (2.75). The NLSE possesses

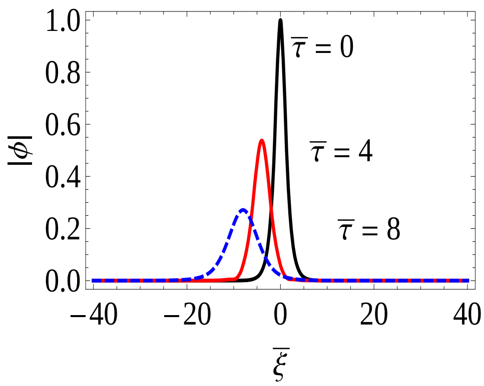

Figure 2.5: (color online) Time-dependent numerical solution of the equation (2.72) with $\bar{\gamma} = 0.1$ and initial amplitude $a = 1$.

another class of nonlinear solution known as rational solutions play a major role in the theory of rogue waves. [148–150] The first-order rational solution of NLSE is known as Peregrine Soliton [151] which is localized in both space and time.

The solutions are the space-periodic breather [152] and the time-periodic breather [153] type solutions. The Peregrine Solitons appear as a bright (i.e. a high peak between two troughs) as well as dark or hole (i.e. an isolated deep trough between two crests) Peregrine Soliton depending on the phase of the underlying carrier wave. [151]

However, here we have considered only the formation of dissipative rouge wave, possible breather solution and rouge wave holes. For this initial excitations of the rouge wave in the simulation, based on the soliton solution on a continuous wave background, we have considered the following Gaussian-type perturbation pulse as the initial condition:

$$\phi(\bar{\xi}, 0) = \phi_{00} + \epsilon \ \exp\left(-\sigma\bar{\xi}^2\right), \ \bar{\xi} \in [-L, L], \tag{2.76}$$

where ϕ_{00} is the initial plane wave solution of NLSE (which is a non-negative constant), ϵ is a weak modulation amplitude and σ represents the inverse of the width of initial perturbation pulse. The time-dependent simulation results are shown in Figs. 2.6 and 2.7. One can see from the left panel of the Fig. 2.6 that in absence of dissipation ($\bar{\gamma} = 0$) at time $\bar{\tau} = 5$, the maximum wave amplitude at $\bar{\xi} = 0$

$$\mid \phi(\bar{\xi} = 0, \bar{\tau} = 5) - \phi_{00} \mid_{max} = 0.15$$

exceeds the modulated wave amplitude ($\epsilon = 0.05$) by a factor of three, which is the main characteristics of a bright Peregrine soliton (the localization of wave in both space and time, where the carrier amplitude amplified by a factor of three). [151]

Then in the simulation we have introduced the electron-ion collision induced dissipative effects. The simulation result is shown graphically in the right panel of

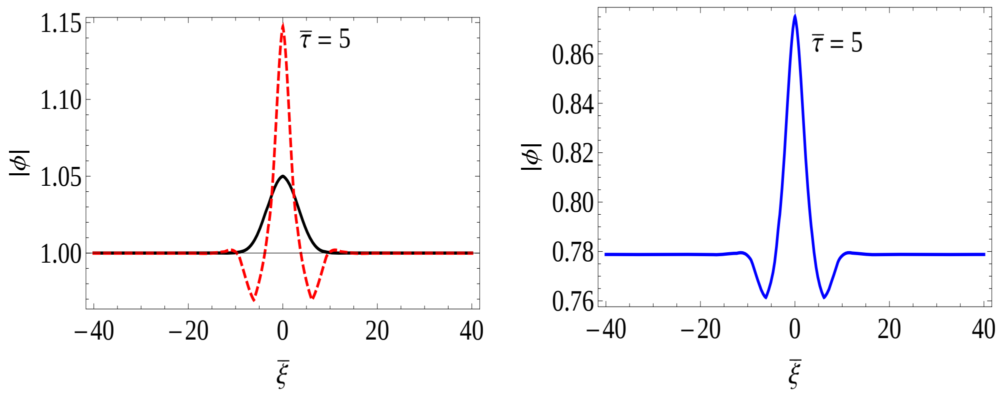

Figure 2.6: (color online) Time-dependent numerical simulation of the equation (2.72) with Eq. (2.76) as the initial condition. The numerical values of the parameters are $\phi_{00} = 1$, $\sigma = 0.05$ and $\epsilon = 0.05$. The left figure is drawn for no dissipation, whereas, the right figure is drawn in presence of dissipation with $\bar{\gamma} = 0.05$. In the left figure, the solid (black) curve is the initial perturbation pulse and the dotted curve (red) represents the typical profile of a bright Peregrine Soliton at $\bar{\tau} = 5$. The right figure represent the same in presence of dissipation.

the Fig. 2.6. One can see from this figure that the amplitude of the nonlinear wave decreases in presence of dissipation, resulting dissipative rouge wave is formed.

Further, we have performed numerical simulations of the time evaluation of the localized initial pulse given by Eq. (2.76) at time $\bar{\tau} = 8$ (in absence of dissipation) and $\bar{\tau} = 11$ (in presence of dissipation). The results are summarized in Fig. 2.7 which reveals the characteristic behavior of the localized breathing soliton. The left panel of this Fig. 2.7 demonstrate that the maximum amplitude of the breather is eight times of the initial modulation wave amplitude in absence of dissipation. We can see from the right panel of this Fig. 2.7 that the dissipation present in the system lowers the amplitude of the continuous wave background as well as the nonlinear wave as mentioned in Eq. 2.62. Thus the observed breathers are indeed giant breathers and the collision introduces the usual damping.

Then in order to excite hole Peregrine soliton, we have performed numerical simulations taking $\epsilon = -0.05$ in the initial perturbation pulse given by Eq. 2.76.

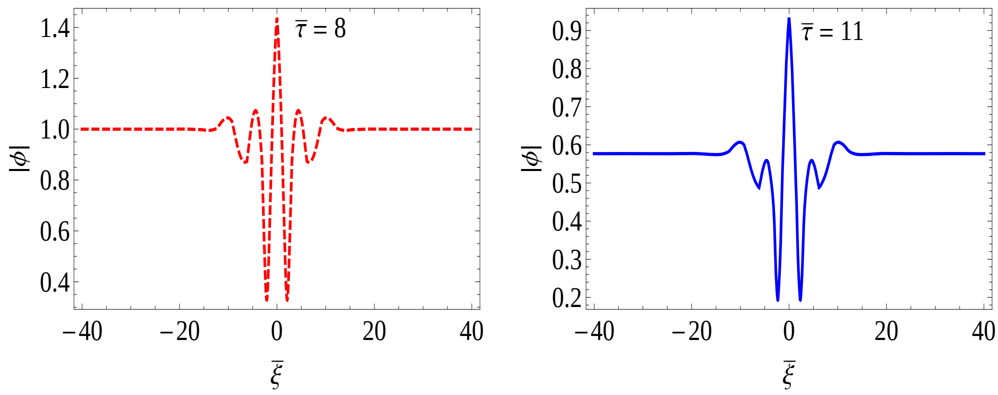

Figure 2.7: (color online) The typical profiles of Breathers. The left figure (red dashed) represents the Breather profile in absence of dissipation at time $\bar{\tau} = 8$. The right figure (blue solid) represents the same profile in presence of dissipation with $\bar{\gamma} = 0.05$ at time $\bar{\tau} = 11$. The initial condition is same as in Fig. 2.6.

The simulation results are shown in Fig. 2.8. One can see from the left panel of the Fig. 2.8 that in absence of dissipation ($\bar{\nu} = 0$) at time $\bar{\tau} = 5$, the maximum amplitude of hole at $\bar{\xi} = 0$

$$| \phi(\bar{\xi} = 0, \bar{\tau} = 5) - \phi_{00} |_{max} = 0.12$$

exceeds twice the modulated wave amplitude ($|\epsilon| = 0.05$), which satisfies the characteristics of a hole Peregrine Soliton (the localized soliton in both space and time, where the amplification factor of the carrier amplitude is greater than twice the modulated wave amplitude). [154] In presence of dissipation rouge wave holes with smaller amplitude are observed as shown in the right panel of the Fig 2.8.

2.7 Summary

The results can be summarized as follows. We have investigated the dynamics of the linearly polarized parallel propagating Alfvén wave. The electron inertia together with ion inertia introduces the dispersive character of the parallel-propagating Alfvén wave in the electron-ion plasma. This finding is unlike the

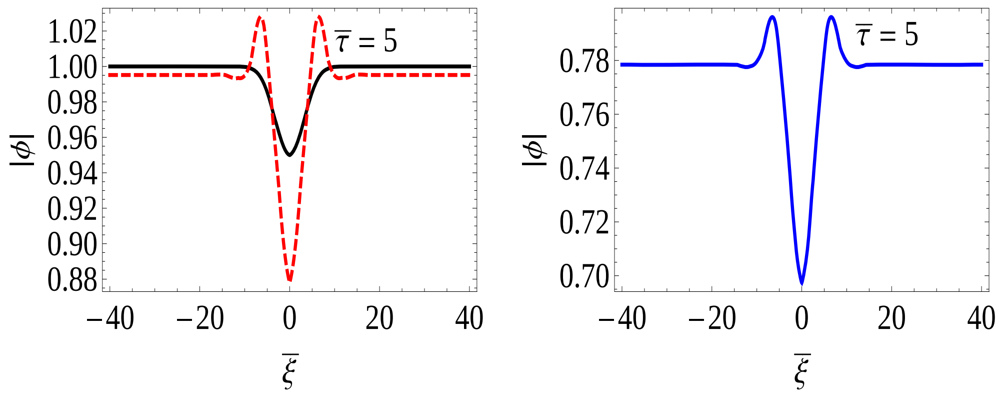

Figure 2.8: (color online) Time-dependent numerical simulation of the equation (2.72) with Eq. (2.76) as the initial condition. The numerical values of the parameters are $\phi_{00} = 1$, $\sigma = 0.05$ and $\epsilon = -0.05$. The left figure is drawn for no dissipation, whereas, the right figure is drawn in presence of dissipation with $\bar{\gamma} = 0.05$. In the left figure, the solid (black) curve is the initial perturbation pulse and the dotted curve (red) represents the typical profile of a dark or hole Peregrine Soliton at $\bar{\tau} = 5$. The right figure represent the same in presence of dissipation.

case investigated earlier where the electron mass is neglected [77] which turns out to be the source of dispersion. It has been found that, the nonlinearity and dispersion are balanced to form soliton like structures. We have also shown that in quasi-linear limit, in absence of collision, the Alfvén wave dynamics satisfy mKdV equation which also has similar solutions. And the dynamics of the weakly nonlinear shear Alfvén wave is found to be governed by a mKdV-Burgers equation. The Burgers term which is responsible for the generation of shock arises due to the electron-ion collision. This nonlinear equation is analyzed by means of analytic and computation. The numerical results predict the formation of both oscillatory (dispersive) shock for weak dissipation and monotonic shock for strong dissipation. Also, numerical solution predicts the breather-like structures of nonlinear shear Alfvén wave.

We have also investigated the wave modulation characteristics of the nonlinear shear Alfvén wave in the long wavelength limit. Our investigation shows that there is a possibility of the trapping of Alfvén wave in a hole created by the wave itself in the medium and the dynamics of this modulated wave is governed by a damped NLSE in which the damping is proportional to the electron-ion collision. The analytical and numerical simulation reveal that this modulated wave exhibits weakly dissipative bright (envelope) solitons. Numerical simulation of the damped NLSE also predict the formation of localized (both space and time: short-lived) large amplitude nonlinear structures known as rogue waves or freak waves, giant breathers and rouge wave holes.

The magnetic field plays a decisive role in the dynamics of inter stellar molecular clouds and the star formation process. [155] This process belongs to the MHD regime, characterized by highly supersonic, strongly magnetized compressible medium, where self-gravity overpowers the thermal pressure over a wide range of scales. [155] The supersonic motion that observed in molecular clouds might arise from the Alfvén type MHD waves which have $B_\perp/B_0 = v_\perp/v_A$, perpendicular to the mean magnetic field B_0. Numerical simulation predict that the magnetic field significantly reduces the rate of star formation i.e. delays the process. In the present investigation the observed shocks are compressive in nature with sufficient magnetic field enhancement in the upstream side of the shock. Thus one can predict that generation of such strong magnetic field can be a potential mechanism to restrict the collapse of molecular clouds due to self-gravity.

The magnetic filed energy grows with the passing of the shock and the saturation occurs at the upstream side (here the saturation value is $2\sqrt{M}$). After the saturation, the energy stored in the magnetic field is transferred back to the plasma particles, leading to the strong plasma heating and the high energy particles. This high energy particles are responsible for the particle acceleration mechanism. Thus the result of the present investigation could be useful for understanding the observed physical phenomena like particle energization [65, 156] and plasma heating. [68]

Moreover the short-lived large-amplitude magnetic structures are commonly observed in space plasmas. In the upstream of the quasi-parallel bow shock such short-lived large amplitude pulsations with strong amplitude magnetic field enhancement has been observed. [157–159] Thus the observation of Alfvénic rouge waves, giant breathers and rouge wave holes in the present work could be a viable processes to observe short-lived large amplitude excitations in the space plasma.

Chapter 3

Effect of electron inertia on circularly polarized Alfvén wave propagation in an electron-ion plasma

In this chapter, we have extended similar investigation in case of the circularly polarized Alfvén wave propagation in absence of collision. Linear analysis of the governing equations manifests dispersion relation of the circularly polarized Alfvén waves where the electron inertia is found to act as a source of dispersion. In the finite amplitude limit, the nonlinear Alfvén wave is found to be described by the Derivative Nonlinear Schrödinger equation (DNLSE) modified by third order dispersion arising due to finite electron inertia. It has been found that, this electron inertia modified DNLSE is completely integrable and an analytical solution has been demonstrated with vanishing boundary conditions.

3.1 Introduction

As described in the previous chapter, the coupling between the elliptically polarized magnetic field components introduces dispersive effect and the dynamics of the finite amplitude nonlinear Alfvén wave (propagating parallel to the magnetic field) is governed by the well known Derivative Nonlinear Schrödinger equation (DNLSE) [77, 119]. The DNLSE is valid in regions with low beta plasma and magnetic fluctuations having lower order compared to the ambient magnetic field. So near to the Sun, the DNLSE describes the nonlinear evolution of finite-amplitude Alfvén waves very well and also describes Alfvénic soliton, Alfvén wave turbulence etc. [77, 119, 160] efficiently.

In the previous chapter, the weakly nonlinear and dispersive Alfvén wave propagation has been investigated considering one component magnetic field and finite electron inertia. It has been found that one component magnetic field is sufficient to describe the essential features of nonlinear and dispersive Alfvén wave where the electron inertia is found to act as a source of dispersion. In this chapter, we have extended the study considering two component magnetic field and investigated some other important aspects of Alfvén wave. In this case, interestingly the electron inertia is also shown to serve as a dispersive effect causing amplitude decay of perturbed magnetic field. In the quasi-linear limit, we have shown that the dynamics of the weakly nonlinear Alfvén wave is governed by a new type of modified DNLSE with third order dispersion term arising due to the consideration of finite electron inertia. We have also investigated modulational instability which determines the conditions of the existence of solitons. This nonlinear evolution equation is found to be completely integrable. [161] An analytical solution of this novel equation has also been derived.

3.2 Basic equations

We have adopted the same model as discussed in the previous chapter. But in this study we have neglected electron-ion collisional effect. The equation of motion of fluid corresponding to electrons and ions in absence of collisions can written as:

$$m_e n_e \left(\frac{\partial}{\partial t} + \mathbf{V}_e \cdot \nabla \right) \mathbf{V}_e = -n_e q_e \left(\mathbf{E} + \frac{1}{c} \mathbf{V}_e \times \mathbf{B} \right), \tag{3.1}$$

$$m_i n_i \left(\frac{\partial}{\partial t} + \mathbf{V}_i \cdot \nabla \right) \mathbf{V}_i = n_i q_i \left(\mathbf{E} + \frac{1}{c} \mathbf{V}_i \times \mathbf{B} \right), \tag{3.2}$$

the continuity equation for both species are

$$\frac{\partial n_e}{\partial t} + \nabla \cdot (n_e \mathbf{V}_e) = 0, \quad \frac{\partial n_i}{\partial t} + \nabla \cdot (n_i \mathbf{V}_i) = 0, \tag{3.3}$$

and the following Maxwell's equations are

$$\nabla \times \mathbf{E} = -\frac{1}{c} \frac{\partial \mathbf{B}}{\partial t}, \tag{3.4}$$

$$\nabla \times \mathbf{B} = \frac{4\pi \mathbf{J}}{c} = -\frac{4\pi e}{c} \left(n_e \mathbf{V}_e - n_i \mathbf{V}_i \right), \tag{3.5}$$

where summation convention is used. All symbols have their usual meaning. Since Alfvén wave is a low-frequency mode ($\omega \ll \omega_{pe}$, electron plasma frequency), so we can neglect the displacement current compared to particle current in Eq. (3.5) for our study. This low frequency assumption is also consistent with the quasi-neutrality condition $n_i \approx n_e \equiv n$. To describe the Alfvén wave we assume that all the dynamical variables are functions of x and t. On the basis of the above facts, from the continuity equations for both species Eqs. (3.3), we have obtained

$$\frac{\partial}{\partial x} \left[n(V_{ix} - V_{ex}) \right] = 0 \Rightarrow V_{ix} = V_{ex} = v \text{ (say)}, \tag{3.6}$$

where we have assumed that $V_{ix}(0,t) = V_{ex}(0,t) = 0$.

In Alfvén wave dynamics the perturbed magnetic fields B_y and B_z arise from the spatial variation of polarization current and directed along the y-direction and z-direction respectively. In component form, Eq. (3.5) can be written as

$$\frac{\partial B_z}{\partial x} = -\frac{4\pi en}{c}(V_{iy} - V_{ey}), \tag{3.7}$$

$$\frac{\partial B_y}{\partial x} = \frac{4\pi en}{c}(V_{iz} - V_{ez}). \tag{3.8}$$

The above Eqs. (3.7) and (3.8) imply that the conduction currents flow along y and z, the directions perpendicular to the plasma motion. Since the 'quasi-neutrality' condition rule out the x component of electric field, so the total wave electric field becomes $\mathbf{E}(x,t) = E_y(x,t)\hat{e}_y + E_z(x,t)\hat{e}_z$. The velocity filed is $V_j = V_{jx}(x,t)\hat{e}_x + V_{jy}(x,t)\hat{e}_y + V_{jz}(x,t)\hat{e}_z$, with $V_{jx} = v(x,t)$ for both the species, where $j \equiv e, i$. Since, the compressional Alfvén wave propagates parallel to the ambient magnetic field directed along x, i.e., $B_0\hat{e}_x$, the magnetic field arising from the fluctuations of electric field will be directed along both the y and z direction. Therefore, the total magnetic field can be written as $\mathbf{B} = B_0\hat{e}_x + B_y(x,t)\hat{e}_y + B_z(x,t)\hat{e}_z$. In view of these above mentioned conditions, from the continuity equations (3.3) for both species, we have

$$\left(\frac{\partial}{\partial t} + v\frac{\partial}{\partial x}\right) n = -n\frac{\partial v}{\partial x}. \tag{3.9}$$

There is convective operator in the Eqs. (3.1), (3.2) and (3.9). This nonlinear operator can be simplified by introducing the Lagrangian variables (ξ, τ) through the following transformation:

$$\xi = x - \int_0^\tau v(\xi, \tau')d\tau' \quad , \quad \tau = t. \tag{3.10}$$

With this transformation the derivative operators are transformed accordingly similar to discussed in the Sec. 1.3 of the first chapter. Using these transformations, the continuity equation (3.9) is simplified and expressed as: $n(\xi,\tau)/n(\xi,0) = \partial\xi/\partial x$. Expressing momentum Eqs. for both species (3.1) and (3.2) in terms of these newly defined variables we have obtained the total momentum equation of the fluid

$$\frac{\partial}{\partial\tau}(m_e\mathbf{V}_e + m_i\mathbf{V}_i) = \frac{e}{c}(\mathbf{V}_i - \mathbf{V}_e)\times\mathbf{B}. \tag{3.11}$$

Expressing the total magnetic field as $\mathbf{B} = \hat{e}_x B_0 + \hat{e}_y B_y(x,t) + \hat{e}_z B_z(x,t)$, the x, y and z components of Eq. (3.11) become

$$\frac{\partial v}{\partial\tau} = \frac{e}{(m_e+m_i)c}\left[B_z(V_{iy}-V_{ey}) - B_y(V_{iz}-V_{ez})\right], \tag{3.12}$$

$$\frac{\partial}{\partial\tau}(m_eV_{ey} + m_iV_{iy}) = \frac{eB_0}{c}(V_{iz}-V_{ez}), \tag{3.13}$$

$$\frac{\partial}{\partial\tau}(m_eV_{ez} + m_iV_{iz}) = -\frac{eB_0}{c}(V_{iy}-V_{ey}), \tag{3.14}$$

respectively. Here the magnetic field associated with the wave has two components $\hat{e}_yB_y(x,t)$ and $\hat{e}_zB_z(x,t)$ which confirm the current propagation along the z and y direction respectively. These facts can be further verified from the Eqs. (3.7) and Eq. (3.8) which are given by

$$V_{iy} - V_{ey} = -\frac{c}{4\pi en(\xi,0)}\frac{\partial B_z}{\partial\xi}, \tag{3.15}$$

and

$$V_{iz} - V_{ez} = \frac{c}{4\pi en(\xi,0)}\frac{\partial B_y}{\partial\xi}, \tag{3.16}$$

respectively. Finally combining these two Eqs. (3.15) and (3.16) we have in the Lagrangian variable space,

$$(\mathbf{V}_i - \mathbf{V}_e)_\perp = \frac{c}{4\pi en(\xi,0)}\left(\hat{e_x}\times\frac{\partial\mathbf{B}_\perp}{\partial\xi}\right). \tag{3.17}$$

Substituting $V_{iy} - V_{ey}$ and $V_{iz} - V_{ez}$ in Eqs. (3.12), (3.13) and (3.14) we have obtained

$$\frac{\partial v}{\partial \tau} = -\frac{1}{8\pi n(\xi,0)(m_e+m_i)}\frac{\partial |\mathbf{B}_\perp|^2}{\partial \xi}, \tag{3.18}$$

$$\frac{\partial}{\partial \tau}(m_e V_{ey} + m_i V_{iy}) = \frac{B_0}{4\pi n(\xi,0)}\frac{\partial B_y}{\partial \xi}, \tag{3.19}$$

and

$$\frac{\partial}{\partial \tau}(m_e V_{ez} + m_i V_{iz}) = \frac{B_0}{4\pi n(\xi,0)}\frac{\partial B_z}{\partial \xi}, \tag{3.20}$$

respectively. Further combining Eqs. (3.19) and (3.20) we have

$$\frac{\partial}{\partial \tau}(m_e \mathbf{V}_{e\perp} + m_i \mathbf{V}_{i\perp}) = \frac{B_0}{4\pi n(\xi,0)}\frac{\partial \mathbf{B}_\perp}{\partial \xi}. \tag{3.21}$$

The evolution equation for magnetic field can further be expressed by taking curl in the electron momentum equation (3.1), and using Eq. (3.4) we have

$$\frac{\partial \mathbf{B}_\perp}{\partial \tau} + \mathbf{B}_\perp \frac{n}{n(\xi,0)}\frac{\partial v}{\partial \xi} - B_0 \frac{n}{n(\xi,0)}\frac{\partial \mathbf{V}_{e\perp}}{\partial \xi} = \frac{m_e c}{e}\frac{n}{n(\xi,0)}\left[\hat{e_x} \times \frac{\partial}{\partial \xi}\left(\frac{\partial \mathbf{V}_{e\perp}}{\partial \tau}\right)\right] \tag{3.22}$$

The continuity equation in terms of Lagrangian variables becomes

$$\frac{\partial}{\partial \tau}\left(\frac{1}{n}\right) = \frac{1}{n(\xi,0)}\frac{\partial v}{\partial \xi}. \tag{3.23}$$

Further, combining Eqs. (3.18) and (3.23) we have

$$\frac{\partial^2}{\partial \tau^2}\left(\frac{1}{n}\right) = -\frac{1}{8\pi n(\xi,0)(m_e+m_i)}\frac{\partial}{\partial \xi}\left(\frac{1}{n(\xi,0)}\frac{\partial |\mathbf{B}_\perp|^2}{\partial \xi}\right). \tag{3.24}$$

Next, replacing U_{iy} and U_{iz} in Eqs. (3.15) and (3.16) respectively with the help of Eqs. (3.19) and (3.20), and further adding we have obtained

$$\frac{\partial \mathbf{V}_{e\perp}}{\partial \tau} = \frac{B_0}{4\pi n(\xi,0)(m_e+m_i)}\frac{\partial \mathbf{B}_\perp}{\partial \xi} - \frac{m_i c}{4\pi e n(\xi,0)(m_e+m_i)}\left(\hat{e_x} \times \frac{\partial^2 \mathbf{B}_\perp}{\partial \xi \partial \tau}\right). \tag{3.25}$$

Now Eqs. (3.17), (3.22), (3.23) and (3.25) can be combined together to give the following equation in a more compact form as:

$$\frac{\partial^2}{\partial \tau^2}\left(\frac{\mathbf{B}_\perp}{n}\right) - \frac{B_0^2}{4\pi n(\xi,0)(m_e+m_i)}\frac{\partial}{\partial \xi}\left[\frac{1}{n(\xi,0)}\frac{\partial \mathbf{B}_\perp}{\partial \xi}\right] = \\ -\frac{B_0 c(m_i-m_e)}{4\pi e n(\xi,0)(m_e+m_i)}\frac{\partial}{\partial \xi}\left[\frac{1}{n(\xi,0)}\left(\hat{e_x}\times\frac{\partial^2 \mathbf{B}_\perp}{\partial \tau \partial \xi}\right)\right] + \\ \frac{c^2 m_e m_i}{4\pi e^2 n(\xi,0)(m_e+m_i)}\frac{\partial}{\partial \xi}\left[\frac{1}{n(\xi,0)}\frac{\partial^3 \mathbf{B}_\perp}{\partial \tau^2 \partial \xi}\right]. \tag{3.26}$$

Next, we have analyzed the nonlinear system (Eqs. (3.24) and (3.26)) in a simplified form adopting the Lagrangian mass variable technique. [132, 138] For this, let us define the following new Lagrangian mass variable ζ instead of ξ

$$\zeta = \int^{\xi} n(\xi', 0) d\xi',$$

which yields the mathematical operator

$$\frac{\partial}{\partial \zeta} = \frac{1}{n(\xi,0)}\frac{\partial}{\partial \xi}.$$

Then introducing this new mass variable ζ in Eqs. (3.24) and (3.26), we have obtained the following simplified couple equations

$$\frac{\partial^2}{\partial \tau^2}\left(\frac{1}{n}\right) = -\frac{V_A^2}{2}\frac{\partial^2}{\partial \zeta^2}|\mathbf{B}_\perp|^2, \tag{3.27}$$

$$\frac{\partial^2}{\partial \tau^2}\left(\frac{\mathbf{B}_\perp}{n}\right) - V_A^2\frac{\partial^2 \mathbf{B}_\perp}{\partial \zeta^2} = -V_A\lambda\frac{\partial^2}{\partial \zeta^2}\left(\hat{e_x}\times\frac{\partial \mathbf{B}_\perp}{\partial \tau}\right) + \delta^2\frac{\partial^2}{\partial \zeta^2}\left(\frac{\partial^2 \mathbf{B}_\perp}{\partial \tau^2}\right), \tag{3.28}$$

where $\mathbf{B}_\perp \equiv \mathbf{B}_\perp/B_0$, $n \equiv n/n_0$, $V_A = B_0/\sqrt{4\pi n_0(m_e+m_i)}$ is the Alfvén velocity, $\lambda = \left(c^2(m_i-m_e)^2/[4\pi n_0 e^2(m_i+m_e)]\right)^{1/2}$ is the ion inertial length and $\delta = \left(c^2 m_e m_i/[4\pi n_0 e^2(m_e+m_i)]\right)^{1/2}$ is the skin depth arising due to electron's finite mass. These two couple of partial differential Eqs. (3.27) and (3.28) are the governing equations of the nonlinear, dispersive circularly polarized Alfvén wave in electron-ion plasma. These equations are very complicated to solve exactly with their full nonlinearity. Therefore, in Sec. 3.4, we will investigate the finite amplitude nonlinear solutions keeping up to third order nonlinear term.

3.3 Linear analysis

Before going to detailed nonlinear analysis we have implemented the perturbative scheme to identify the basic linear modes involved in this study. So, we linearize Eq. (3.28) by considering the perturbation entities with value much smaller than unity such as $n = 1 + \tilde{n}$ and $\mathbf{B}_\perp = \tilde{\mathbf{B}}_\perp$, and obtain the following linear equation:

$$\left(\frac{\partial^2}{\partial t^2} - V_A^2 \frac{\partial^2}{\partial x^2}\right) \tilde{\mathbf{B}}_\perp = -V_A \lambda \hat{e}_x \times \frac{\partial^3 \tilde{\mathbf{B}}_\perp}{\partial t \partial x^2} + \delta^2 \frac{\partial^4 \tilde{\mathbf{B}}_\perp}{\partial t^2 \partial x^2}. \tag{3.29}$$

Then assuming the solution in the form of Fourier mode $\tilde{f} \sim f_k \exp[-i(\omega t - kx)]$ (where ω and k are the oscillation frequency and wave number), we have obtained the following dispersion relation in dimensionless form:

$$\left(1 + \delta^2 k^2\right)^2 \omega^4 - \left(2 + 2\delta^2 k^2 + \lambda^2 k^2\right) k^2 \omega^2 + k^4 = 0, \tag{3.30}$$

which describes the left-hand (ω_-) and right-hand (ω_+) circularly polarized waves

$$\omega_\pm^2 = k^2 \frac{1 + (\lambda^2 + 2\delta^2)\frac{k^2}{2}}{(1 + \delta^2 k^2)^2} \times \left[1 \pm \sqrt{1 - \left(\frac{(1 + \delta^2 k^2)}{1 + (\lambda^2 + 2\delta^2)\frac{k^2}{2}}\right)^2}\,\right], \tag{3.31}$$

where ω, k, λ and δ are made dimensionless using $\omega \to \omega L/V_A$, $k \to kL$, $\lambda \to \lambda/L$ and $\delta \to \delta/L$ respectively. Here L is the typical system length and V_A is the Alfvén velocity. Here, the wave dynamics is regulated by magnetic pressure, ion inertia and electron inertia. The dispersion relation clearly shows that the waves are dispersive in nature. Here we have focused to study the dynamics of the right-hand

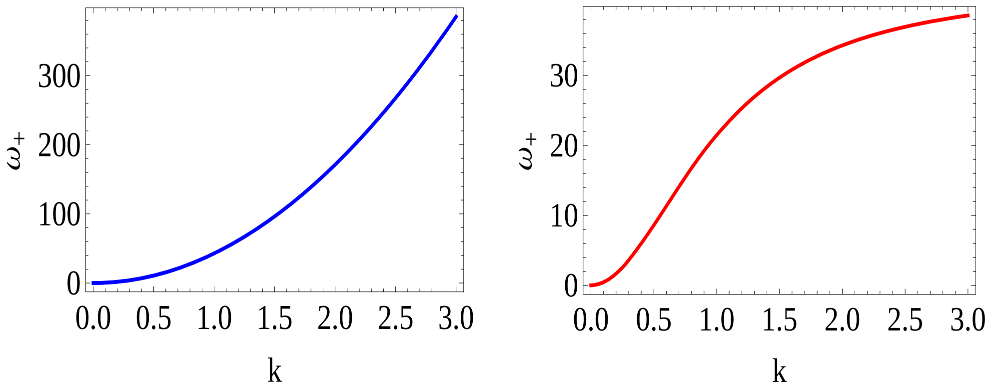

Figure 3.1: (color online) Comparison of the dispersion curve for right-hand polarized wave in absence and presence of electron inertia with $\lambda = 42.8$. The left figure (blue solid curve) is drawn in absence of electron inertia ($\delta = 0$) and the right figure (red solid curve) is drawn in presence of inertia ($\delta = 1$).

polarized wave. Fig. 3.1 presents dispersion relations of right-hand polarized wave in absence and presence of electron inertia. It shows that in absence of electron inertia the dispersive curve asymptotically increases whereas the dispersive effect of electron inertia arrests the wave propagation and saturation occurs.

3.4 Weak amplitude nonlinear dynamics

Having complete perception of the linear modes involved in our study, we continue to study the nonlinear regime of nonlinear Alfvén wave under weak amplitude limit. For dependent variables proposing

$$n = 1 + \tilde{n} \text{ and } \mathbf{B}_\perp = \tilde{\mathbf{B}}_\perp \text{ with } \tilde{n}, \mid \mathbf{B}_\perp \mid < 1,$$

keeping up to second order term and substituting, from Eq. (3.28), we have obtained

$$\left(\frac{\partial^2}{\partial \tau^2} - V_A^2 \frac{\partial^2}{\partial \zeta^2}\right) \tilde{\mathbf{B}}_\perp = -V_A \lambda \left(\hat{e}_x \times \frac{\partial^3 \tilde{\mathbf{B}}_\perp}{\partial \tau \partial \zeta^2}\right) + \delta^2 \frac{\partial^4 \tilde{\mathbf{B}}_\perp}{\partial \tau^2 \partial \zeta^2} + \frac{\partial^2}{\partial \tau^2}(\tilde{\mathbf{B}}_\perp \tilde{n}). \quad (3.32)$$

The above equation represents both left-hand and right-hand polarized Alfvén waves modified by the dispersions (arising due to both ion inertia and electron inertia effect) and nonlinearity.

Moreover the small amplitude nonlinear wave equations are derived by assuming that the equilibrium density is homogeneous i.e. $n(\xi, 0) = 1$, therefore $\zeta = \xi$ [$\equiv x - \int v(\xi, \tau')d\tau'$]. Also in this weak amplitude limit $\xi(\zeta) \equiv x$ and $\tau \equiv t$ (actually in this case, $\xi(\zeta)$ and τ are no longer remain Lagrangian variables but become equivalent to x and t). Therefore, we rewrite the above Eq. (3.32) in the following form:

$$\left(\frac{\partial}{\partial t} - V_A\frac{\partial}{\partial x}\right)\left(\frac{\partial}{\partial t} + V_A\frac{\partial}{\partial x}\right)\tilde{\mathbf{B}}_\perp - \frac{\partial^2}{\partial x^2}(\tilde{\mathbf{B}}_\perp \tilde{n}) - V_A\lambda\left(\hat{e}_x \times \frac{\partial^3 \tilde{\mathbf{B}}_\perp}{\partial t \partial x^2}\right) + \delta^2\frac{\partial^4 \tilde{\mathbf{B}}_\perp}{\partial t^2 \partial x^2}. \tag{3.33}$$

For the Alfvén wave propagating in the positive x direction only, from the above relation, we get

$$\frac{\partial}{\partial t} = -V_A\frac{\partial}{\partial x},$$

and this approximation yields (from Eq. (3.24))

$$\tilde{n} \approx \frac{|\tilde{\mathbf{B}}_\perp|^2}{2}.$$

Then substituting all these in Eq. (3.33) and integrating the transformed equation once with the boundary condition at $x \to \infty$, $|\tilde{\mathbf{B}}_\perp| \to 0$, we obtain

$$\left(\frac{\partial}{\partial t} + V_A\frac{\partial}{\partial x}\right)\tilde{\mathbf{B}}_\perp + \frac{V_A}{4}\frac{\partial}{\partial x}(\tilde{\mathbf{B}}_\perp|\tilde{\mathbf{B}}_\perp|^2) = -\frac{V_A\lambda}{2}\left(\hat{e}_x \times \frac{\partial^2 \tilde{\mathbf{B}}_\perp}{\partial x^2}\right) - \frac{\delta^2}{2}\frac{\partial^3 \tilde{\mathbf{B}}_\perp}{\partial x^3}. \tag{3.34}$$

Finally, a further transformation of coordinates

$$\hat{x} = x - V_A t \quad \text{and} \quad \hat{t} = t,$$

renders the following equation:

$$\frac{\partial \tilde{\mathbf{B}}_\perp}{\partial \hat{t}} + \frac{V_A}{4}\frac{\partial}{\partial \hat{x}}(\tilde{\mathbf{B}}_\perp|\tilde{\mathbf{B}}_\perp|^2) = -\frac{V_A\lambda}{2}\left(\hat{e}_x \times \frac{\partial^2 \tilde{\mathbf{B}}_\perp}{\partial \hat{x}^2}\right) - \frac{\delta^2}{2}\frac{\partial^3 \tilde{\mathbf{B}}_\perp}{\partial \hat{x}^3}. \tag{3.35}$$

Then normalizing the Eq. 3.35 by $\bar{t} \rightarrow \hat{t}/t_0, \bar{x} \rightarrow \hat{x}/L$ and $\tilde{\mathbf{B}}_\perp \rightarrow \alpha \mathbf{b}_\perp$, we arrive at the Vector Derivative Nonlinear Schrödinger Equation (VDNLS) with third order dispersion

$$\frac{\partial \mathbf{b}_\perp}{\partial \bar{t}} + \frac{\partial}{\partial \bar{x}}(\mathbf{b}_\perp |\mathbf{b}_\perp|^2) + \left(\hat{e}_x \times \frac{\partial^2 \mathbf{b}_\perp}{\partial \bar{x}^2} \right) + \frac{\partial^3 \mathbf{b}_\perp}{\partial \bar{x}^3} = 0, \tag{3.36}$$

where,

$$t_0 = \frac{2c(m_e m_i)^2}{eB_0(m_i - m_e)^3}, \; L = \frac{cm_e m_i}{(m_i - m_e)\sqrt{4\pi n_0 e^2 (m_e + m_i)}},$$
$$\text{and} \;\; \alpha = (m_i - m_e)\sqrt{\frac{2}{m_e m_i}}.$$

Finally we can write the Eq. (3.36) as the complex Derivative Nonlinear Schrödinger Equation(DNLSE) for the right-hand polarized Alfvén wave

$$\frac{\partial \phi}{\partial \bar{t}} + \frac{\partial}{\partial \bar{x}} \left(|\phi|^2 \phi \right) - i\frac{\partial^2 \phi}{\partial \bar{x}^2} + \frac{\partial^3 \phi}{\partial \bar{x}^3} = 0, \tag{3.37}$$

where $\phi = b_y - ib_z$. It is very important to note that, the Nonlinear Schrödinger Equation governs only nonlinear modulation of the complex amplitude of carrier wave in contrast to this the DNLSE describes the whole nonlinear modulation of the complex field. In our study the modified DNLSE, with the third order dispersion term arising due to electron inertia effect, describes the nonlinear modulation of the Alfvén wave. For the sake of more generalized equation a parameter ϵ can be set to the Eq. (3.37) as

$$\frac{\partial \phi}{\partial \bar{t}} + \frac{\partial}{\partial \bar{x}} \left(|\phi|^2 \phi \right) - i\frac{\partial^2 \phi}{\partial \bar{x}^2} + \epsilon\frac{\partial^3 \phi}{\partial \bar{x}^3} = 0, \tag{3.38}$$

where ϵ can either be 1 or 0. If we neglect the second order dispersive term, the modified DNLSE (3.37) is reduced to the following well known Complex modified Korteweg-de Vries (CMKdV) equation [162]

$$\frac{\partial \phi}{\partial \bar{t}} + \frac{\partial}{\partial \bar{x}} \left(|\phi|^2 \phi \right) + \epsilon\frac{\partial^3 \phi}{\partial \bar{x}^3} = 0. \tag{3.39}$$

On the other hand, if we put $\epsilon = 0$, we recover the following well known DNLSE

$$\frac{\partial \phi}{\partial \bar{t}} + \frac{\partial}{\partial \bar{x}}\left(|\phi|^2\phi\right) - i\frac{\partial^2 \phi}{\partial \bar{x}^2} = 0. \tag{3.40}$$

Here we must emphasize that the DNLSE was derived in a fluid system (water waves) and its solution, soliton, is applicable in nearly all branches of physics. Thus the derived modified DNLSE (3.37) should be applicable mostly to all physical systems and is a very generalized equation from any point of view.

3.5 Modulational instability

In this section, following the way in references [125, 126, 139, 143–145, 163] we have analyzed the modulational characteristics of the right-hand polarized Alfvén wave. For this purpose, we have performd a linear stability analysis of the plane wave solution for Eq. (3.37). For the simplification of notation removing the bar signs the Eq. (3.37) for the right-hand polarized wave becomes

$$\frac{\partial \phi}{\partial t} + \frac{\partial}{\partial x}\left(|\phi|^2\phi\right) - i\frac{\partial^2 \phi}{\partial x^2} + \frac{\partial^3 \phi}{\partial x^3} = 0. \tag{3.41}$$

It is easy to find out that Eq. (3.41) possesses the plane-wave solution with constant amplitude as

$$\phi = \phi_0 \exp[-i(ax + \gamma t)], \tag{3.42}$$

where ϕ_0 and a are real parameters, and $\gamma = a(a + a^2 - \phi_0^2)$. Therefor for stability analysis, we consider the perturbation about this stable solution in the following standard procedure,

$$\phi = [\phi_0 + \tilde{\phi}(x,t)] \exp[-i(ax + \gamma t)], \tag{3.43}$$

where $\tilde{\phi}(x,t)(|\tilde{\phi}| \ll \phi_0)$ is the perturbed amplitude of the modulated wave. then substitution of this Eq. (3.43) into the Eq. (3.41) yields the following linearized two coupled equations:

$$\frac{\partial\tilde{\phi}_R}{\partial t}+\frac{\partial^3\tilde{\phi}_R}{\partial x^3}+\left(3\phi_0^2-3a^2-2a\right)\frac{\partial\tilde{\phi}_R}{\partial x}+(3a+1)\frac{\partial^2\tilde{\phi}_I}{\partial x^2}=0$$

$$\text{and}\quad \frac{\partial\tilde{\phi}_I}{\partial t}+\frac{\partial^3\tilde{\phi}_I}{\partial x^3}+\left(\phi_0^2-3a^2-2a\right)\frac{\partial\tilde{\phi}_I}{\partial x}-(3a+1)\frac{\partial^2\tilde{\phi}_R}{\partial x^2}-2a\phi_0^2\tilde{\phi}_R=0, \tag{3.44}$$

where $\tilde{\phi}=\tilde{\phi}_R+i\tilde{\phi}_I$, $\phi_{R(I)}$ is the real (imaginary) part of ϕ.

Finally, the space-time dependence of the perturbation of the form $\tilde{\phi}\sim\exp\,(i\vartheta)$, where $\vartheta\,(=\Lambda x-\Omega t)$ is the modulated phase with $(\Lambda\ll a)$ and $\tilde{\Omega}(\ll\gamma)$ are the wave number and modulation frequency, respectively, yields the following dispersion relation:

$$\Omega=\Lambda(2\phi_0^2-3a^2-2a-\Lambda^2)\pm\Lambda\sqrt{(3a+1)^2\Lambda^2-2a(3a+1)\phi_0^2+\phi_0^4}, \tag{3.45}$$

from which we can say that dispersion relation depends on the values of the plane wave amplitude ϕ_0 together with the wave number Λ. When $(3a+1)^2\Lambda^2-2a(3a+1)\phi_0^2+\phi_0^4<0$, the frequency becomes complex at any value of the wave number Λ and the disturbance will grow(decay) into bright(dark) solitons depending on the positive(negative) complex part of the frequency.

3.6 Analytical solution

In this section, we have tried to solve the Eq. (3.37) analytically. As is well known the DNLSE is completely integrable and preserves infinite number of conserved quantities. [164, 165] Like the DNLSE, the newly developed modified DNLSE is also found to be completely integrable and preserves infinite number of conserved quantities. According to the conservation laws the first three of those conserved quantities are

$$\begin{aligned}
\text{Energy}(\mathcal{E}) &= \int_{-\infty}^{+\infty} |\phi|^2 dx, && (3.46)\\
\text{Momentum}(\mathcal{M}) &= \int_{-\infty}^{+\infty} \left[i\left(\phi\phi_x^* - \phi^*\phi_x\right) - |\phi|^4\right] dx, && (3.47)\\
\text{Hamiltonian}(\mathcal{H}) &= \int_{-\infty}^{+\infty} \left[|\phi_x|^2 + \frac{i}{4}|\phi|^2\left(\phi^*\phi_x - \phi\phi_x^*\right)\right] dx. && (3.48)
\end{aligned}$$

So it is possible to find the analytical solution of the derived modified DNLSE (3.41).

Therefore, we have solved the Eq. (3.41) using moving frame analysis. To find out nonlinear solution, we transform Eq. (3.41) into the moving frame $\xi = x - ut$, where u is the phase velocity of the wave. Then the first integral of the transform equation leads to the following equation

$$\frac{d^2\phi}{d\xi^2} + (|\phi|^2 - u)\phi - i\frac{d\phi}{d\xi} = 0, \tag{3.49}$$

subject to the boundary conditions $\phi \to 0$ all derivatives $\to 0$ as $\xi \longrightarrow \pm\infty$. Assuming a stationary solution of the form

$$\phi(\xi) = \sqrt{\psi}(\xi)e^{i\theta(\xi)}, \tag{3.50}$$

with real functions ψ and θ, and substituting in Eq. (3.49) we have obtained a pair of coupled equations for ψ and θ

$$\frac{d^2\psi}{d\xi^2} - \frac{1}{2\psi}\left(\frac{d\psi}{d\xi}\right)^2 - 2\psi\left(\frac{d\theta}{d\xi}\right)^2 + 2\psi\frac{d\theta}{d\xi} + 2(\psi - u)\psi = 0, \tag{3.51}$$

$$2\frac{d\psi}{d\xi}\frac{d\theta}{d\xi} + 2\psi\frac{d^2\theta}{d\xi^2} - \frac{d\psi}{d\xi} = 0 \Rightarrow \frac{d}{d\xi}\left[2\psi\frac{d\theta}{d\xi} - \psi\right] = 0. \tag{3.52}$$

Integrating once using the boundary condition $\phi \to 0$ as $\xi \to \pm\infty$ we have

$$\theta(\xi) = \theta_0 + \frac{1}{2}\xi. \tag{3.53}$$

With Eq. (3.53) we can rewrite the Eq. (3.51) as the second order differential equation in ψ

$$\frac{d^2\psi}{d\xi^2} - \frac{1}{2\psi}\left(\frac{d\psi}{d\xi}\right)^2 + \left(\frac{1}{2} - 2u\right)\psi + 2\psi^2 = 0. \tag{3.54}$$

Multiplying the above Eq. (3.54) by $\frac{2}{\psi}\frac{d\psi}{d\xi}$ we have

$$\frac{d}{d\xi}\left[\frac{1}{\psi}\left(\frac{d\psi}{d\xi}\right)^2\right] = \frac{d}{d\xi}\left[(4u-1)\,\psi - 2\psi^2\right]. \tag{3.55}$$

Integrating the Eq. (3.55) using the boundary conditions $\phi \to 0$ as $\xi \to \pm\infty$ we can arrive at

$$\int \frac{d\psi}{\psi\sqrt{a^2 - 2\psi}} = \xi + c_1, \tag{3.56}$$

where we have defined $a^2 = 4u - 1$, and considered $c_1 = 0$ which is consistent with the boundary conditions.

Finally integrating the Eq. (3.56) we get

$$\psi = \frac{a^2}{2}\mathrm{sech}^2\left(\frac{a\xi}{2}\right). \tag{3.57}$$

Therefore, the final solution is given by

$$\phi = \sqrt{\left(2u - \frac{1}{2}\right)}\mathrm{sech}\left(\sqrt{u - \frac{1}{4}}(x - ut)\right)\exp\left[i\left(\theta_0 + \frac{1}{2}(x - ut)\right)\right]. \tag{3.58}$$

The soliton solution is shown graphically in Fig. 3.2 for wave phase velocity $u = 1$. It is found that the dispersive effect caused by the electron inertia together with ion inertia can balance the nonlinear steepening of waves leading to the formation of a soliton.

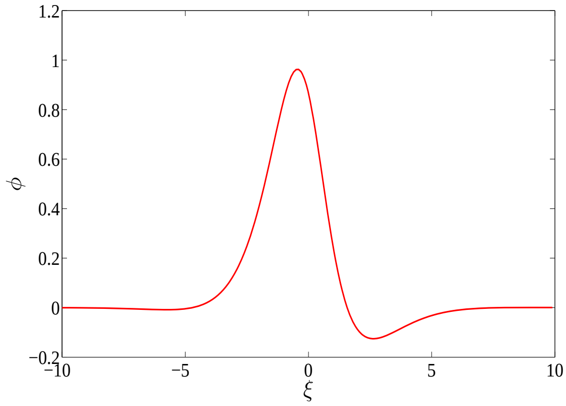

Figure 3.2: (color online) Formation of single soliton in moving frame ξ with $u = 1$

3.7 Summary

In this chapter, we have investigated the effect of electron inertia on the circularly polarized Alfvén wave propagation in the frame work of Lagrangian two fluid model in a cold electron-ion plasma. The right-hand circularly polarized wave dynamics has been inspected in detail. The complete linear analysis indicates the saturation of right-hand polarized wave in presence of the dispersive effect of electron inertia. We have also shown that the dynamics of the weakly nonlinear Alfvén wave is governed by modified DNLSE with third order dispersion term. The equation reflects that the third order dispersion arises solely due to the consideration of finite electron inertia. This nonlinear equation has been analyzed by means of analytical calculation and soliton type solutions are obtained. These results could be useful in interpreting solitary Alfvén wave propagation, reported by satellites in different parts of the auroral ionosphere and the interplanetary plasma.

Chapter 4

Vortex dynamics in a strongly coupled dusty plasma in presence of dust-neutral collisional drag

The formation of vortex, their evolution and interactions have been studied in presence of dust-neutral collisional drag in a strongly coupled dusty plasma by numerically integrating the generalized hydrodynamic equation (GH) after transforming into fourier space using a doubly periodic pseudo-spectral simulation method. Specifically, the nonlinear dynamical response of this strongly coupled system in presence of dust-neutral drag has been presented. In this chapter, it has been shown that the interplay between the nonlinear elastic stress and the dust-neutral drag results in the generation of non-propagating monopole vortex for some duration before it starts to propagate like transverse shear wave. It has also been found that the interaction between two unshielded monopole vortices having both same (co-rotating) and opposite (counter rotating) rotations result in the formation of two propagating dipole vortices of equal and unequal strength respectively.

4.1 Introduction

As discussed in the first chapter, the dusty plasma has been found to reflect visco-elastic property in the intermediate coupling regime of $1 < \Gamma < 1$ (where, Γ is the ratio of the inter-particle potential energy to the kinetic energy) and its dynamics has been provided by the generalized hydrodynamic model (GH) that incorporates the Maxwell's relaxation parameter τ_m to mimic the viscoelastic property. [89] The dusty plasma can often be found in the strongly coupled regime when the coupling parameter Γ becomes greater than or equal to 1, i.e, when the inter-particle potential energy becomes comparable or exceeds the thermal kinetic energy of the particles. This strong coupling enables the system to support transverse shear wave along with the other longitudinal modes, which has been reported theoretically and later verified experimentally. [30–32] In nonlinear regime, it has been shown theoretically that this strongly coupled dusty plasma system can support vortex like structures exploiting the convective nonlinearity of this system which usually comes from the nonlinear fluid advection in two dimensional flows. [6, 33–35] Recently molecular dynamic simulation has shown formation of tripole and dipole vortices from the perturbed shielded Gaussian vortex. [104] In such system the effect of elasticity on vortices makes them quite different from normal Newtonian fluids.

In dusty plasma, the dust particles are subjected to many forces such as ion-drag force and thermophoretic forces in addition to dust-dust coupling effect. [6] In our study, we have excluded such forces except the dust-dust coupling which provides a simple picture of dusty plasma system. In laboratory dusty plasma, the condensation of 'liquid' dusty plasma into 'solid' can be achieved only by increasing the neutral gas pressure. Hence, it is very important to take into account the neutral gas pressure in making the dusty plasma model.

In the above mentioned references on dust vortex flows, [33–35, 104] the effect of gas friction i.e the dust-neutral collisional drag (i.e. friction force exerted on the dust particles due to presence of the neutral gas in complex plasma, known as Epstein drag [6, 166]) has not been considered yet. In a recent article, the dynamical change of the phenomena of vortex merging has been studied numerically by varying the strong coupling parameter ranging from hydrodynamic to strongly coupled limit in the strongly coupled dusty plasma in the framework of the GH model. [167] In this study, they did not consider the dust-neutral collisional drag in their model. Therefore, it has utmost importance to study the effect of neutral gas friction in the context of the dust vortex dynamics. The present chapter is devoted to study the effect of both elastic stress arising due to the strong coupling effect and dust-neutral collisional drag on the vortex dynamics in the strongly coupled dusty plasma.

In this chapter, we have studied an important phenomenon of vortex formation and their evolution and interactions in a strongly coupled dusty plasma in the framework of the GH model modified by dust-neutral collisional drag. Specifically, we have observed how the interplay between the nonlinear elastic stress and the dust-neutral collisional drag determines the dynamics of the vortices in such a strongly coupled system. All the studies have been done by numerically integrating the GH equation after transforming into fourier space using a de-alised doubly periodic pseudo-spectral simulation method.

4.2 Governing equations

The dynamics of the strongly coupled dusty plasma medium has been described using generalized hydrodynamic set of equations (Eqs. (1.1) to (1.5), as discussed in section 1.2.3.1 of the first chapter). To study the phenomena associated with the transverse shear wave, we should consider the modified dust momentum equation (Eq. (1.7) of Sec. 1.2.3.2 of first chapter) for the incompressible dust fluid as:

$$\left[1+\tau_m\left(\frac{\partial}{\partial t}+\mathbf{v}\cdot\nabla\right)\right]\left[\rho_{d0}\left(\frac{\partial}{\partial t}+\mathbf{v}\cdot\nabla\right)\mathbf{v}+\nabla p\right]=\eta\nabla^2\mathbf{v}, \tag{4.1}$$

where q_d is the charge on the individual dust particle, $\mathbf{v}$ is the dust fluid velocity, η is the shear dynamic viscosity coefficient, ρ_{d0} is the equilibrium constant dust density and p is the total pressure of the system.

In this present work, the dust fluid dynamics is studied in a two dimensional horizontal layer of dust particles where all the spatial variations are restricted on 2-D $x-y$ plane and z is the axis of symmetry which means a two dimensional slab coordinate system is used here. Here, we are interested to study the vortex dynamics in presence of dust-neutral collisional drag. So the dust momentum equation in presence of dust-neutral drag can be modified as:

$$\left[1+\tau_m\left(\frac{\partial}{\partial t}+\mathbf{v}\cdot\nabla\right)\right]\left[\left(\frac{\partial}{\partial t}+\mathbf{v}\cdot\nabla\right)\mathbf{v}+\nu\mathbf{v}\right]=\frac{\eta}{\rho_{d0}}\nabla^2\mathbf{v}, \tag{4.2}$$

where ν is the frequency of the dust-neutral collisional drag. Here, we have taken cold dust approximation, i.e, random thermal motion of dust grain is ignored. Hence, the pressure term is not taken into consideration in Eq. (4.2).

The Eq. (4.2) can be written in normalized form as:

$$\left[1+\hat{\tau}_m\left(\frac{\partial}{\partial \hat{t}}+\hat{\mathbf{v}}\cdot\hat{\nabla}\right)\right]\left[\left(\frac{\partial}{\partial \hat{t}}+\hat{\mathbf{v}}\cdot\hat{\nabla}\right)\hat{\mathbf{v}}+\hat{\nu}\hat{\mathbf{v}}\right]=\frac{1}{Re}\hat{\nabla}^2\hat{\mathbf{v}}, \tag{4.3}$$

where normalized parameters are $\hat{\eta} = 1/Re$ (Reynolds number $Re = \frac{UL\rho_{d0}}{\eta}$) , $\hat{\tau}_m = \tau_m U/L$, $\hat{\nu} = \nu L/U$ and $\hat{\mathbf{v}} = \frac{\mathbf{v}}{U}$. We have normalized the length, velocity and time by a typical length scale L , a typical velocity scale U and L/U respectively. Then removing the hat symbols and simplifying the normalized form of the dust momentum Eq. (4.3) we have

$$\frac{\partial^2 \mathbf{v}}{\partial t^2} + \frac{1}{\tau_m}\left[\frac{\partial \mathbf{v}}{\partial t} + \mathbf{v}\cdot\nabla\mathbf{v} + \nu\mathbf{v}\right] + \underbrace{\frac{\partial}{\partial t}\left(\mathbf{v}\cdot\nabla\mathbf{v}\right) + \left(\mathbf{v}\cdot\nabla\right)\frac{\partial \mathbf{v}}{\partial t}} +$$
$$\left(\mathbf{v}\cdot\nabla\right)\left(\mathbf{v}\cdot\nabla\right)\mathbf{v} + \nu\left(\frac{\partial}{\partial t} + \mathbf{v}\cdot\nabla\right)\mathbf{v} = \frac{1}{Re\ \tau_m}\nabla^2\mathbf{v}. \tag{4.4}$$

Further simplifying the second term of the curly bracketed term in Eq. (4.4) by using the identity $\nabla\cdot(\mathbf{AB}) = \mathbf{A}\cdot\nabla\mathbf{B} + (\nabla\cdot\mathbf{A})\mathbf{B}$ and the incompressible condition $(\nabla\cdot\mathbf{v})$ as:

$$\begin{aligned}\left(\mathbf{v}\cdot\nabla\right)\frac{\partial \mathbf{v}}{\partial t} &= \nabla\cdot\left(\mathbf{v}\frac{\partial \mathbf{v}}{\partial t}\right)\\ &= \frac{1}{2}\nabla\cdot\left[\frac{\partial}{\partial t}(\mathbf{vv})\right]\\ &= \frac{1}{2}\frac{\partial}{\partial t}\left[\nabla\cdot(\mathbf{vv})\right]\\ &= \frac{1}{2}\frac{\partial}{\partial t}\left(\mathbf{v}\cdot\nabla\mathbf{v}\right)\end{aligned} \tag{4.5}$$

and substituting this term (4.5) in Eq. (4.4) we obtain

$$\frac{\partial^2 \mathbf{v}}{\partial t^2} + \frac{1}{\tau_m}\left[\frac{\partial \mathbf{v}}{\partial t} + \mathbf{v}\cdot\nabla\mathbf{v} + \nu\mathbf{v}\right] + \frac{3}{2}\frac{\partial}{\partial t}\left(\mathbf{v}\cdot\nabla\mathbf{v}\right) +$$
$$\left(\mathbf{v}\cdot\nabla\right)\left(\mathbf{v}\cdot\nabla\right)\mathbf{v} + \nu\left(\frac{\partial}{\partial t} + \mathbf{v}\cdot\nabla\right)\mathbf{v} = \frac{1}{Re\ \tau_m}\nabla^2\mathbf{v}. \tag{4.6}$$

Taking curl of the Eq. (4.7), we get the vorticity equation of dust fluid as:

$$\frac{\partial}{\partial t}\left(\frac{\partial \omega}{\partial t} + \frac{3}{2}[\psi,\omega] + \frac{\omega}{\tau_m} + \nu\omega\right) + \left(\frac{1}{\tau_m} + \nu\right)[\psi,\omega] + \frac{\nu}{\tau_m}\omega + \frac{\partial}{\partial x}\left[\psi,\left[\psi,\frac{\partial \psi}{\partial x}\right]\right]$$
$$+\frac{\partial}{\partial y}\left[\psi,\left[\psi,\frac{\partial \psi}{\partial y}\right]\right] = \frac{1}{Re\ \tau_m}\nabla^2\omega, \tag{4.7}$$

where ψ ($\mathbf{v} \equiv \hat{e}_z \times \nabla\psi$) is the velocity stream function, $\omega \equiv \hat{e}_z \cdot (\nabla \times \mathbf{v}) \equiv \omega = \nabla^2\psi$ is the vorticity and $[\phi, \chi] \equiv \hat{e}_z \times \nabla\phi \cdot \nabla\chi \equiv \partial_x\phi\partial_y\chi - \partial_y\phi\partial_x\chi$ is Poissons bracket notation; where ∂_j is the partial derivative with respect to the variable j. The vortex equation is of 2nd order in time and has been broken into two the following two 1st order time evolution equations for the sake of numerical integration as:

$$\frac{\partial\omega}{\partial t} + \frac{3}{2}[\psi, \omega] + \left(\frac{1}{\tau_m} + \nu\right)\omega = \phi, \tag{4.8}$$

$$\begin{aligned}\frac{\partial\phi}{\partial t} + \left(\frac{1}{\tau_m} + \nu\right)[\psi, \omega] + \frac{\nu}{\tau_m}\omega + \frac{\partial}{\partial x}\left[\psi, \left[\psi, \frac{\partial\psi}{\partial x}\right]\right] + \\ \frac{\partial}{\partial y}\left[\psi, \left[\psi, \frac{\partial\psi}{\partial y}\right]\right] = \frac{1}{Re\ \tau_m}\nabla^2\omega.\end{aligned} \tag{4.9}$$

For small amplitude perturbation, the nonlinear convective term is not effective in first order and for large τ_m, the equation leads to a linear shear wave equation. In 2d plane, it manifests the propagation of rotational structures of fluid particles like generation of surface waves on lake when struck with stones.

4.3 Numerical investigation

For the study of evolution of vortices in strongly coupled plasmas, the Eqs. (4.8) and (4.9) are numerically integrated using a doubly periodic de-aliased pseudo-spectral code, discussed in the Sec. 1.4 of the first chapter. The dynamic variables ϕ, ω and ψ are expanded in Fourier modes as:

$$\omega(x, y) = \sum_{k_x=-Nx/2}^{N_x/2} \sum_{k_y=-N_y/2}^{N_y/2} \omega_{k_x,k_y} \exp\left(\frac{2\pi i k_x x}{l_x}\right) \exp\left(\frac{2\pi i k_y y}{l_y}\right).$$

where l_x and l_y are the size of the computational domain and N_x and N_y are number of spatial grid points. The time integration is done by Runge-Kutta-gill time integration method. In our simulations, Courant Friedrichs Lewy condition

(CFL condition) is well satisfied. [168] For our simulation, parameters used are of spatial grid points $N_x = N_y = 512$, initial vorticity $\omega_0 = 50$, step in time $\delta t = 0.0001$, step in space $\delta x = \frac{2\pi}{N_x}$, CFL $= \frac{\omega_0 \delta t}{\delta x}$ value is 0.407, which is quite smaller than 1. Aliasing error is minimized using standard $\frac{2}{3}$ de-aliasing method (zero padding method). [116] The results of the spectral code simulation of the article [36] are reproduced and matched accurately using our spectral code. The Eq. (4.7) leads to the vortex equation (3 in the ref. [36]) in the limit $\tau_m = 0$ and $\nu = 0$. Also, our code accurately represent the results in linear regime of shear wave propagation as shown in the article. [167] In the linear regime of the equation (4.7), shear wave propagates with phase velocity $c_{sh} = \sqrt{1/Re\tau_m}$. So, if we start with small amplitude monopole vortex (Gaussian shaped), the structure will propagate. The linear wave equation looks like

$$\frac{\partial^2 \omega}{\partial t^2} = c_{sh}^2 \nabla^2 \omega \tag{4.10}$$

Multiplying both side of equation (4.10) with $(\partial\omega/\partial t)$ and after integrating over 2d space, we get one invariant quantity

$$2I = \int \left(\omega_t^2 + c_{sh}^2 \nabla\omega \cdot \nabla\omega\right) dxdy.$$

Here and throughout the study, we have used that the vorticity ω should be differentiable in the whole domain and that it vanishes at the boundary. In fourier space the invariant quantity can be written as:

$$2I_k = \sum_k \omega_t(\vec{k})\omega_t^*(\vec{k}) + c_{sh}^2 k^2 \omega(\vec{k})\omega^*(\vec{k}).$$

where $\dfrac{\partial\omega}{\partial t}$ is denoted by ω_t for simplicity and * denotes complex conjugate. This invariant quantity has been checked to be constant for all time with higher accuracy. Now, we multiply both side of equations (4.8) and (4.9) with ω and then integrate over 2d space to get

$$\int \omega\omega_t dxdy + \frac{3}{2}\int \omega\left[\psi,\omega\right]dxdy + \left(\frac{1}{\tau_m}+\nu\right)\int \omega^2 dxdy = \int \phi\omega dxdy, \quad (4.11)$$

$$\int \omega\phi_t dxdy + \left(\frac{1}{\tau_m}+\nu\right)\int \omega\left[\psi,\omega\right]dxdy + \frac{\nu}{\tau_m}\int \omega^2 dxdy + \int \omega\frac{\partial}{\partial x}\left[\psi,\left[\psi,\frac{\partial\psi}{\partial x}\right]\right]dxdy + \int \omega\frac{\partial}{\partial y}\left[\psi,\left[\psi,\frac{\partial\psi}{\partial y}\right]\right]dxdy = \frac{1}{Re\ \tau_m}\int \nabla\omega\cdot\nabla\omega dxdy. \quad (4.12)$$

The consistency of the balance of right and left hand sides of each equations has been checked after few time intervals. The accuracy of difference between left and right hand sides are found to be 10^{-16} to 10^{-18}.

4.4 Dynamical evolution of vortices

A typical fluid flow contains different types of vortices. In our present study, we have considered initial Gaussian shaped monopole vortex given by $\omega(x,y) = \omega_0\exp(-((x-x_c)^2+(y-y_c)^2)/a_c^2)$; where ω_o is the total circulation (positive sign indicates clockwise rotational direction) and a_c is the vortex core radius. The numerical investigation has been carried out for $a_c = 0.7$ and $x_c = y_c = 0$.

After benchmerking our code with known results of the published article, [36] we have studied evolution and interaction of vortices starting from initial Gaussian shaped monopole vortex as mentioned above. We have mainly studied the role of higher order nonlinearities in the GH equation and hence the effect of nonlinear elastic stress on dust vortex motion. For the initial Gaussian shaped monopole vortex of higher amplitude (5.8), the propagation is shown in Fig. 4.1 in different times. At first, the initial monopole vortex starts to shrink and steepen due to the nonlinear effect that leads to a small area vortex with higher vorticity. As time goes on, the nonlinear effect leads to a singular solution but the dust-neutral drag (ν) provides the necessary damping for which a steady vortex structure is formed between time $t = 1.2$ to 2.8. After time $t = 2.8$, the nonlinear collision term ($\nu[\psi, \omega]$) becomes sufficiently strong so that collisions overpower the effect of nonlinearity and finally the strength of vorticity starts to diminish. The continuous damping effect with background media decreases the amplitude and when it comes to the linear regime, the structure propagates like a linear shear wave. Such singular behavior of nonlinear terms in GH equation has been analytically studied and reported recently for longitudinal waves in strong coupling limit. [169]

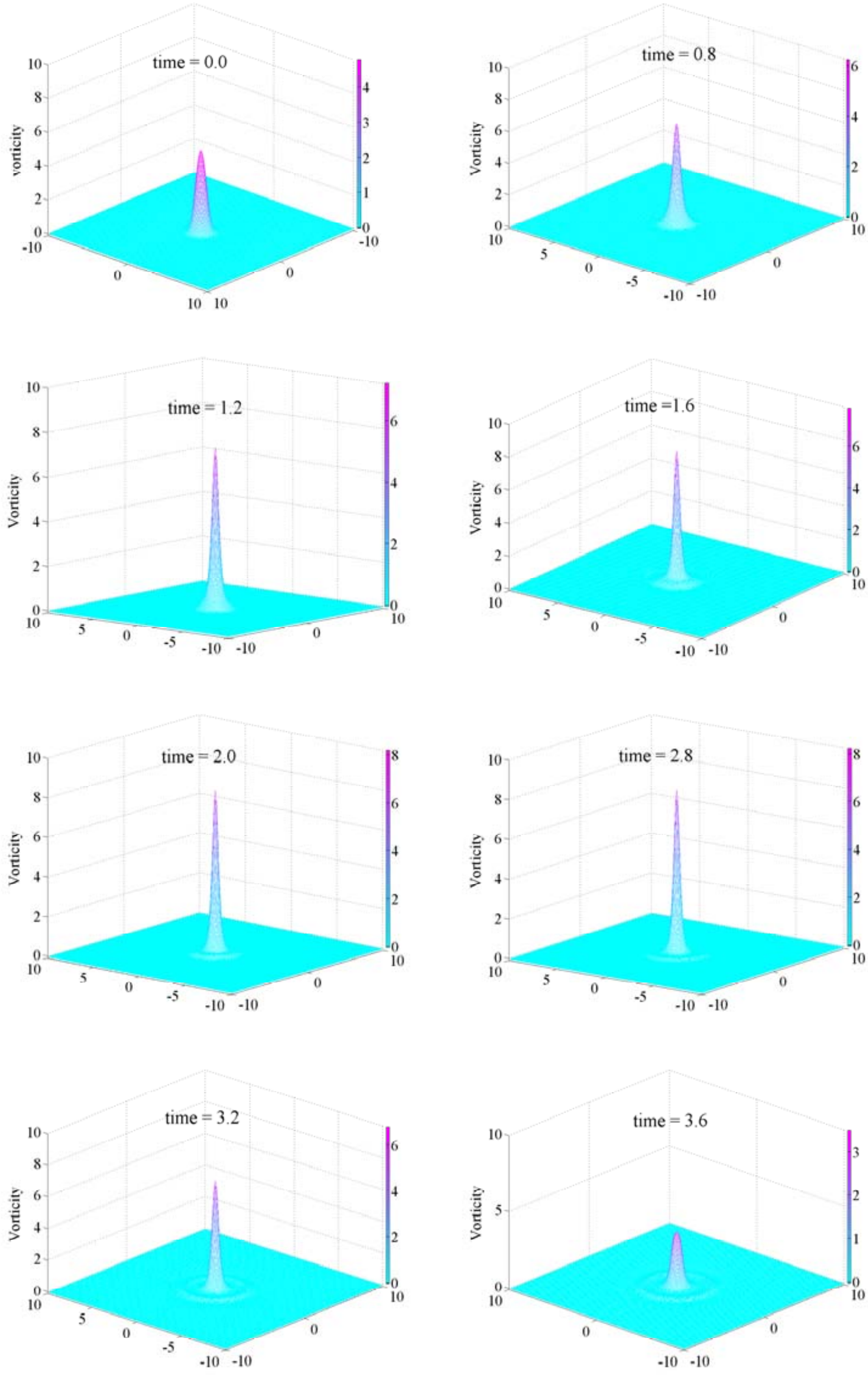
time = 0.0
vorticity
time = 0.8
vorticity
time = 1.2
Vorticity
time =1.6
Vorticity
time = 2.0
Vorticity
time = 2.8
Vorticity
time = 3.2
Vorticity
time = 3.6
Vorticity

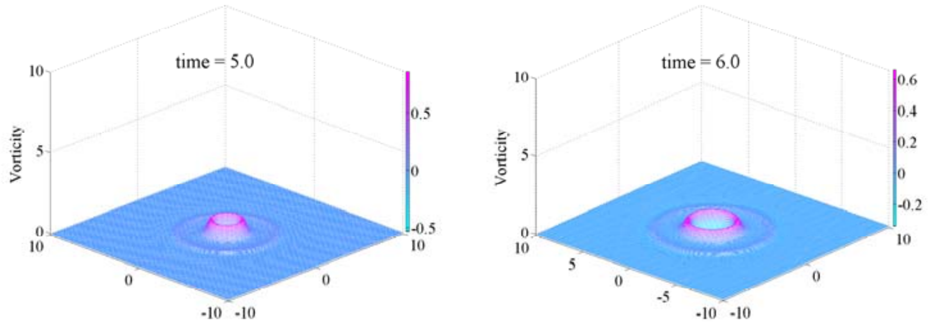

Figure 4.1: (Color online) Evolution of large amplitude (amplitude 5.8 in normalized unit) Gaussian formed monopole vortex in time with length scale $L = 1mm$ and velocity scale $U = 1mm/s$ so that the simulation box would be $20mm \times 20mm$. Velocity scale is chosen keeping in mind the typical shear wave velocity in mm/s. Mode numbers are taken as 512×512 and collision frequency $\nu = 0.0225$, $Re = 0.1$ and $\tau_m = 20$. Here, vorticity is plotted as 3D surface on $x - y$ plane.

For low amplitude, nonlinear terms cannot be stronger than linear propagating term and thus the initial structure expands like propagating shear wave. The propagation of small amplitude vortex is shown in Fig. 4.2 where it is observed that the nonlinear term is unable to resist the spreading of monopole vortex. The amplitude of initial disturbance should be quite high so that nonlinearity can take necessary role for generating non-propagating monopole vortex. Then we have explained the results from kinetic energy and total squared vorticity (enstrophy) point of view for rotating dust fluid. The kinetic energy of dust fluid is expressed as:

$$E = \frac{1}{2} \int |\vec{v} \cdot \vec{v}| dxdy.$$

In k-space energy per unit area can be written as:

$$E_k = \frac{1}{2} \sum_{k_x, k_y} (k_x^2 + k_y^2) \psi(k_x, k_y) \psi^*(k_x, k_y).$$

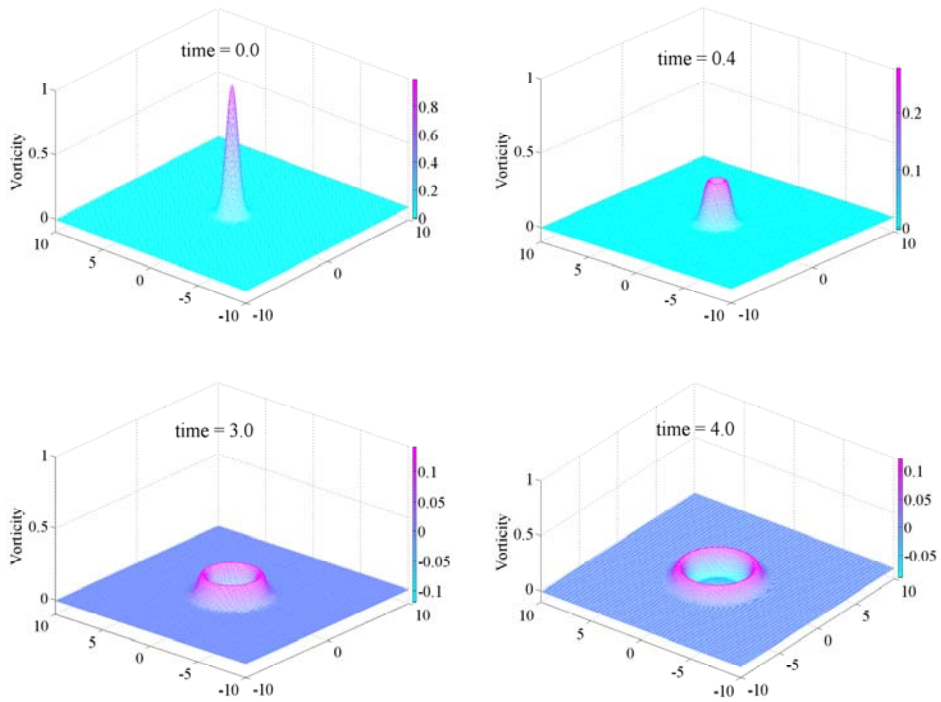

Figure 4.2: (Color online) Evolution of small amplitude (1.0 in normalized unit) Gaussian formed monopole vortex in time. Others parameters remain same like previous Fig. 4.1. Nonlinearity could not exceed the strength of linear term and thus initial structure propagates with shear wave velocity.

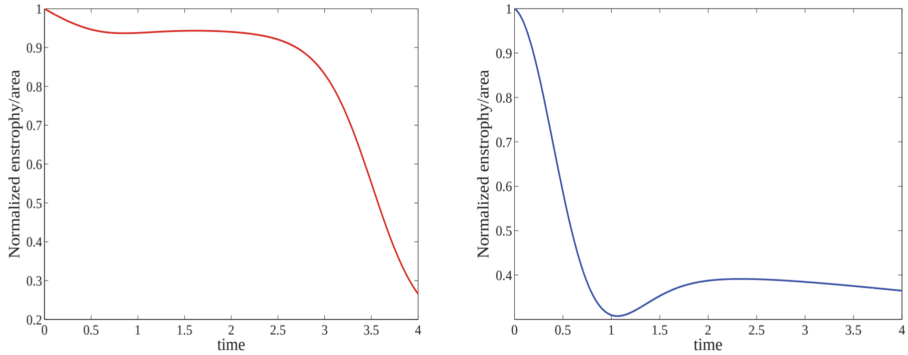

Figure 4.3: (Color online) Normalized enstrophy per unit area is plotted for comparison of linear and nonlinear case. Graph on left side represents nonlinear case and the right one is for linear case.

The enstrophy of rotating dust fluid is expressed as:

$$\Omega = \frac{1}{2}\int \omega^2 dx dy,$$

and in k-space enstrophy per unit area can be written as:

$$\Omega_k = \frac{1}{2}\sum_{k_x,k_y} \omega(k_x, k_y)\omega^*(k_x, k_y).$$

Fig. 4.3 shows a comparison of enstrophy per unit area with time for both low and high amplitude. For high amplitude (left graph), the balance between the nonlinearity and the dust-neutral collisional drag helps to get steady non-propagating vortex between time approximately $t = 0.8$ to $t = 3.0$ and the enstrophy per unit area shows almost constant value in this time regime. After time $t = 3.0$, the nonlinear collision term ($\nu[\psi, \omega]$) becomes sufficiently strong so that the collision overpowers the effect of nonlinearity and finally the strength of vorticity diminishes with time. For low amplitude, the enstrophy per unit area decreases rapidly with shear wave propagation. Fig. 4.4 shows variation of corresponding kinetic energy per unit area with time. For nonlinear case (left graph), the kinetic energy per unit

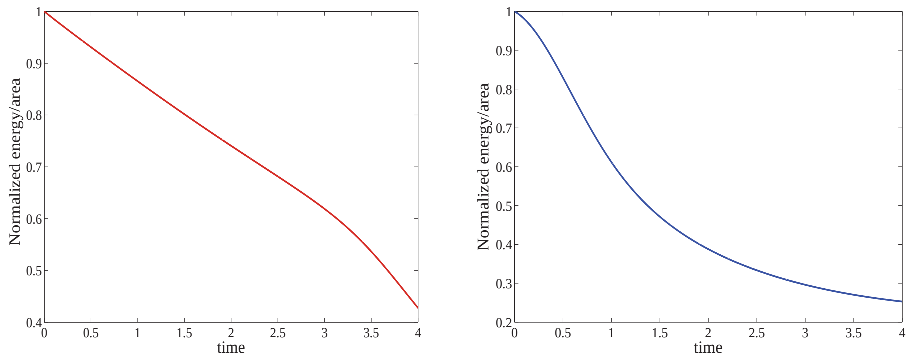

Figure 4.4: (Color online) Normalized energy per unit area is plotted for comparison of linear and nonlinear case. Graph on left side represents nonlinear case and the right one is for linear case.

area decreases linearly upto time $t = 3.0$, after that it decreases more rapidly. But the enstrophy per unit area remains almost constant within this time duration. These observations can be understood by noticing that for the nonlinear case, the vorticity remains almost constant within the time duration, approximately $t = 1.2$ to 2.8, as shown in Fig. 4.1. As we know that enstrophy depends on vorticity, so it also remains constant. Linear velocity depends on both angular velocity (angular velocity is nothing but vorticity) and radial size of the vortex and from Fig. 4.1, it is clear that the radial size of the vortex decreases with time which results in the decrease of kinetic energy per unit area with time. For linear case, the kinetic energy per unit area diminishes more rapidly which is similar to the enstrophy per unit area graph at low amplitude.

In our second case, we have investigated interaction between two monopole vortices for both cases of same and opposite direction of rotation. In both cases, dipoles are formed and for higher strength vortices, these dipoles move away from each other. The interaction between monopole vortices in dusty plasma has been recently reported in non collisional regime. [167] Like as the results of this article, [167] we have not observed any merging of co-rotating vortices. But, in our spectral simulation, we have first time reported dipole formation from interaction between two monopole vortices. Fig. 4.5 shows formation of dipoles of unequal strength and their propagation after interaction between two counter rotating monopole vortices. The overall strength of the dipole vortices remain same upto time 2.2, and then due to the damping effect of ν the dipole vortices start to decay. Hence the dipoles start to move away from each other. In weakly coupled limit ($\tau_m = 0.1$), when we repeat the same run, no dipole formation occurs and the initial structure decays due to the viscosity of the dust fluid as shown in Fig. 4.6. So, this phenomena of dipole formation and its propagation solely depends on the strong coupling property (elastic behavior) of dust fluid. In Fig. 4.7, the generation of dipole vortices is shown from the interaction between two counter rotating monopole vortices of low amplitude 16. Here, we have noticed that generated dipole vortices are of small amplitude and thus they are not propagating but due to the nature of shear wave at linear regime they start to expand and come to bigger size. Fig. 4.8 shows the formation and propagation of dipole vortices generated from the interaction between two co-rotating monopole vortices. Unlike counter rotating case, generated dipoles are of equal strength and they also propagate. Fig. 4.9 shows the interaction between two co-rotating vortices of smaller amplitude 16, resulting two non-propagating dipole vortices of equal strength.

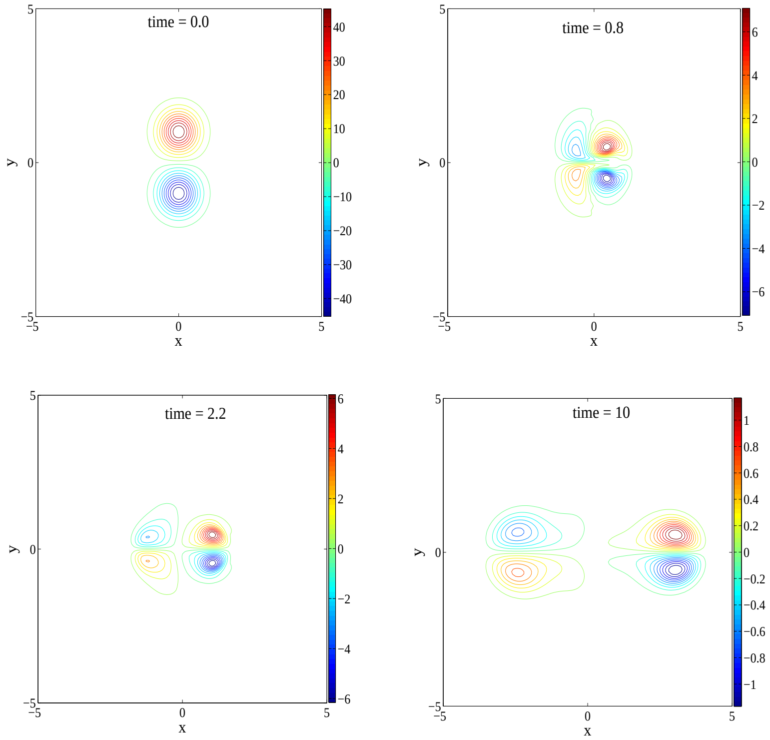

Figure 4.5: (Color online) Formation and evolution of dipole vortices from two counter rotating monopole Gaussian vortices in time. Mode numbers are taken as 512×512 and initial amplitude 50 in normalized unit. Collision frequency $\nu = 45.5, Re = 0.1$ and $\tau_m = 20$. The simulation box size is $20mm \times 20mm$ but here we have taken $10mm \times 10mm$ for better resolution. Here, vorticity is plotted as contour on $x - y$ plane.

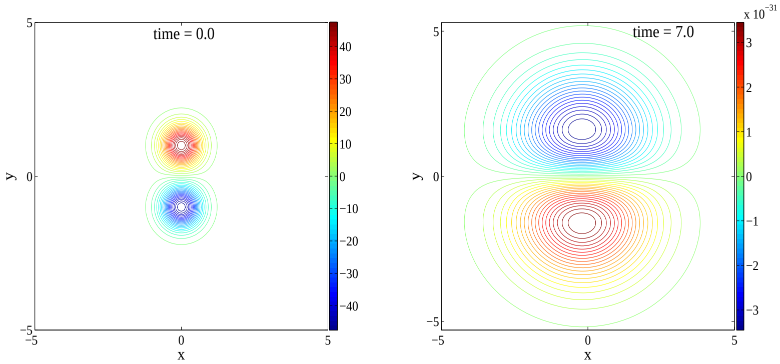

Figure 4.6: (Color online) Formation and evolution of dipole vortices from two counter rotating monopole Gaussian vortices in time. Mode numbers are taken as 512×512 and initial amplitude 50 in normalized unit. Collision frequency $\nu = 45.5, Re = 0.1$ and $\tau_m = 0.1$. The simulation box size is $20mm \times 20mm$ but here we have taken $10mm \times 10mm$ for better resolution. Here, vorticity is plotted as contour on $x - y$ plane.

4.5 Summary

The formation, evolution and interactions of gaussian vortices for a strongly coupled dusty plasma in the framework of GH model have been investigated in this chapter. The results shown here are new compared to the existing results discussed in the recent article [167] as the collisional effect of background neutrals is taken into account. In elastic limit, viscosity does not provide dissipative effect and hence, only dissipative role comes from dust-neutral collisional drag. Due to shear wave propagation in elastic limit (large τ_m), small amplitude initial monopole always propagates with shear wave velocity and thus non-propagating localized monopole vortex is not formed. This is expected as it represents linear regime which is nothing but a simple wave equation. However, the study with the large amplitude vortex shows that, as time increases, nonlinear effect becomes important and the higher order nonlinearity becomes responsible for steeping and shrinking

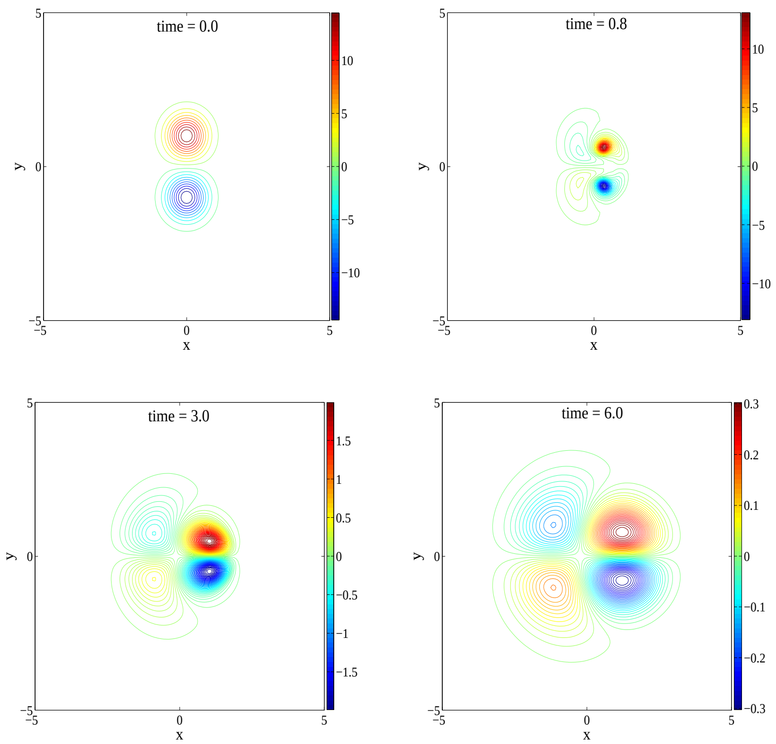

Figure 4.7: (Color online) Formation and evolution of dipole vortices from two counter rotating monopole Gaussian vortices in time. Mode numbers are taken as 512×512 and initial amplitude 16 in normalized unit. Collision frequency $\nu = 7.36, Re = 0.1$ and $\tau_m = 20$. The simulation box size is $20mm \times 20mm$ but here we have taken $10mm \times 10mm$ for better resolution. Here, contour plot of vorticity on $x - y$ plane is shown.

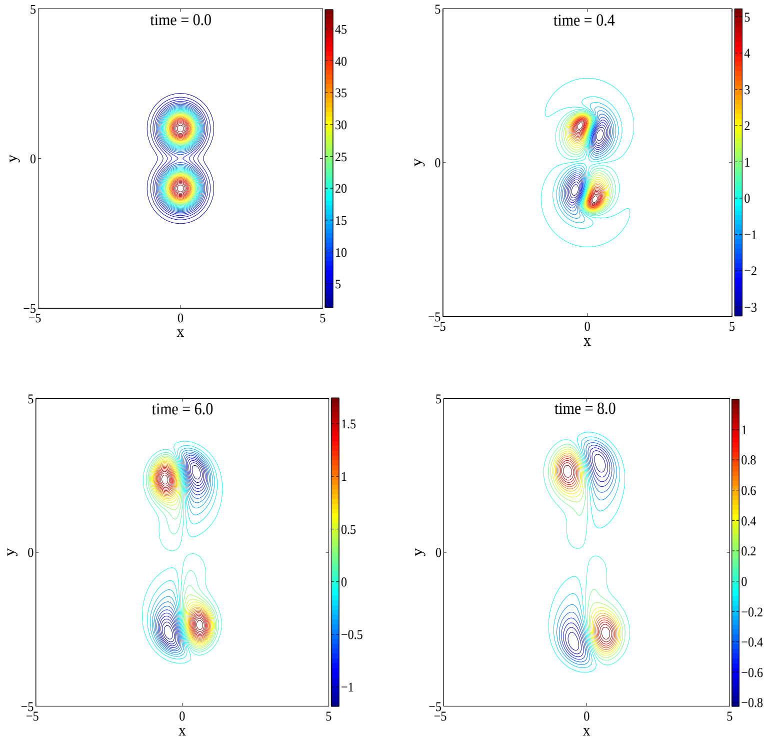

Figure 4.8: (Color online) Formation and evolution of dipole vortices from two co-rotating monopole Gaussian vortices in time. Mode numbers are taken as 512×512 and initial amplitude 50 in normalized unit. Collision frequency $\nu = 47.5$, $Re = 0.1$ and $\tau_m = 20$. The simulation box size is $20mm \times 20mm$ but here we have taken $10mm \times 10mm$ for better resolution. Here, vorticity is plotted as contour on $x - y$ plane.

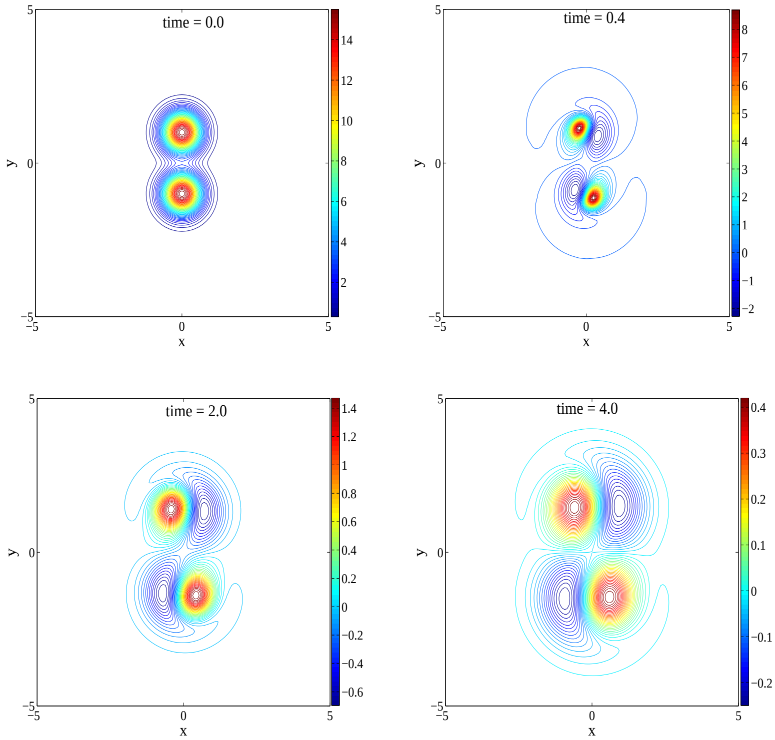

Figure 4.9: (Color online) Formation and evolution of dipole vortices from two co-rotating monopole Gaussian vortices in time. Mode numbers are taken as 512×512 and initial amplitude 16 in normalized unit. Collision frequency $\nu = 7.36$, $Re = 0.1$ and $\tau_m = 20$. The simulation box size is $20mm \times 20mm$ but here we have taken $10mm \times 10mm$ for better resolution. Here, contour plot of vorticity on $x - y$ plane is shown.

of initial profile and finally it goes to a singular solution. But, physically, the presence of collision provides necessary and sufficient balance to generate localized non-propagating (means not like linear case) monopole structure for some time duration. After that the damping nature of collisions finally diminishes the structure. Although recent investigation has shown continuous generation of shear wave even in nonlinear stage, [167] but our simulated results have no such signature. The balance between convective nonlinearity and dissipation is analogous to soliton like structure formation of longitudinal perturbation. But, in case of soliton, the balance against steepening behavior of convective nonlinearity is provided by physical dispersion. So, our prediction is that one can experimentally find non-propagating monopole vortex varying the discharge power and neutral pressure.

Furthermore, we have studied interaction between two monopoles having both co-rotating and counter rotating initial forms. In absence of collision, the recent investigation [167] has shown the continuous emission of waves and no dipole formation has been reported. However, our studies show that dipolar vortices are formed due to the interaction between both same (co-rotating) and opposite (counter rotating) vortices. For large amplitude the diplole vortices move away from each other keeping their form nearly unchanged, whereas, for relatively smaller amplitude, the strength of the dipole falls in the linear regime and then due to wave propagation property, they expand into digger sizes. The result of the dipole formation after interaction between two monopoles at the balanced condition of convective nonlinearity and dust-neutral collisional drag has been first time observed in our study. There are few recent experimental observations of monopolar, dipolar and quadrupolar dust vortices in strongly coupled dusty plasma [99, 170]. It would also be interesting to study experimentally the interaction between two monopolar dust vortices with different rotation profiles in different coupling regime. Our numerical results on vortices may lead to explain future experimental observations of interaction of dust vortices. This type of study of vortex evolution could be helpful for both basic understanding of nonlinear shear wave phenomena and also for the characterization of different parameters in strongly coupled dusty plasma system.

Chapter 5

Stability analysis of an elliptical vortex in a strongly coupled dusty plasma in presence of dust-neutral collisional drag

The stability of a long scale equilibrium vortex structure to short scale perturbations has been studied in a strongly coupled dusty plasma in the framework of a generalized hydrodynamic model (GH) modified by dust-neutral collisional drag. The analysis has been carried out using a mathematical technique employed by Bayly. The stability domain of the vortex for arbitrary values of ellipticity (ϵ) has been obtained by performing an extensive numerical study of the final stability equation in the standard Hill form. It has been found that the free energy associated with the velocity shear of the vortex can drive secondary instabilities consisting of transverse shear waves when the collision modified secondary wave frequency matches with the mean rotation frequency of the vortex or one of its integer multiples.

5.1 Introduction

The break up of vortex structures is usually associated with the onset of turbulence in the medium and hence a knowledge of the stability properties of vortices is an important requisite for gaining a better understanding of turbulence. A number of past studies have addressed this problem and looked at the stability of vortices in fluids [74] and in weakly coupled plasmas (where the potential energies of the constituent particles $\ll$ their kinetic energies). [171] As described in the fourth chapter, nonlinear two dimensional vortex like structures can be generated in strongly coupled regime (where the potential energy of the constituent particles $\gg$ their kinetic energy) of the dusty plasma in the context of the transverse shear wave. [33, 167, 172, 173] The transverse shear wave nonlinearly saturated into vortex like structures exploiting the convective nonlinearity of the GH equation. The present chapter is devoted to understand the stability features of vortices in strongly coupled regime of dusty plasma. The motivation behind such investigation came from the question of nonlinear saturation of low frequency instabilities as follows: generally the nonlinearity present in the system leads to an accumulation of energy to the long scale vortex structures due to inverse cascade process and thus prevent the attainment of a stationary state, therefore how does the nonlinear saturation occur? In order to investigate the saturation mechanism, we have studied the stability of long scale vortex structures to short scale secondary perturbations. Specifically, we have considered a model of stationary vortex at equilibrium with finite ellipticity (ϵ) at the core and studied its stability to secondary shear wave perturbations.

In this present study, the stability analysis has been carried out using a mathematical technique employed by Bayly [174] in the context of a fluid dynamics problem. The final stability equation can be cast into the form of a Hill's equation. An extensive numerical study of this equation has been carried out to obtain the stability domain of the vortex for arbitrary values of ellipticity (ϵ). We have also obtained estimates of the growth rate of the instability by using a multiple time scale method.

5.2 Governing equations

For this study, we have considered the same model as the previous work and started with the normalized form of the modified dust momentum equation (Eq. (4.3) of the fourth chapter) given as:

$$\left[1+\tau_m\left(\frac{\partial}{\partial t}+\mathbf{v}\cdot\nabla\right)\right]\left[\left(\frac{\partial}{\partial t}+\mathbf{v}\cdot\nabla\right)\mathbf{v}+\nu\mathbf{v}\right]=\frac{\eta}{\rho_{d0}}\nabla^2\mathbf{v}, \tag{5.1}$$

here hat symbols are removed for simplicity. The primary concern of this chapter is the investigation of the vortex stability. We have obtained the vorticity evolution equation by taking the curl of Eq. (5.1) as:

$$\nabla\times\left[\left\{1+\tau_m\left(\frac{\partial}{\partial t}+\mathbf{v}\cdot\nabla\right)\right\}\left\{\left(\frac{\partial}{\partial t}+\mathbf{v}+\nu\cdot\nabla\right)\mathbf{v}\right\}\right]=\frac{\eta}{\rho_{d0}}\nabla^2(\nabla\times\mathbf{v}). \tag{5.2}$$

The above equation is the vorticity equation in the GH system. Taking the z component of the above equation we have

$$\begin{aligned}&\left[1+\tau_m\left(\frac{\partial}{\partial t}+\hat{e}_z\times\nabla\psi\cdot\nabla\right)\right]\left(\frac{\partial}{\partial t}+\nu+\hat{e}_z\times\nabla\psi\cdot\nabla\right)\\&\nabla_\perp^2\psi+\tau_m\left\{\left(\hat{e}_z\times\nabla\frac{\partial\psi}{\partial x}\cdot\nabla\right)\left(\frac{\partial}{\partial t}+\hat{e}_z\times\nabla\psi\cdot\nabla\right)\frac{\partial\psi}{\partial x}\right.\\&\left.\left(\hat{e}_z\times\nabla\frac{\partial\psi}{\partial y}\cdot\nabla\right)\left(\frac{\partial}{\partial t}+\hat{e}_z\times\nabla\psi\cdot\nabla\right)\frac{\partial\psi}{\partial y}\right\}=\eta^*\nabla^2\nabla_\perp^2\psi,\end{aligned} \tag{5.3}$$

where $\eta^* = \eta/\rho_{d0}$. In the recent past it has been shown [30] that in the kinetic limit $\omega\tau_m \gg 1$ the above equation yields a propagating shear mode and subsequently its linear and nonlinear properties have been further studied. Nonlinear vortex like solutions have been reported both analytically [33] as well as in molecular dynamics simulations. [173] These nonlinearly driven vortex like solutions display an elliptically shaped core.

5.3 Equilibrium

We have taken such an elliptical core vortex as our basic equilibrium state and study the excitation of secondary instabilities in a localized region around it. We have approximated the two dimensional velocity potential as:

$$\psi_0(x, y) = \frac{\Omega}{2}\left(\frac{x^2}{\epsilon} + \epsilon y^2\right),$$

where Ω is the constant vortex rotation frequency and ϵ is the ellipticity parameter of the vortex. It may be mentioned that this form represents the simplest distortion of the equilibrium around the o-point of a vortex where the higher order distortions like x^3, y^3 terms [triangularity of the constant velocity potential surfaces $\psi_0(x, y)$] have been ignored. In this analysis we have also assumed that the secondary wave scales to be much shorter than the equilibrium scale. Substituting $\psi_0(x, y)$ in the equilibrium form of the vorticity Eq. (5.3) we have

$$\nu\Omega\left(\frac{1}{\epsilon} + \epsilon\right) - \tau_m\Omega^3\left(\frac{1}{\epsilon} + \epsilon\right) = 0. \tag{5.4}$$

This implies $\Omega = \sqrt{\nu/\tau_m}$. From the above relation we can say that the vortex rotation frequency Ω, depends on the collisional drag and also on the relaxation parameter at the equilibrium condition.

5.4 Stability analysis of two dimensional elliptical vortex

With the equilibrium discussed above we have studied the stability of the elliptical vortex to short scale secondary perturbations. As Eq. (5.3) is a single variable equation it is easy to introduce the velocity potential perturbation $\psi_1(x, y, t)$ around the equilibrium velocity potential ψ_0. Now we may write the perturbation equation around this 2-D vortex equilibrium from Eq. (5.3) as:

$$\begin{aligned}
&\left[1+\tau_m\left(\frac{\partial}{\partial t}+\hat{e}_z\times\nabla\psi_0\cdot\nabla\right)\right]\left(\frac{\partial}{\partial t}+\nu+\hat{e}_z\times\nabla\psi_0\cdot\nabla\right)\nabla_\perp^2\psi_1\\
&+\tau_m\left[\left(\hat{e}_z\times\nabla\frac{\partial\psi_0}{\partial x}\cdot\nabla\right)\left(\frac{\partial}{\partial t}+\hat{e}_z\times\nabla\psi_0\cdot\nabla\right)\frac{\partial\psi_1}{\partial x}\right.\\
&+\left(\hat{e}_z\times\nabla\frac{\partial\psi_0}{\partial x}\cdot\nabla\right)\left(\hat{e}_z\times\nabla\psi_1\cdot\nabla\right)\frac{\partial\psi_0}{\partial x}+\left(\hat{e}_z\times\nabla\frac{\partial\psi_1}{\partial x}\cdot\nabla\right)\\
&\left(\hat{e}_z\times\nabla\psi_0\cdot\nabla\right)\frac{\partial\psi_0}{\partial x}+\left(\hat{e}_z\times\nabla\frac{\partial\psi_0}{\partial y}\cdot\nabla\right)\left(\frac{\partial}{\partial t}+\hat{e}_z\times\nabla\psi_0\cdot\nabla\right)\\
&\frac{\partial\psi_1}{\partial y}+\left(\hat{e}_z\times\nabla\frac{\partial\psi_0}{\partial y}\cdot\nabla\right)\left(\hat{e}_z\times\nabla\psi_1\cdot\nabla\right)\frac{\partial\psi_0}{\partial y}\\
&\left.+\left(\hat{e}_z\times\nabla\frac{\partial\psi_1}{\partial y}\cdot\nabla\right)\left(\hat{e}_z\times\nabla\psi_0\cdot\nabla\right)\frac{\partial\psi_0}{\partial y}\right]=\eta^*\nabla^2\nabla_\perp^2\psi_1
\end{aligned} \tag{5.5}$$

and then further simplifying the final equation can be written as:

$$\begin{aligned}
&\left[1+\tau_m\left\{\frac{\partial}{\partial t}+\left(\frac{\Omega x}{\epsilon}\frac{\partial}{\partial y}-\Omega\epsilon y\frac{\partial}{\partial x}\right)\right\}\right]\left\{\frac{\partial}{\partial t}+\nu+\left(\frac{\Omega x}{\epsilon}\frac{\partial}{\partial y}-\Omega\epsilon y\frac{\partial}{\partial x}\right)\right\}\nabla_\perp^2\psi_1\\
&+\frac{\tau_m\Omega}{\epsilon}\frac{\partial}{\partial y}\left\{\frac{\partial}{\partial t}+\left(\frac{\Omega x}{\epsilon}\frac{\partial}{\partial y}-\Omega\epsilon y\frac{\partial}{\partial x}\right)\right\}\frac{\partial\psi_1}{\partial x}-\frac{\tau_m\Omega^2}{\epsilon^2}\frac{\partial^2\psi_1}{\partial y^2}-\tau_m\Omega^2\frac{\partial^2\psi_1}{\partial x^2}\\
&-\tau_m\Omega\epsilon\frac{\partial}{\partial x}\left\{\frac{\partial}{\partial t}+\left(\frac{\Omega x}{\epsilon}\frac{\partial}{\partial y}-\Omega\epsilon y\frac{\partial}{\partial x}\right)\right\}\frac{\partial\psi_1}{\partial y}-\tau_m\Omega^2\epsilon^2\frac{\partial^2\psi_1}{\partial x^2}-\tau_m\Omega^2\frac{\partial^2\psi_1}{\partial y^2}=\eta^*\nabla^2\nabla_\perp^2\psi_1.
\end{aligned} \tag{5.6}$$

We have used Bayly's method [174] to solve the above equation. In this method one eliminates the space dependent terms arising from the equilibrium flows by assuming the wave vector to be an explicit function of time. Taking a perturbation of the type $\psi_1 \sim \phi(t)\exp[i\mathbf{k}(t)\cdot\mathbf{r}]$ (i.e. Fourier analyzing in space and not in time and taking the time dependent wave vector $\mathbf{k} = \mathbf{k}(t)$), one can eliminate the equilibrium flow terms by adjusting the explicit time dependence of $\mathbf{k}$. Substituting this ψ_1 in Eq. (5.6) we have

$$\begin{aligned}
&\left[1 + \tau_m \left\{\frac{d}{dt} + i\dot{\mathbf{k}}\cdot\mathbf{r} + \left(\frac{\Omega x}{\epsilon} i k_y - \Omega\epsilon y i k_x\right)\right\}\right] \\
&\left\{\frac{d}{dt} + \nu + i\dot{\mathbf{k}}\cdot\mathbf{r} + \left(\frac{\Omega x}{\epsilon} i k_y - \Omega\epsilon y i k_x\right)\right\}(-k_\perp^2\phi) \\
&+\frac{\tau_m\Omega}{\epsilon}(ik_y)\left\{\frac{d}{dt} + i\dot{\mathbf{k}}\cdot\mathbf{r} + \left(\frac{\Omega x}{\epsilon} i k_y - \Omega\epsilon y i k_x\right)\right\}(ik_x\phi) \\
&-\frac{\tau_m\Omega^2}{\epsilon^2}(-k_y^2\phi) - \tau_m\Omega^2(-k_x^2\phi) - \tau_m\Omega\epsilon(ik_x) \\
&\left\{\frac{d}{dt} + i\dot{\mathbf{k}}\cdot\mathbf{r} + \left(\frac{\Omega x}{\epsilon} i k_y - \Omega\epsilon y i k_x\right)\right\}(ik_y\phi) \\
&-\tau_m\Omega^2\epsilon^2(-k_x^2\phi) - \tau_m\Omega^2(-k_y^2\phi) = \eta^* k_\perp^4\phi,
\end{aligned} \tag{5.7}$$

where $\dot{\mathbf{k}}$ implies derivative of $\mathbf{k}$ with respect to time. Equating x, y dependent and the constant terms independently the above equation may then be replaced by

$$\frac{dk_x}{dt} + \frac{\Omega}{\epsilon}k_y = 0, \quad \frac{dk_y}{dt} - \Omega\epsilon k_x = 0, \tag{5.8}$$

and

$$\begin{aligned}
&\left(1 + \tau_m\frac{d}{dt}\right)\left(\frac{d}{dt} + \nu\right)\Phi + \frac{\tau_m\Omega}{\epsilon}k_y\frac{d}{dt}\left(\frac{k_x}{k_\perp^2}\Phi\right) \\
&-\frac{\tau_m\Omega^2}{\epsilon^2}\left(\frac{k_y^2}{k_\perp^2}\Phi\right) - \nu\Phi - \tau_m\Omega\epsilon k_x\frac{d}{dt}\left(\frac{k_y}{k_\perp^2}\Phi\right) \\
&-\tau_m\Omega^2\epsilon^2\left(\frac{k_x^2}{k_\perp^2}\Phi\right) = -\eta^* k_\perp^2\Phi,
\end{aligned} \tag{5.9}$$

where $k_\perp^2\phi = \Phi$. The solution for the k_x, k_y is given by

$$k_x = k_0\cos(\Omega t + \delta), \quad k_y = k_0\epsilon\sin(\Omega t + \delta), \tag{5.10}$$

where k_0, δ are constants and represent the wave vector and the initial phase respectively.

We have first considered the case of $\tau_m = 0$ (i.e. in the weakly coupled regime). The above Eq. (5.9) can then be simplified as:

$$\frac{d\Phi}{dt} = -\eta^* k_\perp^2 \Phi, \tag{5.11}$$

from which the solution is given by

$$\Phi = \Phi_0 \exp\left[-\eta^* \int k_\perp^2(t) dt\right], \tag{5.12}$$

where $k_\perp^2 = (k_0^2/2)[(1+\epsilon^2) + (1-\epsilon^2)\cos 2\Omega t]$. This suggests a decay of the perturbations. This is readily understood as in the weakly coupled regime the system no longer supports the transverse shear wave (due to a lack of strong correlation between the dust particles) and hence we get the usual damping of the wave due to viscosity in this limit. Therefore if there is any instability in the system then one can say that it arises only due to the finite τ_m. Now combining Eq. (5.9) with Eq. (5.10), the time evolution for the perturbation Φ can be written as:

$$\frac{d^2\Phi}{dt^2} + P(t)\frac{d\Phi}{dt} + Q(t)\Phi = 0, \tag{5.13}$$

where

$$P(t) = \left[\left(\nu + \frac{1}{\tau_m}\right) + \frac{\Omega(1-\epsilon^2)\sin 2\Omega t}{(1+\epsilon^2) + (1-\epsilon^2)\cos 2\Omega t}\right], \tag{5.14}$$

and

$$Q(t) = \left[\frac{-4\Omega^2(\sin^2\Omega t + \epsilon^2\cos^2\Omega t)}{\{(1+\epsilon^2) + (1-\epsilon^2)\cos 2\Omega t\}} + \frac{2\Omega^2(1-\epsilon^2)^2\sin^2 2\Omega t}{\{(1+\epsilon^2) + (1-\epsilon^2)\cos 2\Omega t\}} + \frac{\eta * k_0^2}{2\tau_m}\left\{(1+\epsilon^2) + (1-\epsilon^2)\cos 2\Omega t\right\}\right]. \tag{5.15}$$

For simplification of the Eq. (5.13), let us take

$$\Phi = \Psi \exp -\frac{1}{2}\int P(t)dt = \frac{\Psi \exp -\frac{1}{2}\left(\nu + \frac{1}{\tau_m}\right)t}{\left[(1+\epsilon^2) + (1-\epsilon^2)\cos 2\Omega t\right]^{-1/4}}, \tag{5.16}$$

and then substituting the Eq. (5.16) in the Eq. (5.13) and further simplifying the following equation is obtained

$$\begin{aligned} \frac{d^2\Psi}{dt^2} + \Bigg[\frac{k_0^2 c_{sh}^2}{2}\{(1+\epsilon^2) + (1-\epsilon^2)\cos 2\Omega t\} - \frac{1}{4}\left(\nu_d + \frac{1}{\tau_m}\right)^2 \\ -\frac{\Omega}{2}\left(\nu_d + \frac{1}{\tau_m}\right)\frac{(1-\epsilon^2)\sin 2\Omega t}{(1+\epsilon^2)+(1-\epsilon^2)\cos 2\Omega t} - \Omega^2\frac{2(1+\epsilon^2)-(1-\epsilon^2)\cos 2\Omega t}{(1+\epsilon^2)+(1-\epsilon^2)\cos 2\Omega t} \\ +\frac{3\Omega^2}{2}\frac{(1-\epsilon^2)^2(1-\cos 4\Omega t)}{\{(1+\epsilon^2)+(1-\epsilon^2)\cos 2\Omega t\}^2}\Bigg]\Psi = 0, \end{aligned} \tag{5.17}$$

where the parameter $c_{sh}(= \sqrt{\eta * /\tau_m})$ stands for the shear wave velocity. Since this is a low frequency vortex, $\Omega \ll 1$, we can neglect all terms proportional to Ω^2 in the above Eq. (5.17) without any loss of generality. This will help us to reduce the algebra without taking away much from the essential physics. The simplified equation can be written as:

$$\begin{aligned} \frac{d^2\Psi}{dt^2} + \Bigg[\frac{k_0^2 c_{sh}^2}{2}(1+\epsilon^2)(1+\xi\cos 2\Omega t) - \frac{1}{4}\left(\nu + \frac{1}{\tau_m}\right)^2 \\ -\frac{\Omega}{2}\left(\nu + \frac{1}{\tau_m}\right)\frac{\xi \sin 2\Omega t}{1+\xi\cos 2\Omega t}\Bigg]\Psi = 0, \end{aligned} \tag{5.18}$$

where

$$\xi = \left(\frac{1-\epsilon^2}{1+\epsilon^2}\right).$$

Normalizing time by the vortex rotation time Ω^{-1} i.e. $\Omega t = \tau$ and considering a rigidly rotating circular vortex flow ($\epsilon = 1, \xi = 0$), the above equation (5.18) can be written as:

$$\frac{d^2\Psi}{d\tau^2} + \left[\frac{k_0^2 c_{sh}^2}{\Omega^2} - \frac{1}{4\Omega^2}\left(\nu + \frac{1}{\tau_m}\right)^2\right]\Psi = 0. \tag{5.19}$$

Hence for a rigidly rotating circular vortex the above equation gives us a collision modified secondary shear wave but no instability. Thus it is clear that, secondary instabilities, if any, must be related to deviation of ϵ from 1 i.e. $\xi \neq 0$. Physically, a rigidly rotating circular vortex has no free energy source in contrast to an elliptical vortex which has a free energy source arising due to the velocity shear of its flow.

To demonstrate the instability, we have first used a multiple time scale analysis [175] to examine the behavior of the solution of Eq. (5.18) in the limit of weak flow ellipticity when ξ is very small. In this limit ξ can be used as an expansion parameter. We have applied this method by introducing a new variable $\tau_1 = \xi\tau$ and assuming a perturbation expansion of the form $\Psi(\tau) = \Psi_0(\tau,\tau_1) + \xi\Psi_1(\tau,\tau_1) + \xi^2\Psi_2(\tau,\tau_1)\cdots$. Substituting Ψ in Eq. (5.18) and equating equal powers of ξ from both sides we get,

$$\frac{\partial^2\Psi_0}{\partial\tau^2} + \frac{1}{\Omega^2}\left[\frac{k_0^2 c_{sh}^2(1+\epsilon^2)}{2} - \frac{1}{4}\left(\nu + \frac{1}{\tau_m}\right)^2\right]\Psi_0 = 0, \tag{5.20}$$

$$\frac{\partial^2\Psi_1}{\partial\tau^2} + \frac{1}{\Omega^2}\left[\frac{k_0^2 c_{sh}^2(1+\epsilon^2)}{2} - \frac{1}{4}\left(\nu + \frac{1}{\tau_m}\right)^2\right]\Psi_1 =$$
$$-2\frac{\partial}{\partial\tau}\left(\frac{\partial\Psi_0}{\partial\tau_1}\right) - \frac{k_0^2 c_{sh}^2(1+\epsilon^2)}{2\Omega^2}\Psi_0\cos 2\tau + \frac{1}{2\Omega}\left(\nu + \frac{1}{\tau_m}\right)\Psi_0 \sin 2\tau, \tag{5.21}$$

The above equations may be solved by proposing

$$\frac{k_0^2 c_{sh}^2(1+\epsilon^2)}{2} - \frac{1}{4}\left(\nu + \frac{1}{\tau_m}\right)^2 = \Omega^2,$$

which is the condition for resonance between the dissipation modified secondary wave frequency and the vortex rotation frequency. Under this condition the solution for Eq. (5.20) is given by

$$\Psi_0(\tau,\tau_1) = A(\tau_1)\cos\tau + B(\tau_1)\sin\tau, \tag{5.22}$$

where the integration constants A, B are taken to be slow functions of time. Now the dependence of A, B on τ_1 may be obtained by substituting Ψ_0 in Eq. (5.21) and demanding that the resulting equation has a solution that is free of secular terms. This condition leads to the following dependence of A, B on τ_1:

$$\left(\frac{d}{d\tau_1} + \alpha\right) A = -\beta B, \tag{5.23}$$

$$\left(\frac{d}{d\tau_1} - \alpha\right) B = -\beta A, \tag{5.24}$$

where

$$\alpha = \frac{1}{8\Omega}\left(\nu + \frac{1}{\tau_m}\right), \quad \beta = \frac{1}{2}\left[1 + \frac{1}{4\Omega^2}\left(\nu + \frac{1}{\tau_m}\right)^2\right].$$

The above equations imply that both A and B grow exponentially. This is given by $A, B \sim \exp(\sqrt{\alpha^2 + \beta^2}\tau_1)$, which implies that for small ξ, the amplitude of the secondary perturbation grows exponentially with growth rate $\sim \xi\Omega$. At this point we must remember that this analysis is done for the transformed variable Ψ. For the actual physical variable ϕ we have to transform back and the exponential factor will change. Hence to obtain the actual growth rate we have to multiply the above growth rate with the factor $\exp[-({\tau_m}^{-1} + \nu)\tau/2\Omega]$. Essentially, in the presence of dissipation the secondary wave still grows but the growth rate is reduced by the above mentioned exponential factor. Since ξ is proportional to $(1 - \epsilon^2)$ therefore we can conclude that for a circularly symmetric vortex ($\epsilon = 1$) i.e. $\xi = 0$, there is no growth for the secondary perturbation. For $\epsilon \neq 1$ the growth rate is finite and we can say that the ellipticity of the vortex is responsible for the growth of the shear wave of the secondary perturbation and that it occurs at the rate of the vortex rotation frequency.

We have next investigated the general case with arbitrary ξ i.e. with $\epsilon \neq 1$, starting with Eq. (5.17). This equation has the general form of the standard Hill equation and can be solved by the method of the Floquet theory. [176] We have expressed Eq. (5.18) in the standard Hill form [176]

$$\frac{d^2\Psi}{d\tau^2} + \left[A_0 + 2\sum_{m=1}^{\infty} A_m \cos(2m\tau + \delta_m)\right]\Psi = 0, \tag{5.25}$$

where

$$A_0 = \frac{{k_0}^2{c_{sh}}^2}{2\Omega^2}(1+\epsilon^2) - \frac{1}{4\Omega^2}\left(\nu + \frac{1}{\tau_m}\right)^2, \quad A_m = \sqrt{a^2 + {a_m}^2},$$

$$\delta_m = \tan^{-1}\left(-a_m/a\right), \quad a = \frac{\xi {k_0}^2 {c_{sh}}^2}{4\Omega^2}(1+\epsilon^2), \quad a_m = \frac{\xi}{4\Omega}\left(\nu + \frac{1}{\tau_m}\right)(\theta_{m+1} - \theta_{m-1}),$$

$\theta_j = \theta_0 \left(\frac{1-\theta_0}{\xi\theta_0}\right)^j$, and $\theta_0 = \frac{1}{\sqrt{1-\xi^2}}$.

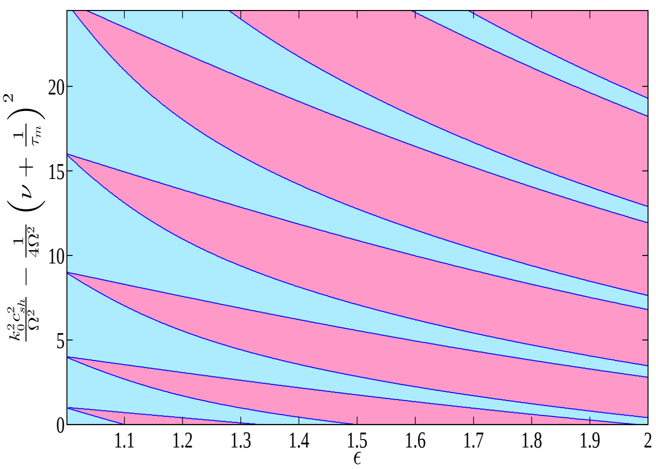

Figure 5.1: (color online) Plot of $[k_0^2 c_{sh}^2 - \frac{1}{4}\left(\nu + {\tau_m}^{-1}\right)^2]/\Omega^2$ vs. ϵ (ellipticity of the vortex). The pink colored regions show the unstable domains.

The general solution to Eq. (5.25) has the Floquet form [176]

$$\Psi = \exp(\mu\tau)\sum_n a_n \exp(2in\tau), \tag{5.26}$$

where the characteristic exponent is denoted by μ, which also determines the growth rate of the solution. This μ can be obtained from the following equation

$$\sin^2\left(\frac{i\pi\mu}{2}\right) = D_\infty(0)\sin^2\left(\frac{\pi\sqrt{\Theta_0}}{2}\right), \tag{5.27}$$

where $D_\infty(0)$ is the determinant of the infinite dimensional Hill's matrix evaluated at $\mu = 0$. The elements of this matrix are given by the expression $D_{mm} = 1$ and $D_{mn} = -A_{m-n}/(4m^2 - A_0)$, where both m and n take values from $-\infty$ to ∞.

For fixed values of ν, τ_m and arbitrary values of ϵ the above characteristic exponent equation (5.27) has to be solved numerically. In Fig. 5.4 the pink colored regions show unstable domains in the parameter space defined by $[A_0, \epsilon]$. From this figure (Fig 5.4) it is clear that when the flow ellipticity is small i.e. for $\epsilon \approx 1$ the bands of instability originate near the resonant frequencies

$$\frac{k_0^2 c_{sh}^2}{\Omega^2} - \frac{1}{4\Omega^2}\left(\nu + \frac{1}{\tau_m}\right)^2 = n^2 (n = 1, 2, 3 \cdots).$$

Note that at these resonance frequencies the elliptical vortex flow starts to drive the instability of the dissipation modified secondary shear waves. For larger flow ellipticities i.e. for $\epsilon > 1$, the bands of instability widen significantly and for high values of ϵ, the unstable domains come close to each other. Hence we find that the flow ellipticity of the elliptical vortex acts as a free energy source and drives these secondary waves unstable in these bands covering broad regions of parameter space. In this context we emphasize that these secondary waves lose their energy on leaving the vortex region and get damped by the usual natural damping mechanisms.

5.5 Summary

In this chapter, we have investigated the stability of a long scale elliptical vortex to short scale secondary perturbations. It is shown that for circular vortices there is no instability because these vortices rotate rigidly and hence have no source of free energy. Vortices with finite ellipticity are, however, shown to be unstable to the excitation of secondary perturbations. The basic physical mechanism for this instability may be understood in terms of a parametrically driven oscillator. In the frame rotating with the mean rigid angular velocity of the plasma, the waves have a time dependent wave vector $k_\perp(t)$ whose dependence arises through the ellipticity parameter $(1-\epsilon^2)$. This can resonantly drive the shear waves (kc_{sh}) provided that certain resonance conditions are satisfied. For a large deviation from circularity, off resonance driving is also possible as seen from the stability diagram Fig. 5.4. The relevance of the secondary instability excitation in a complex dusty plasma is as follows. One of the challenges faced by nonlinear theories describing low-frequency plasma turbulence is that the conventional cascade mechanisms transfer energy towards long scales where the natural damping mechanisms are negligible. This can lead to an indefinite accumulation of energy in the longest scale and prevent the attainment of a stationary state. It seems clear that when the energy in the long scale becomes large, it must find a nonlinear mechanism of dissipation to arrive at a stationary state. Our present calculation points to a possible mechanism that can make the long scale vortex radiate energy in the form of short scale secondary waves that can propagate out of the vortex and get damped in the plasma by conventional damping channels. Such a mechanism would happen beyond a threshold amplitude as obtained from the instability condition described above. The secondary instability can act as a seed for the onset of turbulence and may in turn also act as a nonlinear saturation mechanism of the vortex structures.

Chapter 6

Conclusion

In this chapter, the results obtained in this thesis have been summarized. Some future prospects of our study have also been discussed in addition.

6.1 Summary

In the field of plasma physics, it has utmost importance to understand linear and nonlinear plasma dynamics and their associated transport phenomena. In this connection, the present thesis covers the studies on some novel aspects of nonlinear coherent structures related to both the Alfvén wave in an electron-ion plasma and also transverse shear wave in a strongly coupled dusty plasma which have not been considered yet. In case of Alfvén waves study, the Lagrangian two fluid model has been adopted and both analytical and numerical analysis have been done in a very elaborative way. The generalized hydrodynamic model (GH) is a simplified phenomenological model for depicting weakly coupled to strongly coupled behavior of fluid. This model has been used for the purpose of describing the dusty plasma medium in strongly coupled regime. For the numerical simulation of GH equations, a de-aliased doubly periodic pseudo-spectral code has been employed.

- In chapter I, a brief overview of our work has been presented. An introduction to several types of coherent structures and the probable causes of formation of such structures in fluid medium and plasmas have been presented briefly. We have given an introduction to the Alfvén wave and the motivation behind our work. Also, the GH equations describing the dusty plasma dynamics and novel transverse shear wave along with its associated nonlinear phenomena related to vortices have been described in detail. The usefulness of the Lagrangian technique compared to the Eulerian technique in treating convective nonlinearity in plasma has been discussed. An idea about the efficiency of the pseudo-spectral method in handling plasma nonlinearity has been described.

- In chapter II, we have studied the linearly polarized Alfvén wave propagation taking into account the electron inertial effect and also the electron-ion collisional effect in a cold electron-ion plasma. It has been found that, the electron inertia together with the ion inertia introduces the wave dispersion which is different from the previous study where the electron mass is neglected. [77] In the weak amplitude limit, it has been found that the Alfvén wave propagation is governed by a mKdV-Burgers (mKdvB) equation. In this mKdVB equation, the electron inertia is found to act as a source of dispersion and the electron-ion collision serves as a dissipation. The collisional dissipation is eventually responsible for the Burgers term in mKdVB equation. The numerical results predict the formation of both oscillatory (dispersive) shock for weak dissipation and monotonic shock for strong dissipation. Also numerical solution predicts the breather-like structures of nonlinear Alfvén wave. In this present study, the observed shocks are compressive in nature due to the strong magnetic field enhancement at the upstream side of the shock, thereby they can be a potential mechanism to restrict the collapse of molecular clouds due to self gravity. Also, after the saturation at the upstream side, due to the energy transfer to the plasma particles strong plasma heating is possible which could initiate the particle acceleration.

  We have also analyzed the wave modulation phenomenon in the long wavelength limit. It has been shown that, there is a possibility of trapping of the Alfvén wave in a hole created by the wave itself in the medium. It has been shown that the dynamics of the modulated wave is described by a damped

NLSE equation in which the damping is provided by the electron-ion collision. The modulated wave exhibits weakly dissipative bright soliton similar to bright solitons described by the NLSE in optical fiber communication. Numerical simulation of the damped NLSE also predicts the formation of localized large amplitude nonlinear structures known as rogue waves or freak waves, giant breathers and rouge wave holes. The results could be useful in interpreting the nonlinear phenomena behind the observed magnetic structures in space plasmas.

- In chapter III, we have extended same investigation in case of circularly polarized Alfvén wave propagation in absence of collision. The right-hand circularly polarized wave dynamics has been inspected in detail. The linear analysis shows that the right-hand polarized wave saturates due to the dispersive effect of electron inertia. The newly developed modified DNLSE with third order dispersion term has also been analyzed and soliton type solutions are obtained.

- Chapter IV contains the study on vortex formation, evolution and interaction in strongly coupled dusty plasma in presence of dust-neutral collisional drag. All the studies have been investigated numerically using a doubly periodic de-aliased pseudo-spectral method. We have observed the vortex phenomena by interplaying the nonlinear elastic stress arising from the strong coupling between the dust particles and the dust-neutral collisional drag. In this work we have found two interesting aspects of vortex evolution which are as follows: 1) a sensitive balance between the nonlinear elastic stress and the dust-neutral collisional drag results in the generation of non-propagating monopole vortex before it starts to propagate like shear wave and 2) the interaction between two unshielded monopole Gaussian vortices having both same (co-rotating) and opposite (counter rotating) rotations produce two propagating dipole vortices of equal and unequal strength respectively when there is a sensitive balance between the nonlinear elastic stress and the dust-neutral collisional drag.

The results are different compared to the existing results discussed in a recent article. [167] In the first study i.e. the case with monopole vortex, the recent investigation shows continuous generation of shear wave even in non-linear regime, whereas our analysis shows the formation of non-propagating monopole vortex. In the second study i.e. two monopoles having both co-rotating and counter rotating initial forms, formation of two dipoles are reported while in contrary the recent investigation shows continuous emission of wave and no dipole formation. Therefore, neutral drag has a strong impact on the vortex dynamics in strongly coupled dusty plasma.

Our study expands the possibility of observing such types of monopole vortex formation and also dipole formations in laboratory experiments on dusty plasma, condensed matter system and astrophysical systems such as neutron star, interior of white dwarfs etc.

- In chapter V, the stability analysis of the long scale equilibrium vortex to short scale shear wave perturbation has been presented. It has been shown that for circular vortices no instability arises, because these vortices rotate rigidly and hence have no source of free energy. However, it has been found that the free energy associated with the ellipticity of the vortex can be responsible for an instability that parametrically drives secondary waves when the collision modified secondary wave frequency matches with the mean rotation frequency of the vortex or one of its multiples.

Therefore, such a process can transfer energy from the long scale vortex to the short scale secondary wave and thereby can provide a saturation mechanism for long scale vortices in complex plasmas.

6.2 Future scope of the work

The study on coherent structures, which is the topic of the thesis, could lead to a better way in understanding transport phenomena in space and astrophysical plasmas as well as in laboratory plasma experiments. We hope that our studies and findings will provide further future scope in this direction. In this regard, we will present point wise discussions over further possibilities leading from the present thesis.

- In Alfvén waves study, various physical factors like finite temperature, viscosity have not been taken into account. In reality, one should take these factors to get better realistic understanding about the system.

- We have investigated the nonlinear evolution of circularly polarized Alfvén wave by solving the modified DNLS equation in absence of collisional effect. If we consider the collisional effect then the governing modified DNLS equation with dissipation term no longer remain as an integrable system. However, this non-integrable system can be investigated by treating the dissipation term as the perturbation term by means of soliton perturbation theory. [177] It might lead to some other aspects of the Alfvén wave dynamics which will be investigated in our future study.

- In the present GH model, we have considered the viscosity as a constant parameter. In actual dusty plasma medium, the vortex dynamics would be interesting to study where the viscosity has a functional dependence on space and time. The effects of such investigation will help us to look at more realistic view of dusty plasma.

- We have assumed the electrons and ions as inertialess species in this dust vortex study. However, in actual dusty plasma experiment on vortices, the ions dynamics is also taken into consideration along with the dust dynamics. [178, 179] So, it would be necessary to incorporate ion dynamics along with the dust dynamics to study vortex phenomena in dusty plasma.

- The studies on dusty plasma assume dust particles carrying static charge. But, the charge fluctuation is an important physical phenomena in dusty plasma research. So, the inclusion of charge fluctuation may be interesting.

- We have considered dust vortex flows in 2-D plane only. But under micro-gravity conditions dust particles form 3-D cloud instead of 2-D layer. Therefore, an extension to 3-D case would yield better understanding about the realistic scenario under microgravity conditions.

- In case of vortex stability analysis, only core instability of the stationary state vortex has been studied. There is no known analytical method to do the stability analysis of the vortex with its full complex shape, so it would be interesting to do the global stability analysis using numerical method.

- We have focussed on the studies of strongly coupled dusty plasma in absence of magnetic field. However, in laboratory experiments, there are several studies on magnetized dust particles. [100, 101] So, consideration of magnetic field will open up an entirely new regime of exploration of strongly coupled dusty plasma. To carry out such investigations, the GH model used in our study has to be modified by the inclusion of magnetic field.

Finally, we sincerely hope that the works presented in this thesis will improve our knowledge on nonlinear physics in general and nonlinear plasma physics in particular and will enlighten our way to proceed furthermore in this direction.

Bibliography

[1] L. Tonks and I. Langmuir, Phys. Rev. **33**, 195 (1929).

[2] F. F. Chen, *Introduction to Plasma Physics and Controlled Fusion;Vol 1: Plasma Physics: Second Edition* (Sringer, Los Angeles, 1983).

[3] D. R. Nicholson, *Introduction to Plasma Theory* (John Wiley and Sons, New York, 1983).

[4] J. A. Bittencourt, *Fundamentals of Plasma Physics, Third edition.* (Sringer, New York, 2004).

[5] P. M. Bellan, *Fundamental of Plasma physics* (The Cambridge Univ. Press, Cambridge, 2006).

[6] P. K. Shukla and A. A. Mamun, *Introduction to Dusty Plasma Physics* (Institute of Physics Publication, Bristol, 2002).

[7] G. S. Selwyn, J. Singh, and R. S. Bennett, J. Vac. Sci. Technol. **A 7**, 2758 (1989).

[8] W. Kleber and B. Makin, Part. Sci. Technol. **16**, 43 (1998).

[9] A. Bouchoule, *Dusty Plasmas: Physics, Chemistry and Technological impacts in Plasma Processing.* (Wiley, New York, 1999).

[10] P. R. i Cabarrocas, P. Gay, and A. Hadjadj, J. Vac. Sci. Technol. **A 14**, 655 (1996).

[11] http://www.iter.org/proj/iterandbeyond. (2008).

[12] T. H. Stix, Phys. Fluids **3**, 19 (1960).

[13] N. Kroll, A. Bon, and N. Bostoker, Phys. Rev. Lett. **13**, 83 (1964).

[14] M. N. Rosenbluth and C. S. Liu, Phys. Rev. Lett. **29**, 701 (1972).

[15] T. H. Stix, Phys. Rev. Lett. **15**, 878 (1965).

[16] B. I. Cohen, A. N. Kaufman, and K. M. Watson, Phys. Rev. Lett. **29**, 581 (1972).

[17] A. N. Kaufman and B. I. Cohen, Phys. Rev. Lett. **30**, 1306 (1973).

[18] B. I. Cohen, M. A. Mostram, D. R. Nicholson, and *et al.*, Phys. Plasmas **18**, 470 (1975).

[19] S. I. Popel, S. V. Vladimirov, and P. K. Shukla, Phys. Plasmas **2**, 716 (1995).

[20] D. A. Tidman and N. A. Krall, *Shock waves in collisionless plasmas* (Wiley-Interscience New York, 1971).

[21] A. B. Mikhalovskii, V. P. Lakhin, L. A. Mikhailovskaya, and G. Onishchenko, Zh. Eksp. Teor. Fiz **86**, 2061 (1984).

[22] A. Hasegawa, C. G. Maclennan, and Y. Kodama, Phys. Fluids **22**, 2122 (1979).

[23] E. I. El-Awady and W. M. Moslem, Phys. Plasmas **18**, 082306 (2011).

[24] V. M. Chmyrev, S. V. Bilichenko, O. A. Pokhotelov, V. A. Marchenko, V. I. Lazarev, A. V. Streltsov, and L. Stenflo, Phys. Scripta **38**, 841 (1988).

[25] A. Retinò, D. Sundkvist, A. Vaivads, F. Mozer, M. André, and C. J. Owen, Nat. Phys. **3**, 236 (2007).

[26] S. D. Bale, P. J. Kellogg, D. E. Larsen, R. P. Lin, K. Goetz, and R. P. Lepping, Geophys. Res. Lett. **25**, 2929 (1998).

[27] J. W. Belcher, L. D. Jr., and E. J. Smith, J. Geophysics. Res. **74**, 2302 (1969).

[28] D. A. Gurnett, R. L. Huff, J. D. Menietti, J. L. Burch, J. D. Winningham, and S. D. Shawhan, J. Geophysics. Res. **89**, 8971 (1984).

[29] H. Ikeji, Phys. Fluids **29**, 1764 (1986).

[30] P. K. Kaw and A. Sen, Phys. Plasmas **5**, 3552 (1998).

[31] J. Pramanik, G. Prasad, A. Sen, and P. Kaw, Phys. Rev. Lett. **88**, 17500 (2002).

[32] P. Bandyopadhyay, G. Prasad, A. Sen, and P. K. Kaw, Phys. Lett. A **372**, 5467 (2008).

[33] M. S. Janaki and N. Chakrabarti, Phys. Plasmas **17**, 053704 (2010).

[34] P. K. Shukla, Phys. Lett. A **306**, 134 (2002).

[35] V. E. Fortov, I. T. Iakubov, and A. G. Khrapak, *Physics of strongly coupled plasma* (Clarendon Press, Oxford, 2006).

[36] A. H. Nielsen and J. J. Rasmussen, Phys. Fluids **9**, 982 (1997).

[37] R. C. Davidson, *Methods in Nonlinear Plasma Theory* (Academic, New York, 1972).

[38] J. S. Russell, Proc. R. Soc. Edinburgh **11**, 319 (1844).

[39] D. J. Korteweg and G. de Vries, Philos. Mag. **39**, 422 (1895).

[40] N. J. Zabusky and M. D. Kruskal, Phys. Rev. Lett. **15**, 240 (1965).

[41] A. Xie, L. van der Meer, W. Hoff, and R. H. Austin, Phys. Rev. Lett. **84**, 5435 (2000).

[42] E. Polturak, P. G. N. de Vegvar, E. K. Zeise, and D. M. Lee, Phys. Rev. Lett. **46**, 1588 (1981).

[43] F. K. Abdullaev, A. Gammal, A. M. Kamchatnov, and L. Tomio, Int. J. of Mod. Phys. **19**, 3415 (2005).

[44] V. V. Konotop, *in Dissipative Solitons, edited by n. akhmediev* (Sringer, 2005).

[45] F. Tappert, *Reminiscences on Optical Soliton Research with Akira Hasegawa* (1998).

[46] H. Washimi and T. Taniuti, Phys. Rev. Lett. **17**, 996 (1966).

[47] H. Ikezi, R. J. Taylor, and D. R. Baker, Phys. Rev. Lett. **25**, 11 (1970).

[48] P. K. Shukla and L. Stenflo, Phys. Lett. A **315**, 244 (2003).

[49] L. Draper, Mar. Obs. **35**, 193 (1965).

[50] A. Ankiewicz, N. Devine, and N. Akhmediev, Phys. Lett. A **373**, 3997 (2009).

[51] K. Hammani, B. Kibler, C. Finot, P. Morin, J. Fatome, J. M. Dudley, and G. Millot, Opt. Lett. **36**, 112 (2011).

[52] N. Akhmediev, J. M. Soto-Crespo, and A. Ankiewicz, Phys. Rev. A **80**, 043818 (2009).

[53] A. N. Ganshin, V. B. Efimov, V. G. Kolmakov, L. P. Mezhov-Deglin, and P. V. E. McClintock, Phys. Rev. Lett. **101**, 065303 (2008).

[54] A. Montina, U. Bortolozzo, S. Residori, and F. T. Arecchi, Phys. Rev. Lett. **103**, 173901 (2009).

[55] Y. V. Bludov, V. V. Konotop, and N. Akhmediev, Phys. Rev. A **80**, 033610 (2009).

[56] L. Stenflo and M. Marklund, J. Plasma Phys. **76**, 293 (2010).

[57] W. M. Moslem, Phys. Plasmas **18**, 032301 (2011).

[58] J. Pedlosky, *Geophysical fluid dynamics.* (Sringer, 1987).

[59] S. A. Balbus and J. F. Hawley, Rev. Mod. Phys. **70**, 1 (1998).

[60] D. J. Wu, G. L. Huang, and D. Y. Wang, Phys. Rev. Lett **77**, 4346 (1996).

[61] Z. Lin, T. Hahm, W. Lee, W. Tang, and R. White, Science **281**, 1835 (1998).

[62] H. Alfvén, MNRAS **107**, 211 (1947).

[63] N. F. Cramer, *The Physics of Alfvén Waves* (WILEY-VCH, Germany, 2001).

[64] H. Alfvén, Nature (London) **150**, 405 (1942).

[65] D. J. Wu and L. Yang, Astron. Astrophys. **452**, L7 (2006).

[66] J. R. Wygant, A. Keiling, C. A. Cattell, R. L. Lysak, M. Temerin, F. S. Mozer, C. A. Kletzing, J. D. Scudder, V. Streltsov, W. Lotko, et al., J. Geophysics. Res. **107**, 24 (2002).

[67] R. A. López, F. A. Asenjo, V. Muñoz, C.-L. C. Abraham, and J. A. Valdivia, Phys. Rev. E. **88**, 023105 (2013).

[68] M. N. Rosenbluth and P. H. Rutherford, Phys. Rev. Lett. **34**, 1428 (1975).

[69] G. Vlad, F. Zonca, and S. Briguglio, Rev. Nuovo Cimento **22**, 1 (1999).

[70] P. K. Shukla, R. Bingham, B. Eliasson, M. E. Dieckmann, and L. Stenflo, Plasma Phy. Controlled Fusion **48**, B249 (2006).

[71] T. Mastumoto and T. K. Suzuki, MNRAS **440**, 971 (2014).

[72] K. Stasiewicz, P. Bellan, C. Chaston, C. Kletzing, R. Lysak, J. Maggs, O. Pokhotelov, C. Seyler, P. Shukla, L. Stenflo, et al., Space Sci. Rev. **92**, 423 (2000).

[73] C. C. Chaston, J. W. Bonnell, L. M. Peticolas, C. W. Carlson, and J. P. McFadden, Geophys. Res. Lett. **29**, 11 (2002).

[74] A. Groisman and V. Steinberg, Nature **405**, 53 (2000).

[75] A. A. Schekochihin, S. V. Nazarenko, and T. A. Yousef, Phys. Rev. E **85**, 036406 (2012).

[76] H. L. Pecseli, *Waves and Oscillations in Plasmas* (CRC. Press, 2012).

[77] C. F. Kennel, B. Buti, T. Hada, and R. Pellat, Phys. Fluids **31**, 1949 (1988).

[78] J. Zhao, Phys. Plasmas **22**, 042115 (2015).

[79] K. Stasiewicz, J. Geophys. Res.: Space Physics **110** (2005).

[80] G. S. Selwyn, J. Sing, and R. S. Bennett, J. Vac. Sci. Technol. **A7**, 2758 (1989).

[81] H. Thomas, G. E. Morfill, V. Demmel, J. Goree, B. Feuerbacher, and D. Möhlmann, Phys. Rev. Lett. **73**, 652 (1994).

[82] J. H. Chu and L. Lee, Phys. Rev. Lett. **72**, 4009 (1994).

[83] Y. Hayashi and K. Tachibana, Jpn. J. Appl. Phys. **33**, L804 (1994).

[84] A. Melzer, T. Trottenberg, and A. Piel, Phys. Lett. A **191**, 301 (1994).

[85] H. Thomas and G. E. Morfill, Nature **379**, 806 (1996).

[86] S. Ichimaru, Rev. Mod. Phys. **54**, 1017 (1982).

[87] M. A. Bervosky, Phys. Lett. A **166**, 365 (1992).

[88] Y. Feng, J. Goree, and B. Liu, Phys. Rev. E **82**, 036403 (2010).

[89] Y. I. Frenkel, *Kinetic Theory of Liquids* (Clarendon, Oxford, 1946).

[90] S. Jana, D. Banerjee, and N. Chakrabarti, Phys. Plasmas **22**, 083704 (2015).

[91] S. Ichimaru, H. Iyetomi, and S. Tanaka, Phys. Rep. **149**, 91 (1987).

[92] W. L. Slattery, G. D. Doolen, and H. E. DeWitt, Phys. Rev. A **21**, 2087 (1980).

[93] W. L. Slattery, G. D. Doolen, and H. E. DeWitt, Phys. Rev. A **26**, 2255 (1980).

[94] H. Ohta and S. Hamaguchi, Phys. Rev. Lett. **84**, 6026 (2000).

[95] G. E. Morfill, H. M. Thomas, U. Konopka, H. Rothermal, M. Zuzic, A. V. Ivlev, and J. Goree, Phys. Rev. Lett. **83**, 1598 (1999).

[96] M. R. Akdim and W. J. Goedheer, Phys. Rev. E **67**, 056405 (2003).

[97] G. E. Morfill, M. Rubin-Zuzic, H. Rothermel, A. V. Ivlev, B. A. Klumov, H. M. Thomas, and U. Konopka, Phys. Rev. Lett. **92**, 175004 (2004).

[98] S. Mitic, R. Sütterlin, A. V. Ivlev, H. Höfner, M. H. Thomas, S. Zhdanov, and G. E. Morfill, Phys. Rev. Lett. **101**, 235001 (2008).

[99] T. Bockwoldt, O. Arp, K. O. Menzel, and A. Piel, Phys. Plasmas **21**, 103703 (2014).

[100] U. Konopka, D. Samsonov, A. V. Ivlev, J. Goree, V. Steinberg, and G. E. Morfill, Phys. Rev. E **61**, 1890 (2000).

[101] N. Sato, G. Uchida, T. Kaneko, S. Shimizu, and S. Iizuka, Phys. Plasmas **8(5)**, 1786 (2001).

[102] M. Schwabe, S. Zhdanov, C. Räth, D. B. Graves, H. M. Thomas, and G. E. Morfill, Phys. Rev. Lett. **112**, 115002 (2014).

[103] A. K. Agarwal and G. Prasad, Phys. Lett. A **309**, 103 (2003).

[104] J. Ashwin and R. Ganesh, Phys. Rev. Lett. **106**, 135001 (2011).

[105] T. Kakutani, H. Ono, T. Taniuti, and C. C. Wei, J. Phys. Soc. Jpn. **24**, 1159 (1968).

[106] T. Kakutani and H. Ono, J. Phys. Soc. Jpn. **26**, 1305 (1969).

[107] K. Mio, T. Ogino, K. Minami, and S. Takeda, J. Phys. Soc. Jpn. **41**, 265 (1976).

[108] E. Mjølhus and J. Wyller, Phys. Scripta **33**, 442 (1986).

[109] E. Mjølhus, Phys. Scripta **40**, 227 (1989).

[110] E. Mjølhus and T. Hada, *Nonlinear waves and chaos in space plasmas* (edited by T. Hada and H. Matsumoto, Terrapub, Tokio, 1997).

[111] J. P. Boyd, *Chebyshev and Fourier Spectral Methods* (DOVER Publications, Inc., New York, 2000).

[112] D. Gottlieb and S. A. Orszag, CBMS-NSF Reg. Conf. Ser. in Appl. Math. **26**, 170 (1977).

[113] C. Canuto, M. Y. Hussaini, A. Quarteroni, and T. A. Zang, *Spectral Methods in Fluid Dynamics* (SpringerVerlag, New York/Berlin, 1988).

[114] Y. Salu and G. Knorr, J. Comput. Phys. **17**, 68 (1975).

[115] G. Knorr, F. R. Hansen, J. P. Lynov, H. L. Pécseli, and J. J. Rasmussen, Phys. Scripta **38**, 892 (1988).

[116] E. A. Coutsias, F. R. Hansen, T. Huld, G. Knorr, and J. P. Lynov, Phys. Scripta **40**, 270 (1989).

[117] W. H. Press, S. A. Teukolsky, W. T. Vetterling, and B. P. Flannery, *Numerical Recipes in FORTRAN 77* (Cambridge University Press, 1986).

[118] B. Buti, V. L. Galinski, V. I. Shevchenko, G. Lakhina, B. T. Tsurutani, B. E. Goldstein, P. Diamond, and M. V. Medvedev, Astrophys. J. **523**, 849 (1999).

[119] E. Mjolhus, J. Plasma Phys. **19**, 437 (1978).

[120] A. W. Hood, D. González-Delgado, and D. Ireland, Astron. Astrophys. **324**, 11 (1997).

[121] I. D. Moortel, A. W. Hood, J. Ireland, and T. D. Arber, Astron. Astrophys. **346**, 641 (1999).

[122] J. Heyvaerts and E. R. Priest, Astron. Astrophys. **117**, 220 (1983).

[123] T. A. Carter, B. Brugman, P. Pribyl, and W. Lybarger, Phys. Rev. Lett. **96**, 155001 (2006).

[124] S. Dorfman and T. A. Carter, Phys. Rev. Lett. **110**, 195001 (2013).

[125] A. Panwar, H. Rizvi, and C. M. Ryu, Phys. Plasmas **20**, 052103 (2013).

[126] A. Panwar, H. Rizvi, and C. M. Ryu, Phys. Plasmas **20**, 082101 (2013).

[127] Y. Lin, J. R. Johnson, and X. Wang, Phys. Rev. Lett. **109**, 125003 (2012).

[128] J. S. Zhao, Y. Voitenko, D. J. Wu, and J. D. Keyser, Astrophys. J. **785**, 139 (2014).

[129] J. S. Zhao, Y. Voitenko, J. D. Keyser, and D. J. Wu, Astrophys. J. **799**, 222 (2015).

[130] M. L. Rinawa, N. Gaur, and R. P. Sharma, Phys. Plasmas **22**, 022310 (2015).

[131] J. M. Dawson, Phys. Rev. **113**, 383 (1959).

[132] H. Schamel, Phys. Reports. **392**, 279 (2004).

[133] N. Chakrabarti, C. Maity, and H. Schamel, Phys. Rev. E. **88**, 023102 (2013).

[134] M. J. Lighthill, J. Inst. Math. Appl. **1**, 269 (1965).

[135] M. C. cross and P. C. Hohenberg, Rev. Mod. Phys. **65**, 851 (1993).

[136] A. Scott, *Encyclopedia of Nonlinear Science, Lectures in Applied Mathematics* (Routledge Taylor Francis Group, New York, 2005).

[137] A. Sarkar, N. Chakrabarti, and H. Schamel, Phys. Plasmas **22**, 072307 (2015).

[138] R. Courant, K. Friedrichs, and H. Lewy, IBM journal of Research and Development **11**, 215 (1967).

[139] M. J. Ablowitz and H. Suger, *Solitons and the Inverse Scattereing Transform* (Society for Industrial and Applied Mathematics (SIAM), Philadelphia, 1981).

[140] M. Saito, S. Watanabe, and H. Tanaka, J. Phys. Soc. Japan **53**, 2304 (1984).

[141] V. E. Zakharov and E. A. Kuznetsov, Physica D **18**, 455 (1986).

[142] E. J. Parkes, J. Phys. A **20**, 2025 (1987).

[143] O. Bang, W. Krolikowski, J. Wyller, and J. J. Rasmussen, Phys. Rev. E **66**, 046619 (2002).

[144] W. Krolikowski, O. Bang, J. J. Rasmussen, and J. Wyller, Phys. Rev. E **64**, 016612 (2001).

[145] S. Ghosh, S. Sarkar, M. Khan, and M. R. Gupta, Phys. Rev. E **84**, 066401 (2011).

[146] Y. S. Kivshar and G. P. Agarwal, *Optical Solitons- From Fibres to Photonic Crystals* (Academic Press, San Diego, 1995).

[147] G. L. Lamb, *Elements of Soliton Theory* (Wiley, New York, 1980).

[148] N. Akhmediev and A. Ankiewicz, *Solitons, Nonlinear Pulses and and Beams* (Chapman and Hall, London, 1997).

[149] N. Akhmediev, A. Ankiewicz, and J. M. Soto-Crespo, Phys. Rev. E **80**, 026601 (2009).

[150] K. B. Dysthe and K. Trulsen, Phys. Scr. **T 82**, 48 (1999).

[151] D. H. Peregrine, J. Aust. Math. Soc. Series B Appl. Math. **25**, 16 (1983).

[152] N. N. Akhmediev, V. M. Eleonskii, and N. Kulagin, Theor. Math. Phys.(USSR) **72**, 809 (1987).

[153] Y. C. Ma, Stud. Appl. Math. **60**, 43 (1979).

[154] A. Chabchoub, N. P. Hoffmann, and N. Akhmediev, J. Geophys. Res. **117**, C00J02 (2012).

[155] E. C. Ostriker, J. M. Stone, and C. F. Gammie, Astrophys. J. **546**, 980 (2001).

[156] J. R. Wygant, A. Keiling, C. A. Cattell, R. L. Lysak, M. Temerin, F. S. Mozer, C. A. Kletzing, J. D. Scudder, V. Streltsov, W. Lotko, et al., J. Geophys. Res. **107**, 24 (2002).

[157] S. J. Schwartz and D. Burgess, Geophys. Res. Lett. **18**, 373 (1991).

[158] S. J. Schwartz, D. Burgess, W. P. Wilkinson, R. L. Kessel, M. Dunlop, and H. Luhr, J. Geophys. Res. **97**, 4209 (1992).

[159] D. Burgess, Adv. Space Res. **20**, 673 (1997).

[160] C. F. Kennel and R. Z. Sagdeev, J. Geophys. Res. **72**, 3327 (1967).

[161] M. J. Ablowitz and P. A. Clarkson, *Solitons, nonlinear evolution equations and inverse scattering*, vol. 149 (Cambridge university press, 1991).

[162] C. F. Karney, A. Sen, and F. Y. Chu, Phys. Fluids **22**, 940 (1979).

[163] S. Jana, S. Ghosh, and N. Chakrabarti, Phys. Plasmas **23**, 072304 (2016).

[164] D. J. Kaup and A. C. Newell, J. Math. Phys. **19**, 798 (1978).

[165] J. Borhanian and A. Rezaei, Phys. Plasmas **24**, 022302 (2017).

[166] P. Epstein, Phys. Rev. **23**, 710 (1924).

[167] V. S. Dharodi, S. K. Tiwari, and A. Das, Phys. Plasmas **21**, 073705 (2014).

[168] R. Courant, K. Friedricks, and H. Lewy, Mathematische Annalen **100**, 32 (1982).

[169] A. Das, S. K. Tiwary, P. Kaw, and A. Sen, Phys. Plasmas **21**, 083701 (2014).

[170] G. E. Morfill, H. M. Thomas, U. Konopka, H. Rothermal, M. Zuzic, A. V. Ivlev, and J. Goree, Phys. Rev. Lett. **83**, 1598 (1999).

[171] H. L. Pcseli, J. J. Rasmussen, and K. Thomsen, Phys. Rev. Lett. **52**, 2148 (1984).

[172] S. Ratynskaia, K. Rypdal, C. Knapek, S. khrapak, A. V. milovanov, A. Ivlev, J. J. Rasmussen, and G. E. Morfill, Phys. Rev. Lett. **96**, 105010 (2006).

[173] J. Ashwin and R. Ganesh, Phys. Rev. Lett. **106**, 135001 (2011).

[174] B. J. Bayly, Phys. Rev. Lett. **57**, 2160 (1986).

[175] C. M. Bender and S. A. Orszag, *Advanced Mathametical Methods for Sciencist and Engineers* (McGraw-Hill, Singapore, 1984).

[176] E. T. Whittaker and G. N. Watson, *A Course of Modern Analysis* (Cambridge Univ. Press, Cambridge, 1969).

[177] A. Biswas, Phys. plasmas **12**, 022306 (2005).

[178] M. Kretschmer, U. Konopka, S. K. Zhdanov, H. M. Thomas, G. E. Morill, V. E. Fortov, V. I. Molotkov, A. M. Lipaev, and O. F. Petrov., Plasma Science, IEEE Transactions on **39(11)**, 2758 (2011).

[179] J. Goree, G. E. Morill, V. N. Tsytovich, and S. V. Vladimirov, Phys. Rev. E **59**, 7055 (1999).